Appalachian STATE UNIVERSITY BOONE, NORTH CAROLINA

Southeastern Geology: Volume 43, No. 4 June 2005

Editor in Chief: S. Duncan Heron, Jr.

Abstract

Academic journal published quarterly by the Department of Geology, Duke University.

SOUTHEASTERN GEOLOGY

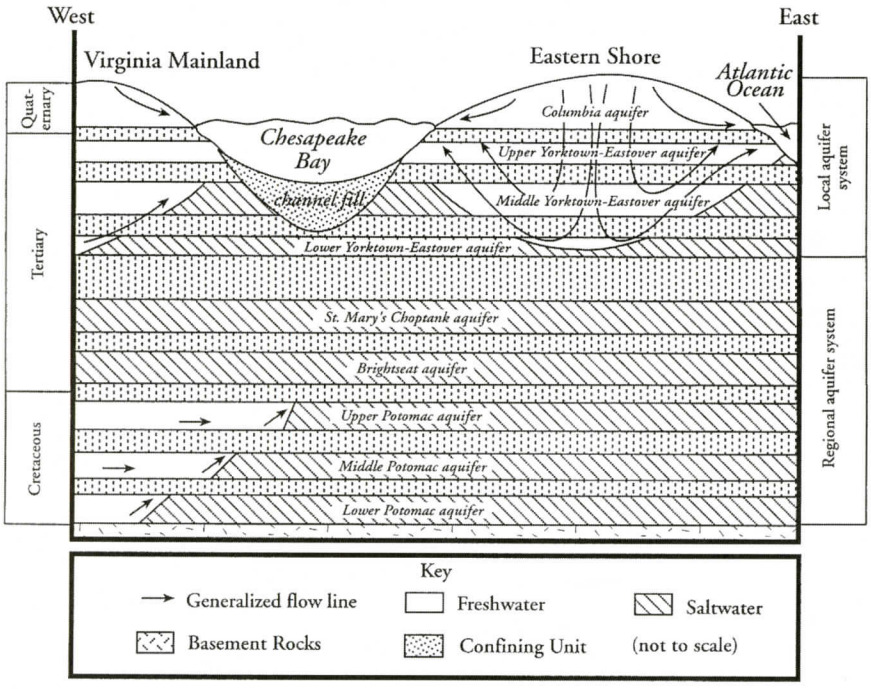

Vol. 43, No. 4 June 2005

SOUTHEASTERN GEOLOGY

PUBLISHED

at

DUKE UNIVERSITY

Editor in Chief:

Duncan Heron

This journal publishes the results of original research on all phases of geology, geophysics, geochemistry and environmental geology as related to the Southeast. Send manuscripts to **DUNCAN HERON, DUKE UNIVERSITY, DIVISION OF EARTH & OCEAN SCIENCES, BOX 90233, DURHAM, NORTH CAROLINA 27708-0233**. Phone: 919-684-5321, Fax: 919-684-5833, Email: duncan.heron@duke.edu Please observe the following:

1) Type the manuscript with double space lines and submit in duplicate, or submit as an Acrobat file attached to an email.
2) Cite references and prepare bibliographic lists in accordance with the method found within the pages of this journal. Data citations examples can be found at http://www.geoinfo.org/TFGeosciData.htm
3) Submit line drawings and complex tables reduced to final publication size (no bigger than 8 x 5 3/8 inches).
4) Make certain that all photographs are sharp, clear, and of good contrast.
5) Stratigraphic terminology should abide by the North American Stratigraphic Code (American Association Petroleum Geologists Bulletin, v. 67, p. 841-875).
6) Email Acrobat (pdf) submissions are encouraged.

Subscriptions to *Southeastern Geology* for volume 43 are: individuals - $23.00 (paid by personal check); corporations and libraries - $33.00; foreign $40. Inquires should be sent to: **SOUTHEASTERN GEOLOGY, DUKE UNIVERSITY, DIVISION OF EARTH & OCEAN SCIENCES, BOX 90233, DURHAM, NORTH CAROLINA 27708-0233**. Make checks payable to: *Southeastern Geology.*

Information about SOUTHEASTERN GEOLOGY is on the World Wide Web including a searchable author-title index 1958-2001 (Acrobat format). The URL for the Web site is: http://www.southeasterngeology.org

SOUTHEASTERN GEOLOGY is a peer review journal.

ISSN 0038-3678

SOUTHEASTERN GEOLOGY

Table of Contents

Volume 43, No. 4 June 2005

SOUTHEASTERN GEOLOGY
V. 43, No. 4, June 2005, p. 173-191

ESTIMATION OF IN SITU POROSITY BY ELECTRIC RESISTIVITY SURVEY: A CASE STUDY IN THE EASTERN SHORE OF VIRGINIA

ALI A. NOWROOZI AND DONALD P. SWIFT

Department of Ocean, Earth and Atmospheric Sciences
Old Dominion University
Norfolk, VA.

ABSTRACT

Inversions of 136 Schlumberger field curves and water quality parameters from 96 screen-elevation wells across the Eastern Shore of Virginia are used to obtain in situ porosity maps at several depths. In addition, empirical equations are derived for estimations of resistivity, formation factor, total dissolved solids and porosity at any depths.

Inversion of surface resistivity field curves over the Eastern Shore of Virginia provides values of rock resistivity (Rs) as a function of depth (h). Rock resistivities are calculated for 3, 5, 10, 20, 30, 40, 50, 60, 70, 100, and 130 m respectively at all 136 locations. The resistivity values are used to construct resistivity maps at these depths as well as resistivity profiles across the area. For the entire Eastern Shore, equation $Rs = 902.46*h^{-0.6336}$, with a multiple correlation coefficient of $R^2 = 0.9773$, gives the average rock or sediment resistivity in ohm–meters (Ωm) with depth. Pore water electrical conductivity (Con) in micro-siemens /cm (μS/cm) and total dissolved solid (TDS) in mg/l are also available for 96 water samples taken from the water of wells in a series of water research stations within the Eastern Shore. Variations in average pore water conductivity (Con) pore water resistivity (Rw), and total dissolved solids with depth (TDS) are calculated by curve fitting. The equations are: $Con = 167.85*e^{0.0272*h}$, $Rw = 67.767*e^{0.0217*h}$ and $TDS = 154.91*e^{0.0251*h}$ with multiple correlation coefficients of 0.8376, 0.8296, and 0.5217, respectively. From these equations, maps and profiles of resistivity formation factor, F, (where F = Rs/Rw) are constructed. Archie's law is then used for a sandy formation, $F = 0.62*\phi^{-2.15}$, to construct porosity maps and porosity profiles. Variation of porosity with depth may result from lenses of high porosity, perhaps related to old paleochannels and sediments with higher clay content. The values of porosity vary between and within each profile, from about 15 to 85%. However, the average porosity between profiles varies from 31.96 to 51.77% with a grand mean of 42%; while, the average value within the profiles varies from 23.07 to 51.43 with a grand mean of 41.15%. The average estimate of resistivity formation factor, total dissolved solids, and porosity at any depth are calculated from equations presented in this work.

INTRODUCTION

Porosity is essential for estimation of the storage capacity of aquifer as well as of petroleum reservoirs. In addition it is vital information for flow modeling, cleaning of the polluted areas, and remediation of soil and rock formations. In the petroleum industry, sonic, density, and neutron logs are tools of choice for estimation of porosity. However, for ground water evaluation in near-surface aquifers, estimates are more commonly based on core samples. There are limited data on porosity of aquifers in the Eastern Shore. The lack of real porosity data forced Richardson (1992) to assign a porosity of 0.25 to all layers in her modeling of ground water flow and saline intrusion in this region. Porosity, however, is not constant for each layer and a higher porosity could affect her conclusions significantly. Swift (2003) reported porosity of core samples from a limited area of the Eastern Shore in vicinity of Oyster, Virginia. His collection is restricted in depth, from surface to about 10 m. An analysis of this data

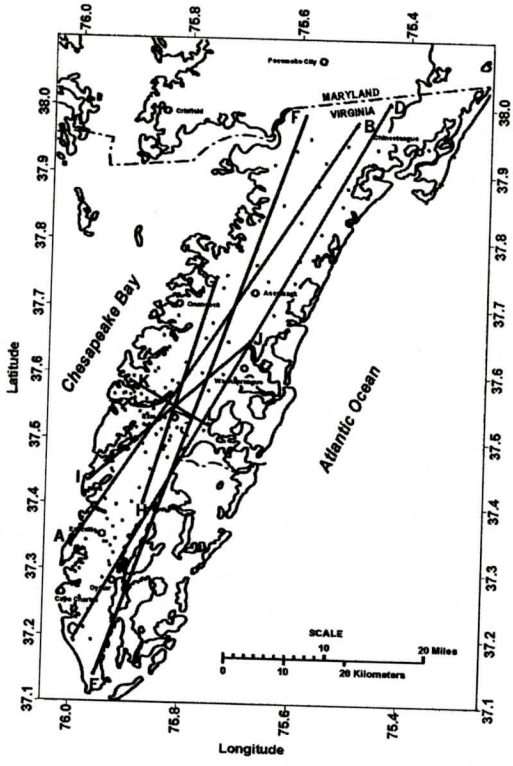

Figure 1. Map of the Eastern Shore of Virginia, indicating the central position for 136 Schlumberger soundings (crosses). Lines AB, CD, EF and others show the positions of profiles.

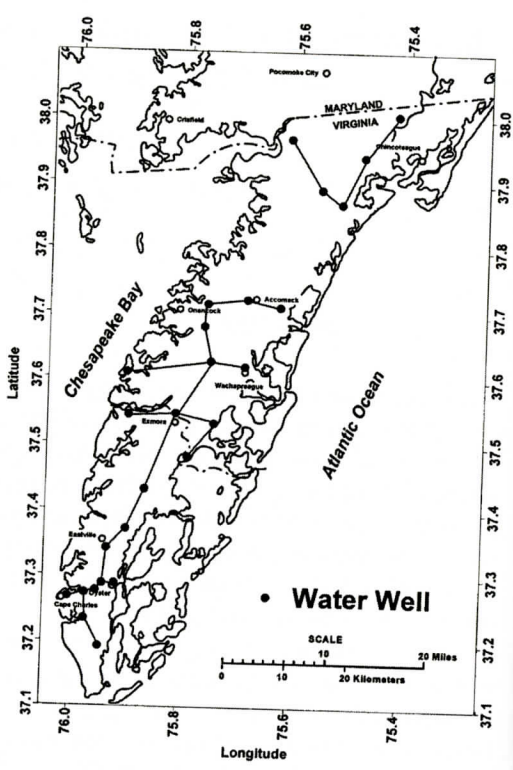

Figure 2. Solid circles show the position of the ground water research stations; each well may have up to six screens. Modified after Fennema and Newton 1982.

shows a nearly normal distribution with a mean porosity of about 36.22% and a mode of 40%.

Goff and others (2002) used extensive box coring and resistivity data from the Eel shelf (Northern California) in modeling two sites. They employed a 7-cm diameter tube core and high resolution Wenner-type resistivity probe to measure the formation factor (Andrews and Bennet, 1981; Wheatcroft and Borgeld, 2000) and employed Archie's equation (1942) to calculate porosity. They assumed that ionic composition and resistance of the bottom water and pore water are the same. Their data are also limited in depth from surface to 15 cm; based on their report, porosity shows a large variability with the mean porosity varying from about 55 to 70%.

In this paper we have assembled inversion results of Schlumberger field curves at 136 locations (Figure 1), and parameters of water quality from 96 screened-elevation wells in the water research stations across the Eastern Shore (Figure 2). Using Archie's equation we calculate porosity and other parameters up to a depth of 130 m.

GEOLOGY AND HYDROGEOLOGY OF THE AREA

Geology

The Eastern Shore is part of the Coastal Plain province of Virginia separating Chesapeake Bay from the Atlantic Ocean. The area is nearly flat with a maximum elevation of about 20 m. The stratigraphy of the area consists of consolidated and unconsolidated sediments of Cretaceous to Holocene age that gently dip and thicken eastward (Foyle and Oertel, 1992). Quaternary sediments unconformably overlay

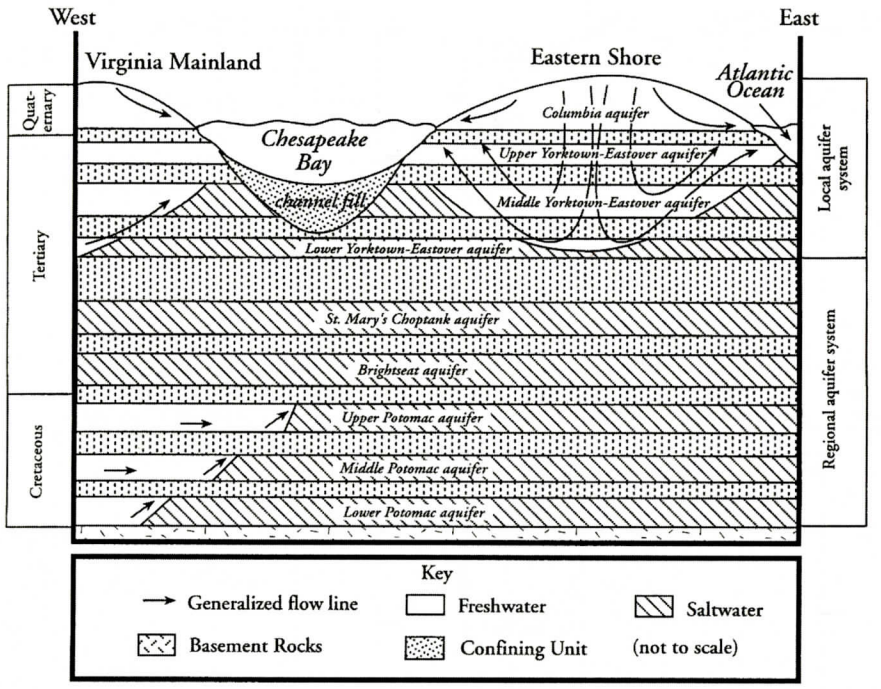

Figure 3. Schematic diagram of aquifers and generalized flow lines of the Eastern Shore from Richardson 1992. The Columbia, upper, middle and lower Yorktown-Eastover aquifers are main sources of freshwater on the Eastern Shore.

Tertiary glauconitic sand and silt that in turn overlies a basement of undifferentiated crystalline rocks of Precambrian to Jurassic age (Mixon, 1985). About 35.5 million years ago an astronomical body is believed to have impacted this area and formed the Chesapeake bolide structure. The impact center is near the city of Cape Charles in the Eastern Shore. The maximum relief of the faulted rim of the bolide structure is about 1.3 km and the thickness of sediments above the impact structure is 300 to 500 m (Poag, 1966). The structure is deeper than the zone of interest for this paper.

Hydrogeology

The study area has one unconfined and several confined aquifers. The near-surface Pleistocene Columbia aquifer is unconfined. The deepest, the Lower Potomac Aquifer, is Lower Cretaceous in age (Meng and Harsh, 1988; Richardson, 1992; Figure 3, this paper). The water quality measurements by Fennema and Newton (1982) are limited to the Pleistocene, and to Upper, Middle, and Lower Miocene strata. Therefore, our analysis is valid only for these units. They report that several wells reach to sediments of the Lower Miocene age at a depth of about 100 m. The Pleistocene aquifer consists of fine to medium sand, separated by layers of silt from underlying Miocene aquifers. The three Miocene aquifers consist of a combination of fine gravel, sand, silt, clay and shell fragments. Generally silt layers separate the Miocene aquifers from each other, but in some areas these units are not easily distinguished. The lithology varies laterally much more in the East-West direction than in the North-South direction. Using stream resistivity surveys in Delmarva coastal bays and analysis of core samples, Manheim and others (2002) discovered a large-scale submarine discharge distributed in the middle Delmarva coastal region to a depth of 30 m below the sea floor; they attributed this discharge to sharp changes in vertical lithology of coastal and submarine sediments.

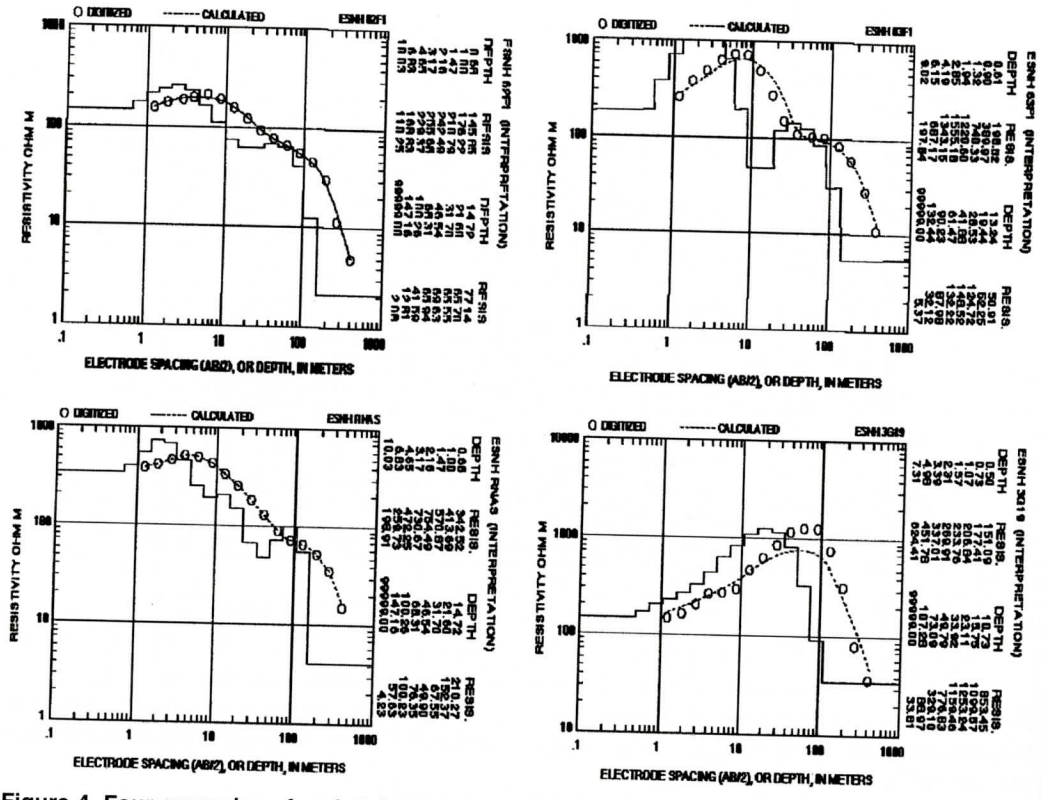

Figure 4. Four examples of resistivity field curves and their interpretation. Open circles are the digitized field curves; the staircase lines are the interpreted models, the dashed lines are the result of calculation for the given model. The results of interpretation are also presented.

FIELD WORK AND INTERPRETATION

Schlumberger Resistivity Soundings

The central positions of 136 Schlumberger resistivity soundings and the direction and length of several profiles are presented in Figure 1. The details of field methods and the inversion processes are explained in Nowroozi and others (1999 and 2003) and are not repeated here. Briefly, the AB/2 spacings are: 1, 2, 3, 5, 7, 10, 12, 16, 20, 24, 30, 40, 50, 60, 80, 100, 120, 150, 200, 250, and may even include some 300 and 400 m. The MN/2 spacing varies from 0.2 m to about 10 m, depending on the potential drop across the M and N electrodes. Always AB/2 was greater than 5 times MN/2; this is a recommendation for deployment of the Schlumberger arrays. The maximum current electrodes spacing employed in the field is sufficient for a penetration depth of 130 m or more.

Interpretation of Resistivity Field Curves

For interpretation of the field curves several programs were used (Zhdanov, and Keller, 1993, Interprex Limited 1999, Zohdy and Bisdorf 1989a and 1989b). For brevity, four field curves and their interpretations are presented in Figure 4. Assuming horizontal layering, the inversion process produces rock resistivity, or sediment resistivity, Rs, as function of layer thickness or depth, h. The results for all the soundings were put in the form of a large data matrix. The matrix has 15 columns, where the columns represented station number, station name, their latitude, longitude and resistivity at

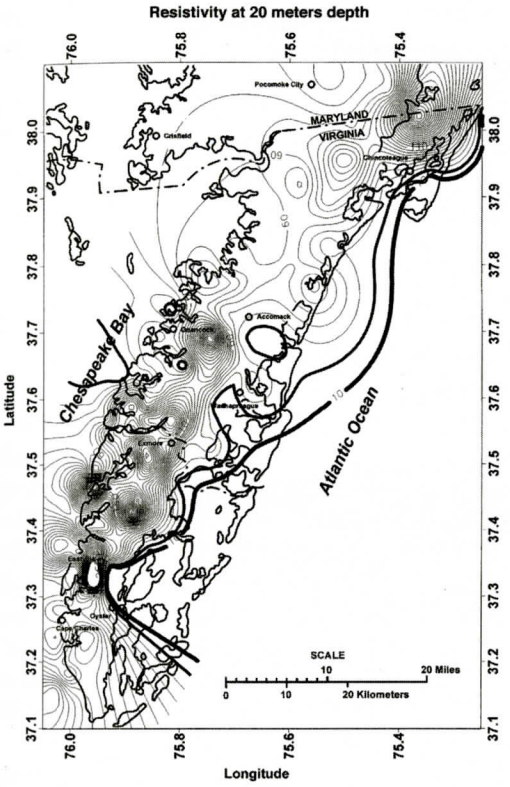

Figure 5. Resistivity map for 20 m depth; contour interval is 10 m. The 10 and 20 ohm –meter contour lines are presented by heavy lines. They may represent the interface between brine and fresh water.

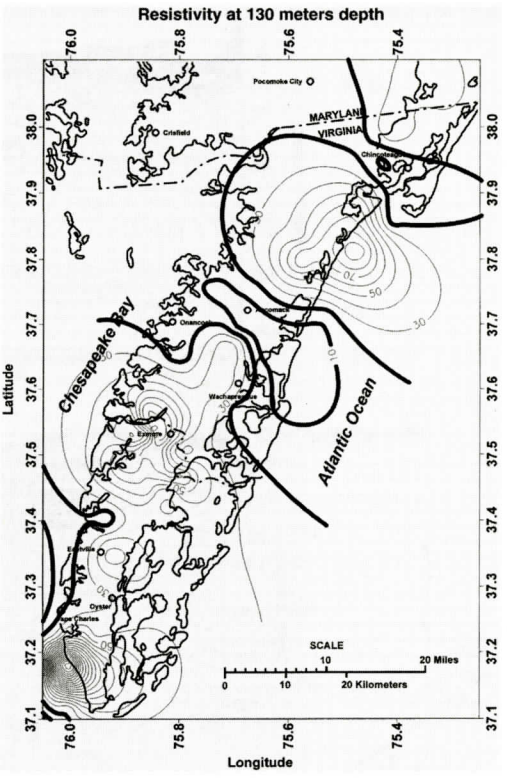

Figure 6. Resistivity map for 130 m depth; the contour interval is 10 -m. The 10 and 20 10 -m contour lines are presented by heavy lines. At this depth saltwater appears in the area of Wachapreague, Acomack, Onancook, Chincoteague and bay side of Eastville.

depth of 3, 5, 10, 20, 30, 40, 50, 60, 70, 100 and 130 m respectively. The rows of this matrix consist of information related to the 136 field stations. Contour maps of resistivity are produced at 11 depths, from 3 to 130 m. They may show the position of saltwater intrusion and paleochannels as discussed by Nowroozi and others (1999 and 2003). For example, Figure 5, and Figure 6 show resistivity maps at 20 and 130 m depths respectively. Heavy contour lines indicate the areas covered by resistivity values less than 20 Ωm. Most probably, they show the horizontal extent of brine water intrusion at these depths. In construction of resistivity profiles, sections are made from each map at various directions as shown in Figure 1. The sections are marked as AB CD, EF and others. The results are put in another large-grid data matrix. This matrix has latitude, longitude, resistivity and a constant depth for each crossing of the resistivity map. The Surfer program (Golden software, 1994, version 6) is used to create the grid matrix. It is also used for construction of the resistivity maps and profiles. Figure 7 shows the resistivity profiles along GH, IJ, and KL directions. Heavy lines mark the interpreted locations of the paleochannels; the brine water intrusions are marked by heavy dashed line.

On following pages, we present a procedure for calculation of porosity using the electric sounding method. In addition we display several porosity maps and porosity cross sections in the Eastern Shore. We use the average resistivity at each depth, resistivity maps, resistivity cross-sections, and water quality data reported by Fennema and Newton (1988) to present

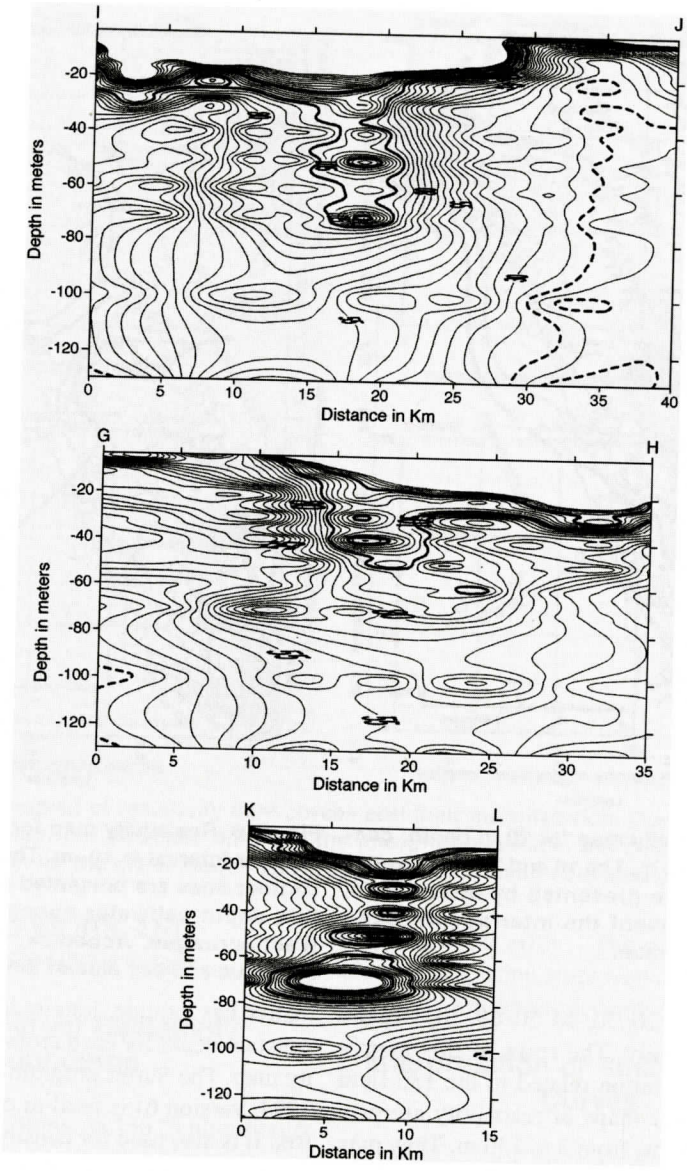

Figure 7. Resistivity profiles along IJ, GH, and KL directions. The dashed lines indicate resistivity contours with less than 20 Ω-m; they may represent the freshwater-brine water interface. The heavy solid lines indicate contour lines with resistivities of 100 to 130 Ω-m. They may indicate paleochannel boundaries.

these findings.

METHODS OF CALCULATION

Basic Data

Fennema and Newton (1982) present water quality measurements for 110 wells; however only 96 measurements include both conductivity and total dissolved solids. In addition to well numbers, each observation is identified by letters S, A, B, C, D and E. The letters refer to water-well screening classifications. They also provided the screen elevation. Screen S is in Pliocene, while Screen A is in Upper, B in Middle and C, D and E are in Lower Miocene strata.

Table 1: Mean value of conductivity in μS/cm, total dissolved solids in mgr/L and pore water resistivity in ohm – meter. The STD next to each column is the standard error of the mean for that parameter.

Screen Name	Depth	Con	STD	TDS	STD	Rw	STD
S	7.381	235.1	17.39	145.9	10.93	44.72	3.47
A	29.551	299.96	24.18	546.74	313.57	52.01	11.97
B	52.358	787.48	208.82	515.77	154.69	23.96	2.38
C	79.209	2520.74	539.31	3440.44	1794.87	15.50	3.07
D	71.065	983.86	59.00	580.67	63.76	10.24	0.62
E	77.470	893.50	12.50	481.00	15.00	11.19	0.16

Variability of the entire 96 data points is rather large, but a large variation in conductivity appears to be normal for the aquifers in the Coastal Plain of Virginia. More recent measurements also show large variation in water quality data; for example, Focazio and others (1993) reported 250 to 4380 μS/cm for conductivity in the Yorktown-Eastover aquifer. They also reported a range of 250 to 8000 and 171 to 10,200 μS/cm for other aquifers in the Coastal Plain.

Table 1 presents the means and standard error of the means (STD), for Con, TDS and Rw as a function of depth. We assume that these data are a good representative for the entire Eastern Shore, and develop functional relationships between depth and different parameters.

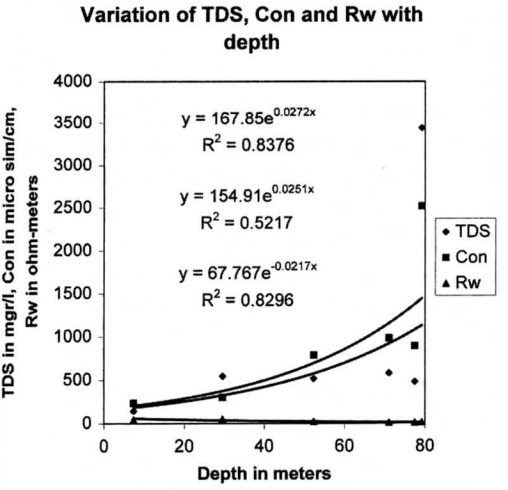

Figure 8. Variation of average total dissolved solid, TDS, Conductivity, Con, and pore water resistivity, Rw, with depth.

ANALYSIS OF WATER QUALITY DATA

General

Equation (1) presents an exponential relationship between conductivity and depth, h in meters.

$$Con = 167.85 * e^{-0.0272 * h} \quad (1)$$

The multiple correlation coefficients (R^2) for this relationship is 0.8376, this is corresponding to a correlation coefficient of 0.915, which is very satisfactory.

The pore water resistivity is given by, Rw = 10000 / Con, where resistivity is in Ω-m, and conductivity is in μS/cm. The relationship between Rw and h is:

$$Rw = 67.767 * e^{-0.0217 * h} \quad (2)$$

The value of multiple correlation coefficients is 0.8296 corresponding to a correlation coefficient of 0.911, which is again very satisfactory. The relation between total dissolved solids and depth is

$$TDS = 154.91 * e^{-0.0251 * h} \quad (3)$$

This relationship has a multiple correlation coefficient of 0.5217 corresponding to correlation coefficient of 0.72, which is acceptable. Figure 8 shows the plot of equation 1, 2 and 3 and the average parameters. Also, there is a linear relation between total dissolved solids and conduc-

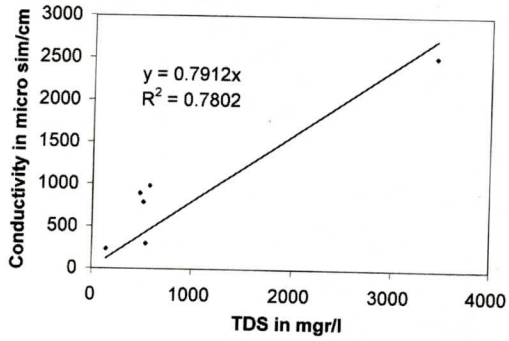

Figure 9. Linear relationship between pore water conductivity and total dissolved solids.

tivity in the form

$$Con=0.7921*TDS \quad (4)$$

This relationship, Figure 9, has a multiple correlation coefficient of 0.7802; this is equivalent to a correlation coefficient of 0.88. The experimental work of Greenberg and others (1980) also required a linear relationship between total dissolved solids and conductivity in the form of TDS= K*Con, where constant k varies between 0.98 and 0.55.

Calculation of Average Rock Resistivity

The rock resistivity was calculated from inversion of 136 field curves. The means of Rs for 136 inversion field curves at depth 3 to 130 were calculated. A power law best represents the variation of Rr with respective depth:

$$Rs = 902.46*h^{-0.6336} \quad (5)$$

Equation (5) has a multiple correlation coefficient of 0.9773. This corresponds to an excellent correlation coefficient of 0.989; a plot of the original data and equation 4 is shown in Figure 10.

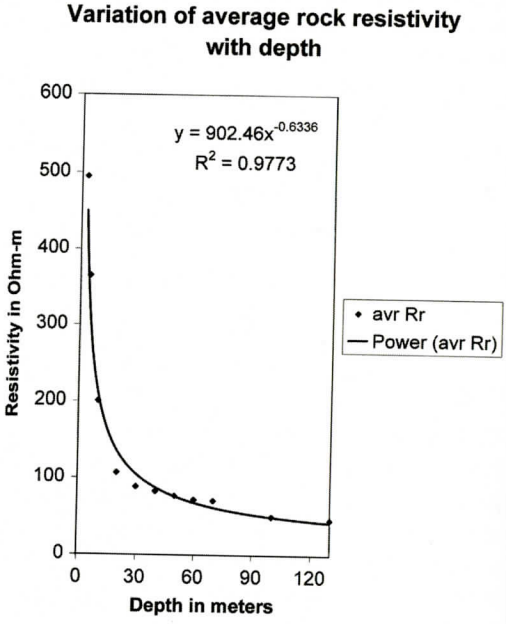

Figure 10. Variation of average rock resistivity, Rs, with depth.

RESISTIVITY FORMATION FACTOR AND POROSITY

Archie's Law

The conduction of electric current in saturated sediments and rock formation is mostly electrolytic and depends on pore water resistivity, Rw, rock resistivity Rs, and porosity, Φ. Equation (6) presented by Archie (1942) gives their relationship,

$$F = Rs / Rw = a *\Phi^{-m} \quad (6)$$

(See also Ward, 1990). In this equation F is known as the resistivity formation factor, while a, and m are constants related to rock type. The constant m is commonly known as the porosity exponent or cementation factor, and the constant a is the coefficient of saturation. The value of a is between 0.6 and 1.5, while the value of m falls between 1.6 and 3 (Sheriff, 1981).

Calculation of the Resistivity Formation Factor and Porosity

As the ratio of Rs / Rw is the resistivity formation factor, we obtain after substitution from equation 3 and 2:

$$F = Rs/Rw = (902.46*h^{-0.6336} / 67.767*e^{-0.0217*h}) \quad (7)$$

For sandy sediments similar to the formation in the Eastern Shore a = 0.62 and m =2.15 may be used. Archie's equation with these constants is

Table 2: The mean value of sediment resistivity, Rs, formation factor, F, porosity, ϕ, and the standard error of the means of each parameter are also presented.

Screen Name	Depth	Rr	STD	F	STD	ϕ	STD
S	7.381	341.96	31.39	8.60	2.14	33.91	2.97
A	29.551	175.32	43.94	4.58	0.81	50.48	4.88
B	52.358	79.26	4.98	5.6	1.36	44.51	2.49
C	79.209	57.31	1.22	14.09	2.94	37.23	4.16
D	71.065	60.56	0.00	5.96	0.36	34.99	0.99
E	77.470	57.34	0.00	5.12	0.072	37.44	0.24

known as Humble Formula (Schlumberger web site, 2004), and given by:

$$F = 0.62*\Phi^{-2.15} \quad (8)$$

This equation or its equivalent is applied for studies related to resistivity of brine- saturated sands in pore geometry (Winsauer and others (1952).

After substitution for F from equation 7 we can write

$$(902.46*h^{-0.6336} / 67.767*e^{-0.0217*h}) = 0.62*\Phi^{-2.15} \quad (9)$$

It is also possible to use either conductivity or total dissolved solids for calculation of Rw. Instead $Rw = 67.767*e^{-0.0217*h}$, it is possible to use Con directly, then

$$Rw = 10000 / 167.85*e^{-0.0272*h} \quad (10)$$

In Equation 10, the constant 10000 is introduced to change the units of µS/cm to Ωm. Then Equation 9 changes to

$$(902.46*h^{-0.6336}*167.85*e^{-0.0272*h})/10000=0.62*\Phi^{-2.15} \quad (11)$$

The value of Rw may also be calculated by using total dissolved solids. Using equation 4 and 10 it follows that

$$Rw = 10000/0.7912*TDS = 10000/ 0.792*154.91*e^{-0.0251*h} \quad (12)$$

After substitution, it follows that

$$(902.46* h^{-0.6336}*0.792*154.91* e^{-0.0251* h}) / 10000 = 0.62*\Phi^{-2.15} \quad (13)$$

In equations 7, and left side of equations 11 and 13 all the coefficients are known. Thus, for any value of depth h, the equations give the resistivity formation factor. Also, as left sides of equations 9, 11, and 13 are known; thus, for any given depth h the equations give the porosity. We will see later that the value of porosity does not change more than 2% between calculation based on the resistivity formation factors obtained from Rw, Con or TDS.

The Humble equation has a range of applicability (Winsauer and others (1952); Schlumberger web-site 2004). The equation gives a porosity of 100% if F = Rs/Rw = 0.62. For smaller value of F it will give a porosity value that is erroneously higher than 100%. In few cases when Rs< 0.62*Rw, the calculated porosity was abnormally high. These cases were isolated and discarded. However, when Rs > 0.62*Rw porosity is under 100%. For example for resistivity formation factor of 0.7, 1.0, 4.3 and 60.0, the porosities are 94.5%, 80.06%, 40.63% and 11.92% respectively. The first two cases may result from clay layer saturated with salt water. The last two cases may result from sandy strata saturated with fresh water.

Table 2 presents the values of Rs, F and Φ, and their standard errors of the mean. Figure 11 presents variations in pore water resistivity, resistivity formation factor, and porosity with depth. In this Figure, the equations 2, 5, 6 and 9 are used for calculations of the pore water resistivity, sediment resistivity, formation factor, and porosity, respectively. Depth varies from surface to 130 m in 5-m intervals. These parameters at the screen positions are also plotted. The agreement appears very good.

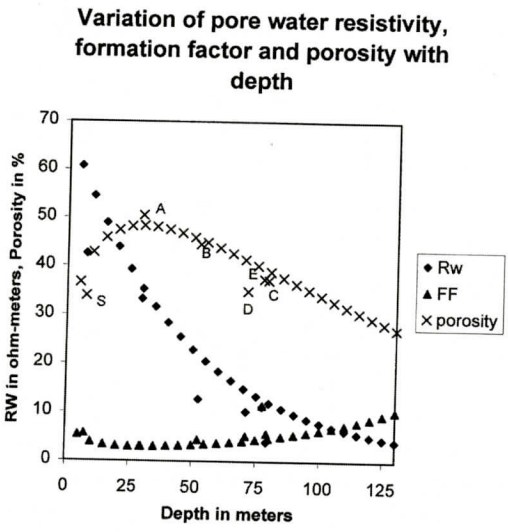

Figure 11. Variation of pore water resistivity, resistivity formation factor and porosity with depth. These parameters at positions of screen S, A, B, C, D and E are also plotted.

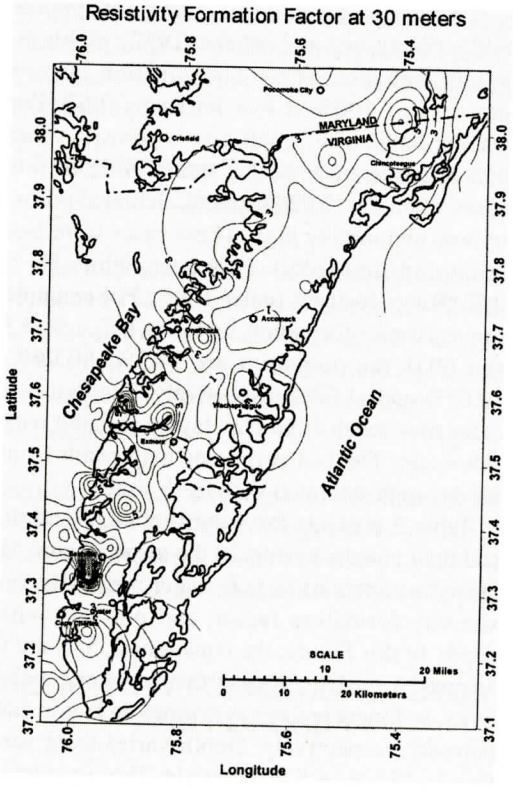

Figure 12. Variation of formation factor at a depth of 30 m.

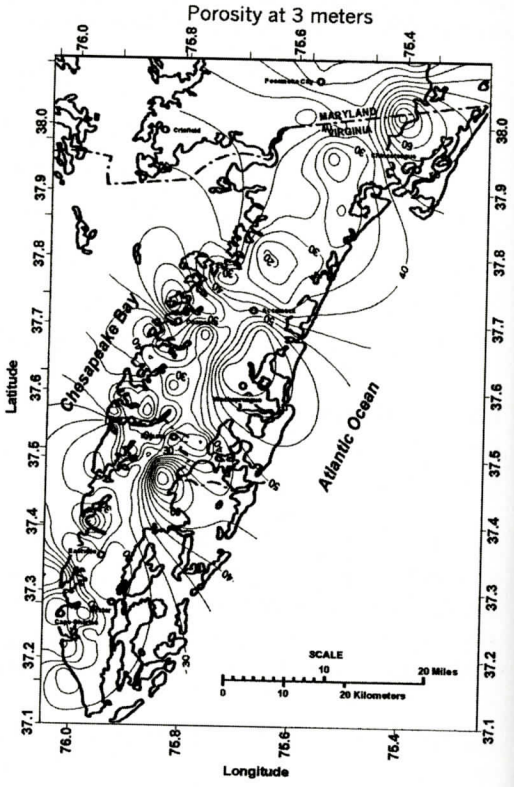

Figure 13. Porosity map at 3 m depth. Porosity values are in%.

CONSTRUCTION OF MAPS

Map of Resistivity Formation Factor

Rock resistivity has been calculated for depths of 3 to 130 meters at each field station; thus the numerical value of Rs is known as a function of latitude, longitude and depth. The Surfer program was used to construct the resistivity map. Two examples of resistivity maps are presented in Figure 5 and 6. Equation 2 provides the pore water resistivity, Rw, for each depth. Thus, the numerical value of resistivity formation F = (Rs/Rw) was calculated as a function of depth, latitude and longitude. As an example, Figure 12 presents the resistivity formation factor at a depth of 30 meters.

Porosity map

When the numerical value of the resistivity

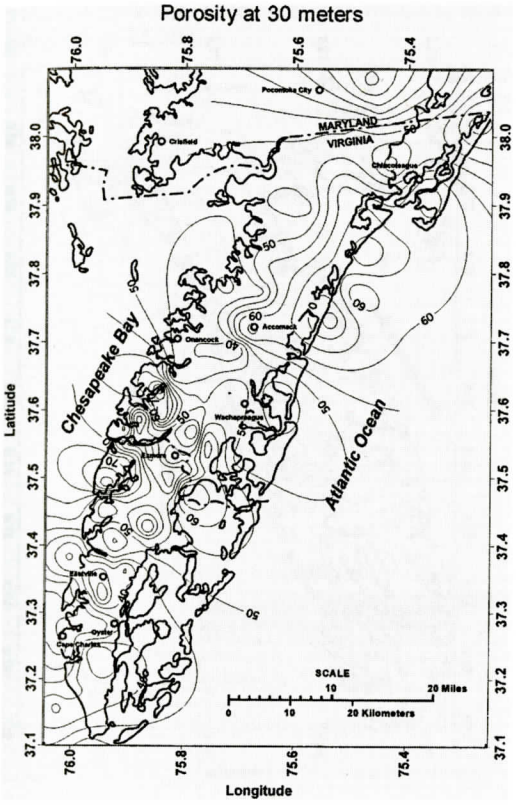

Figure 14. Porosity map at 30 m depth. Porosity values are in%.

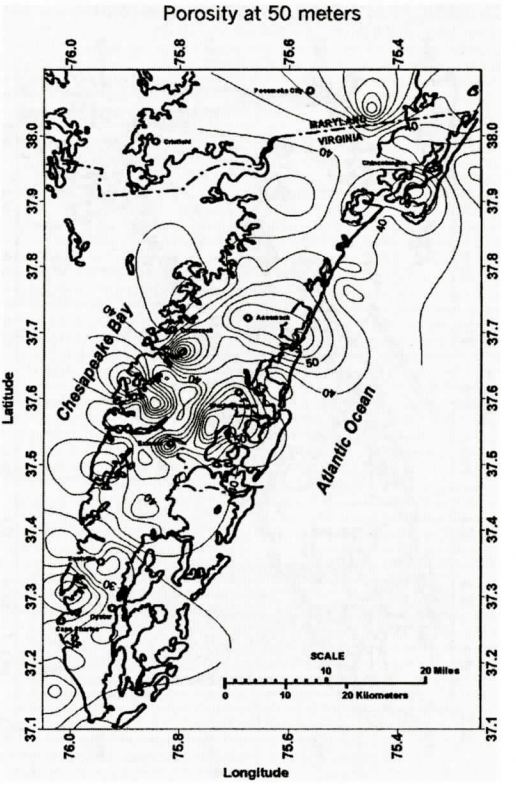

Figure. 15. Porosity map at 50 m depth. Porosity values are in%.

formation factor is available, then the Humble Equation 7 was used to calculate the porosity. For each map, the equation may give the porosity in the range 0f 0.10 to about 0.85; we have multiplied each value by 100 to present the porosity value in percentages. Although the 11 porosity maps are constructed for depths of 3 to 130 m, we only present the porosity maps at 3, 30, 50, 70 and 130- meter depths in Figures 13, 14, 15, 16 and 17 respectively. A comparison between porosity maps shows considerable variation vertically and horizontally from map to map. The average value of porosity and porosity plus and minus one standard deviation for the eleven porosity maps as a function of depth is presented in Figure 18. Table 3 presents the depth and the variation of average porosity, standard deviation of mean, minimum, maximum and the number of grid points. The average porosity shows a smooth variation with depth. Its value varies from 23.07 to 51.43%, with a range of 8.6% to 89.61%. Figure 18 shows the vertical variation of porosity with depth. A broad higher value of 51.43, 49.96, and 46.74% at depths between 20 to 40 meters depths is noted. The broad higher porosity value may be due to contribution of profiles in the paleochannels (Nowroozi and others (2003).

CONSTRUCTION OF PROFILES

Profile of Resistivity Formation Factor

We have used the grid matrix for resistivity profiles and Equation 2 for calculation of the resistivity formation factor. Each grid point has latitude, longitude, depth and sediment resistivity, Rs. Equation 2 provides the pore water resistivity, Rw. Thus the resistivity formation factor F = (Rs/Rw) is known and the profile of resistivity formation factor is easily constructed.

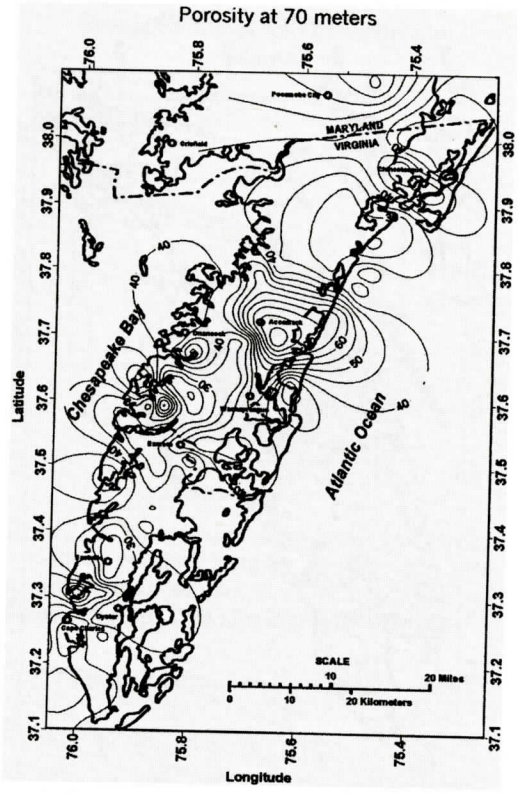

Figure. 16. Porosity map at 70 m depth. Porosity values are in%.

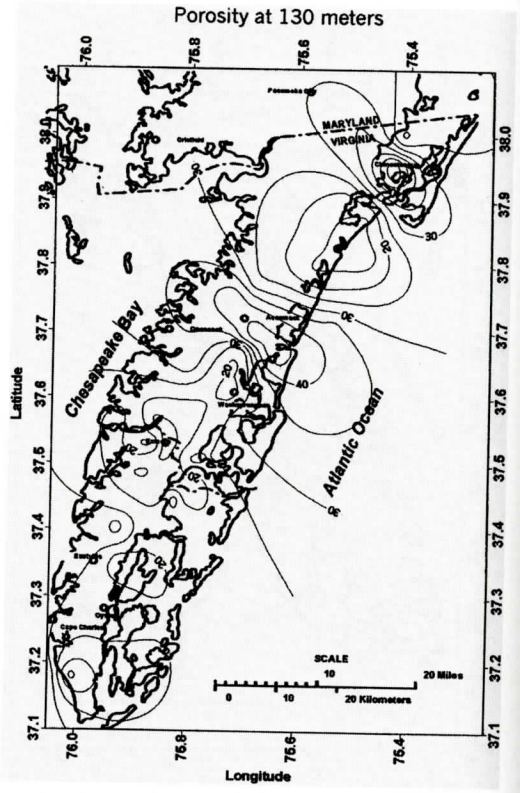

Figure. 17. Porosity map at 130 m depth. Porosity values are in%.

Construction of Porosity Profiles

When the resistivity formation factor at each grid point is calculated then Equation 8 is used to calculate the porosity at that point. After calculation of porosity at all grid points, then porosity profiles are constructed. The direction and length of resistivity profiles are presented in Figure 1. Because the other profiles are based on the resistivity profiles, the length and the direction of profiles for the resistivity formation factors and the porosity profiles are identical. Figure 19 has four panels and presents resistivity profile, pore water profile, resistivity formation factor and porosity profile along section IJ. We have assumed that, the average value is valid for the entire Eastern Shore; thus, the pore water resistivity is constant at each depth. This assumption is reasonable, because Equation 2 is derived from a large number of water quality data from wells that are distributed across this

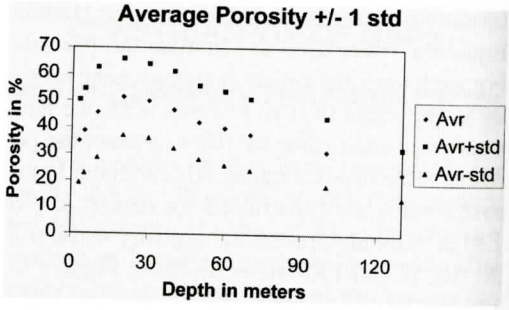

Figure 18. Variations of average porosity across eleven maps as a function of depth, the mean porosity plus and minus one standard deviation are also plotted. Thus, 68% of calculated porosities are within the upper and the lower plots.

area. The longest porosity profiles are presented in Figure 20. They are profiles AB, CD, EF and MN, respectively. They cover the length of the Eastern Shore; their directions are a few degrees east of the north. Figure 21 presents the

Table 3: Variation of the average porosity and other parameters with depth. The grand mean of porosity is 41.15%.

Depth, m	Average porosity in%	Standard deviation of mean	Minimum porosity	Maximum porosity	Grid points
3	34.78	15.59	12.93	88.69	127
5	38.62	15.89	12.51	83.71	127
10	45.56	17.0	17.9	89.61	123
20	51.43	14.44	14.48	89.43	119
30	49.96	13.98	13.36	86.30	122
40	46.74	14.53	14.32	89.80	124
50	41.03	13.87	19.03	85.40	124
60	39.85	13.89	16.91	85.86	123
70	37.52	13.43	12.74	84.78	116
100	31.21	12.73	12.25	85.80	76
130	23.07	9.33	8.63	58.07	65

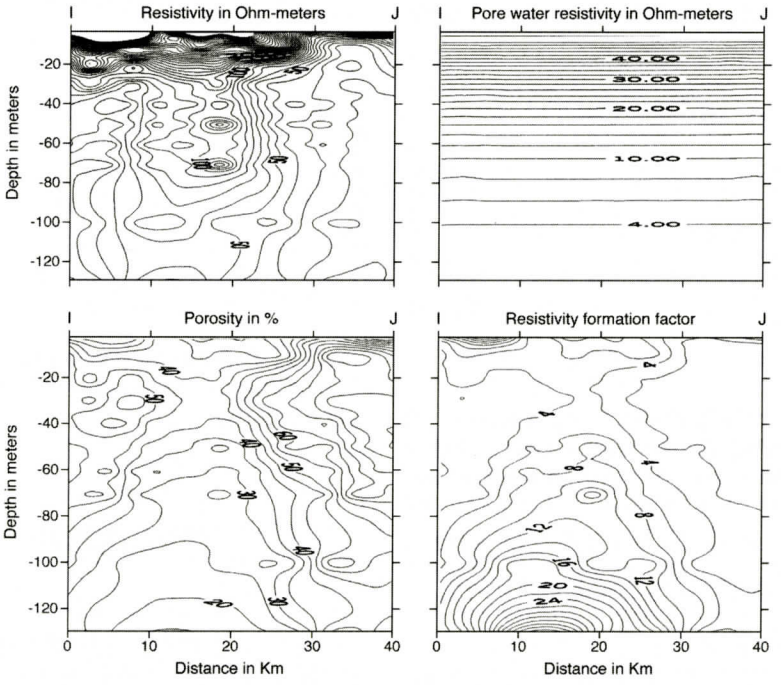

Figure 19. Rock resistivity profile, the pore water resistivity profile, the profile of resistivity formation factor and the porosity profile along IJ direction. Because average pore water resistivity is assumed to be the same across the Eastern Shore, the pore water resistivity map does not show any horizontal variation.

shorter profiles along different directions in the middle area of the Eastern shore. They are profiles GH, KL, and I-Oyster, respectively. Their length is measured in 100 m or 0.1 km. The pattern of porosity distribution varies between and within each profile as is evident from comparison between Figure 20 and 21.

A recalculation of porosity based on Equations 9, 11 and 13 for profile I-Oyster is given in Figure 22. The calculation is based on total

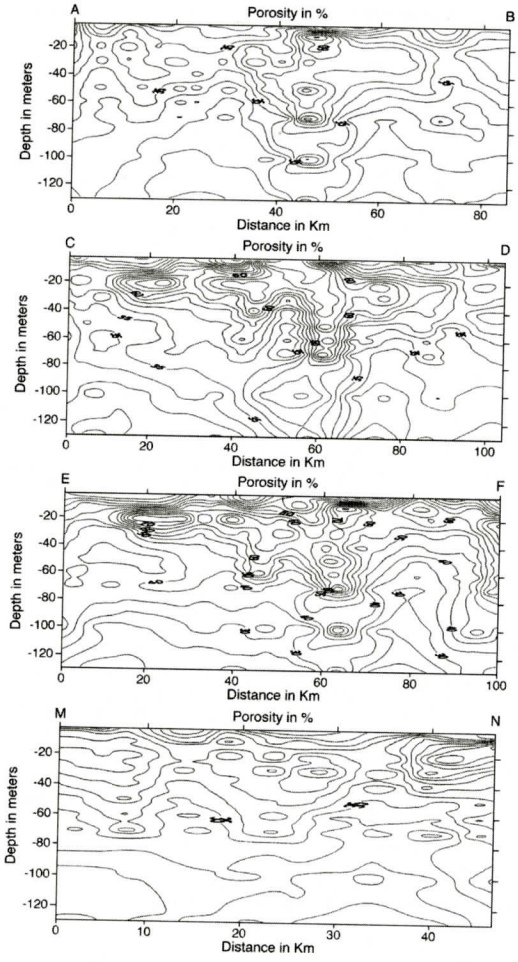

Figure 20. Porosity profile along direction AB, CD, EF, and MN. The horizontal scale is in Km. Porosity values are in%. The direction of profiles is shown in Figure 1.

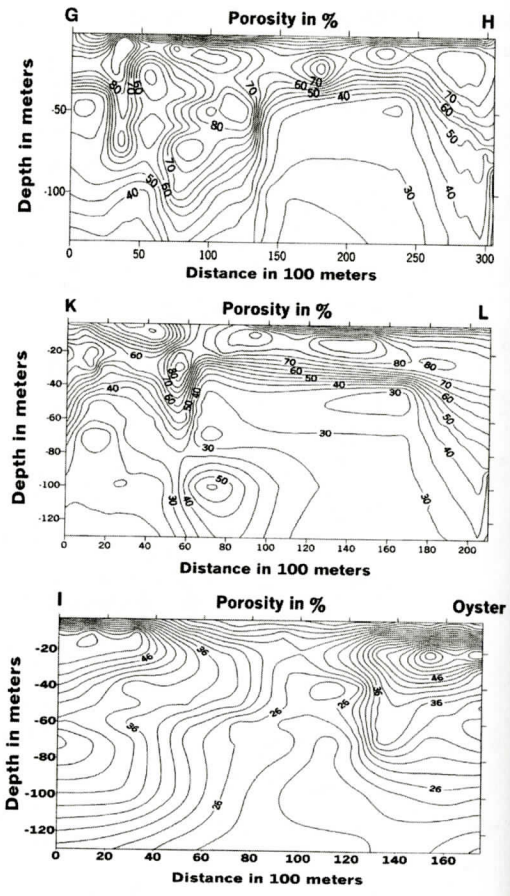

Figure 21. Porosity profiles along direction GH, KL, and I-Oyster. The horizontal scale is in 100 m or 0.1 of Km.

dissolved solid, pore water resistivity and conductivity. As expected the TDS, Rw and Con have only vertical variations with depth, h. A visual inspection of porosity distribution shows that the three profiles show nearly the same pattern especially at depths shallower than 30 m. A plot of porosity based on TDS and Rw is presented in Figure 23. This plot shows a very good correspondence between the two methods of calculation and yields a multiple correlation coefficients of 0.9618. This value corresponds to a correlation coefficient of 0.98071. Thus, the two porosity estimations are differing by less than 2%.

DISCUSSION

Porosity is an important physical property of soil sediments and rock formations. Porosity can be calculated from a sample by measurements of wet and dry masses, grain and fluid density and saturation coefficient (Henry, 1997). For sedimentary rocks, its value depends on rock type, grain size, compaction, cementation, sediment packing, composition, clay content, and geological history of the rock formation. The amount of water bounded to clay particles in sediments is an important parameter for evaluation of porosity. Henry (1997) discussed a correlation between the total

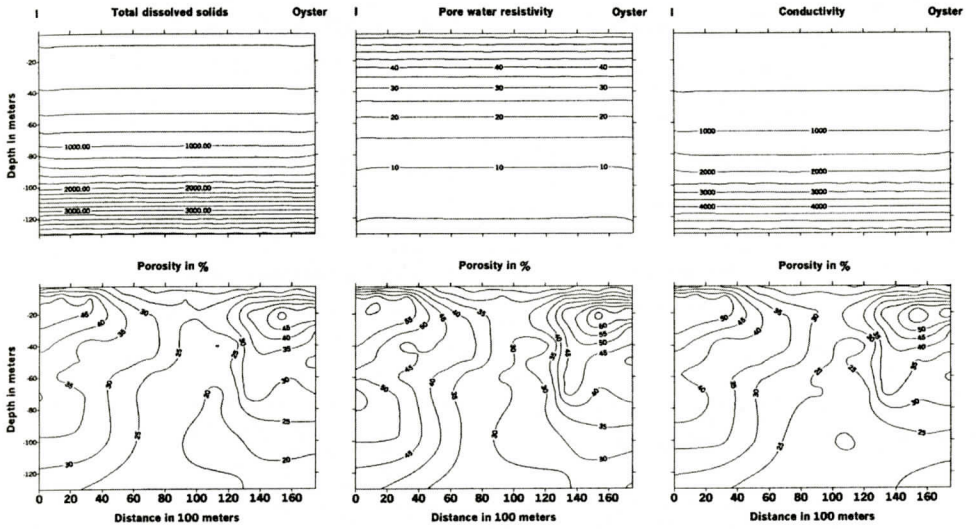

Figure 22. Recalculation of porosity using total dissolved solids, pore water conductivity and pore water resistivity. A comparison between the results of calculations shows that the patterns and distributions of porosity are nearly the same.

water content of the samples and their cation-exchange capacity. He also reported that smectites strongly influence the ability of the sediments to retain both absorbed and pore water. In this work, no sediment samples were available for laboratory examination. Thus, cation exchange capacity, measurement of wet and dry masses, grain and fluid density and saturation coefficient were not measured. It is known however, that wet clay has relatively high electric conductivity; also conductivities have implication for migration of chemical elements (Manheim and Waterman, 1974). Thus, our calculation of porosity may show considerable range of values within each profile and across them due to lithology of sediments and its clay content.

Based on geometry and, assuming spherical grains for a sedimentary rock, porosity for cubical packing is 47.65%, but for rhombohedral packing it is 25.95%. However, a mixture of large and small grain sediments sorting may have smaller values of porosity. Porosity of clean sand may rise to 50%, and that of clay may reach as high as 80% (Fetter, 1980). The large range of variations (15 to 85 per cent) in calculated porosity is very probably the results of different clay content or sediment sorting.

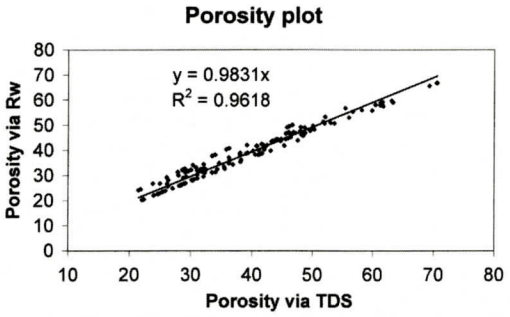

Figure 23. Porosity based on pore water resistivity and porosity based on total dissolved solids. If the values were identical the coefficient of X would have been 1; but it is 0.9831. This is a good indication that the difference between two methods of calculation is less than 2%.

Published measurements of porosity for the Eastern Shore of Virginia are limited. However, in the vicinity of the town of Oyster, Swift (2003) reported over 700 laboratory measurements. This data set is for a depth range of surface to 10 m. Figure 24 shows eight observed distributions reported by Swift (2003) and calculations for profile I-Oyster. The left hand four distributions are from Swift (2003); the top three are individual samples; the last is the distribution for the total samples. It is clear that the

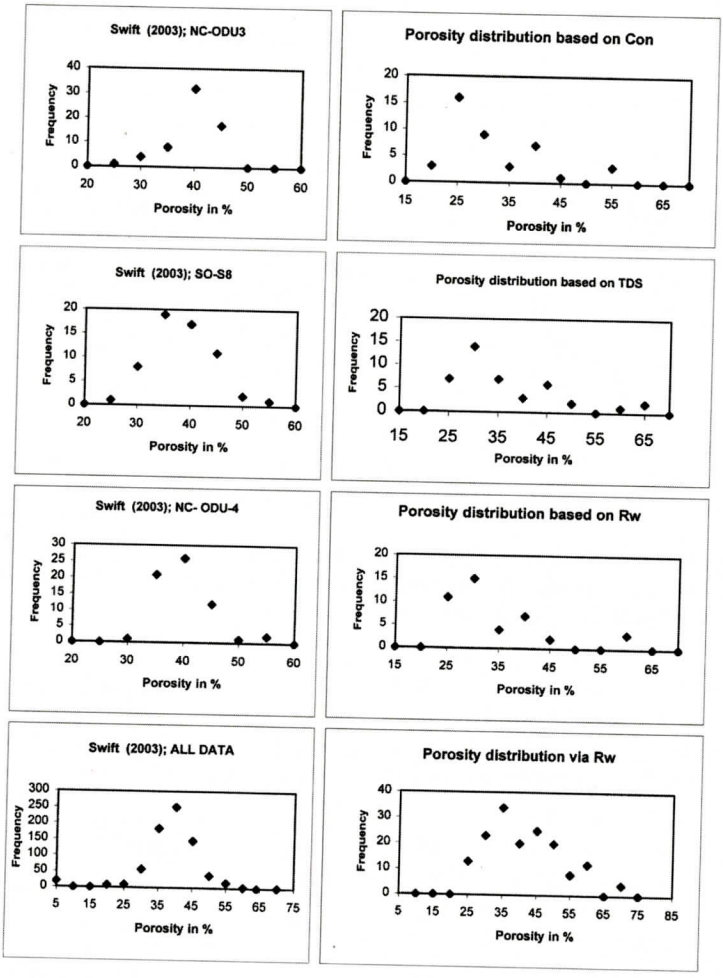

Figure 24. Variability of porosities. Samples NC-ODU3, SO-S8 and NC-ODU4 are measured by Swift and Others, in the vicinity of Oyster in the Eastern Shore. The depth range is from surface to 10 m. The variation of over 700 samples is also presented as ALL DATA. The variability of porosity for profile I-oyster is presented on the right side. The first upper three panels are from surface to 10 m depth. They are calculated based on pore water conductivity, total dissolved solids and pore water resistivity. The last panel shows the distribution for this profile from surface to depth of 130 m. All Data have a mean of 36.22%; calculations for the entire depth range of surface to 130 m show a mean of 38.86%.

distribution varies from sample to sample, but all three samples show a maximum frequency of 35 to 40%; the entire sample, over 700 estimations, indicates a mode of 40% and a mean of 36.22%. The right hand four distributions are along the I-Oyster profiles. The first three distributions are from surface to a depth of 10 m, using Con, TDS and Rw respectively. The last distribution is based on Rw and covers the depth of surface to 130 m. A direct comparison between the left hand panels and the right hand panels is not valid, because Swift's measurements are limited only to vicinity of Oyster. Our calculations are for a profile that is ending at Oyster but it is about 17 km long. It appears that for this profile the mode of porosity calculation in this paper is slightly smaller than the mode of measurements by Swift. However, his measurements are based on core samples. This type of measurement gives the ratio of pore volume to

Table 4: The variation of calculated porosity along various profiles.

Profile	Porosity in%	Standard Deviation	Maximum in%	Minimum in%	Grid points
AB	44.47	14.06	17.9	95	763
CD	39.55	14.5	11.5	83.5	856
EF	42.39	15.14	15.5	83.9	778
GH	51.77	18.58	22.5	89.3	312
IJ	42.96	16.61	14.3	87.1	394
KL	39.27	15.76	14.1	80.3	155
MN	38.62	13.69	13.0	95.1	390
I-Oyster	31.96	9.34	17.3	57.6	160

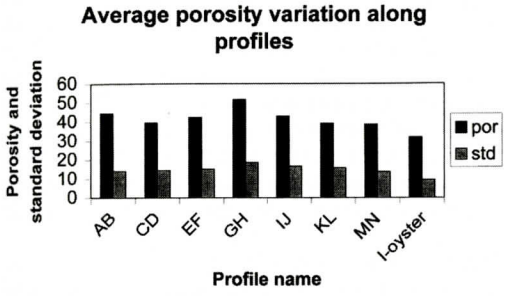

Figure 25. Variation of average porosity and standard deviation of the mean along the eight profiles.

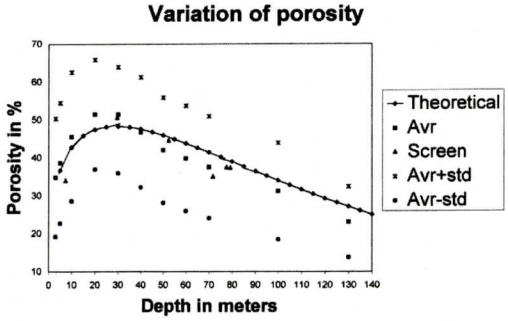

Figure 26. Theoretical calculation of porosity with depth based on equation 9, the average value of eleven porosity maps, and the mean and standard deviation of porosity at the six screen levels.

total volume but measurements based on electric survey give the porosity along the current line over the entire path; thus, a small difference should be expected.

An attempt was made to see the variation of average porosity across various profiles. Table 4 gives profile names, standard deviation of the mean, minimum, maximum porosity and the number of observations or grid points along each profile. Figure 25 shows the graphical plot of this variation. The average values vary from about 51.77% to 31.96%; however, Table 4 gives a grand mean of about 42.06%. The grand mean of porosity in Table 3 is 41.15%. Thus, it appears that the grand mean of the porosity across eleven depths is the same as that across eight profiles.

CONCLUSIONS

We have used water quality data and the results of Schlumberger electric soundings to estimate porosity. The relationships between porosity and depth are given by equations 9, 11 and 13. Results obtained by the equations are consistent.

Figure 26 summarizes the porosity results presented in Tables 2 and 3 and theoretical calculations of porosity based on equation 9. Porosity is shown to a depth of 130 m at 5-meter intervals. The average porosity across eleven porosity maps, the average plus and minus one standard deviation of the mean and the porosity at the six screen levels are also plotted. The average porosity varies from 23.03% at a depth of 130 m to a value of 51.43% at a depth of 20 m, falling to 34.78% at a depth of three m. The grand mean of the average porosity at all depths is 41.15 per cent. Porosity at the screen levels varies from 33.91% at a depth of about 7.4 m to a maximum of 50.48% at a depth of 29.6 m and falling to 37.23% at a depth of 79.2 m. The grand mean of porosity at the six screen levels

is 39.74%. The average porosity values are slightly above the theoretical values from surface to about 30 m; then are slightly under the theoretical values from 50 m depth onward. The difference may indicate a systematic anisotropy of porosity in the eleven horizontal planes. The azimuthally variations of the porosities are presented in Figure 25; however, it appears that the mean of porosities is the same as in the vertical direction. The average porosity along eight vertical profiles with differing directions varies from 31.95% to 51.77%. This shows the azimuthally variation of the porosity perhaps due to sediments sorting and its clay content. The average grand mean for all the profiles is 42.05%. This is very close to the average mean of 41.15 at all depths and the grand mean of 39.74% at the screen levels. Swift (2003) made over 700 estimates between surface and a depth of 10 m; their data has a mean of 36.22%. This is very close to our estimate of 34.78% at a depth of 3 m and 33.91% at a depth of 7.4 m. Thus, although there is a variation of average porosity with depth, no significant variation in horizontal directions is observed.

In this study, we have synthesized all available data in order to provide a model of the distribution of porosity in the shallow aquifers of the Eastern Shore. Although the variation in data is considerable, we were able to develop a functional relationship between pore water conductivity, pore water resistivity, sediment resistivity, resistivity formation factor and porosity with depth. This is essential for ground water flow modeling and solute transport.

ACKNOWLEDGMENTS

This research was supported in part by a seed grant from the Virginia Water Resources Research Center, and in part by grant ER62478-1010025-0001649 from the Subsurface Science Program, Department of Energy.

REFERENCES CITED

Andrews, D., Bennett, A., 1981, Measurement of diffusitivity near the sediment-water interface with a fine-scale resistivity probe: Geochimica Acta v. 45, p. 2169-2175

Archie, G. E., 1942. The electric resistivity log as an aid in determining some reservoir characteristics: Trans. Am. Inst. Min. Metal, and Pet. Eng., v. 146, p. 54-62.

Fennema, R.J., Newton, V.P., 1982, Ground Water Resources of the Eastern Shore of Virginia: Commonwealth of Virginia, State Water Control Board, Richmond, Virginia, Planning Bulletin 332, 74 p.

Fetter, C. W., 1988, Applied Hydrogeology: Merrill Publishing Company: Columbus, Toronto, London, Melbourne, 591 p.

Focazio, Michael J., Seperian, Gary K. and Rowan M, E., 1993, Quality of ground water in the coastal plain physiographic provinces of Virginia. U.S. Geological Survey. Water-Resources Investigations Report 92-4175, 223 p.

Foyle, A.M. and Oertel, G.F., 1992, Seismic stratigraphy and coastal drainage patterns in the Quaternary section of the Southern Delmarva Peninsula, Virginia, USA. Sedimentary Geology, v. 80 p. 261-277.

Golden Software, 1994. Surfer for Windows: Contouring and Mapping. Golden, CO.

Goff, A. John, Wheatcroft, R. A., Lee H., Drake, D. E., Swift, D. J. P. and Fan S., 2002, Spatial variability of shelf sediments in the Strataform natural laboratory, Northern California: Continental shelf Research v, 22, p. 1199-1223.

Greenberg, A. E., Connors, J., and Jenkins, D., 1980, Standard methods for the examination of water and wastewater: American Public Health Association, Washington, DC 20006, and p. 1134.

Henry, P, 1997, Relationship between porosity, electric conductivity and cation exchange capacity in Barbados wedge sediments: *in* Shipley, T. H., Ogawa, Y., Blum, P. and Bahr, J. M., eds., Proceeding of the Ocean Drilling Program, Scientific Results: V. 156, p. 138-149.

Interprex Limited, 1999, RESIX-IP Volume 2, User's manual DC resistivity and induced Polarization Data interpretation Software P.O. Box 839 Golden Colorado 80402-0839.

Meng, A. A. III, and Harsh, J. F. 1988, Hydrologic framework of the Virginia Coastal Plain: U.S. Geological Survey Professional Paper 1404-C. 82p.

Manheim, F.T., Krantz, D. E., Snyder, D. S. and Sturgis, B., 2002, Stream resistivity survey in Delmarva Coastal Bay. Proceeding symposium on the application of Geophysics to environmental and engineering problem SAGEEP). P. 17.

Manheim F. and Waterman, L. S., 1974, Diffusimetry (diffusion constant estimation) on sediments cores by resistivity probe: in von der Boch, C. C. Sclater, J. G. and others Init. Rep. DSDP, 22: Washington, D. C. (U. S. Government Printing Office) p. 660-670.

Mixon, R.B., 1985, Stratigraphic and geomorphic framework of uppermost Cenozoic deposits in the southern Delmarva Peninsula, Virginia and Maryland. U.S. Geological Survey Professional Paper 1067-G, 53 p.

Nowroozi, Ali A., Horrocks, S.B., and Henderson, P.N., 1999, Saltwater intrusion into the freshwater aquifer in the Eastern Shore of Virginia: A reconnaissance electri-

cal resistivity survey. Journal of Applied Geophysics: v. 42, p. 1-22.

Nowroozi, Ali A., Karst, Adam T, and Henderson, Peter N, 2003, Paleochannels and water resources of the Eastern Shore of Virginia: A case study by electric resistivity methods Southeastern Geology: 41,No 4 177-199.

Poag, C.W., 1996, Structural outer rim of Chesapeake Bay impact crater: seismic and borehole evidence. Meteoritics & Planetary Sciences 31,218-226.

Richardson, D.L. 1992). Hydrogeology and Analysis of the Ground-Water Flow System of the Eastern Shore, Virginia. U.S.G.S. Open-file report 91-490, 119 p.

Sheriff, R. F 1981, encyclopedic dictionary of exploration geophysics. Society of Exploration geophysicists, Tulsa Oklahoma, 268p.

Swift, Donald P. 2003, Web Page, Old Dominion University; http://sediment.odu.edu: 8050/

Schlumberger Oilfield Glossary; Web- Page 2004, http://www.glossary.oilfield.slb.com

Ward, S.H., 1990, Geotechnical and Environmental Geophysics v. 1: review and tutorial. Society of Exploration Geophysicists, p. 147-189.

Wheatcroft, R.A and Borgeld 2000, Oceanic flood deposits on the northern California shelf: large-scale distribution and small-scale physical properties. Continental Shelf Research 20. 2163-2190.

Winsauer, W.O., Shearin H. M., Masson P.H. and Williams M. 1952, Resistivity of Brine- saturated sands in relation to pore geometry. American Association of Petroleum Geologists Bulletin 253-377.

Zhdanov, M.S. and Keller, G.V., 1994, The Geo-electric Method in Geophysical Exploration: Elsevier, Amsterdam, the Netherlands, Methods in Geochemistry and Geophysics V 31. 884 p.

Zohdy, A.A.R., 1989, a new method for the automatic interpretation of Schlumberger and Wenner sounding curves. Geophysics, **v.** 54 p. 245-253.

Zohdy, A.A.R., and Bisdorf, R.J., 1989, Programs for the Automatic Processing and Interpretation of Schlumberger Sounding Curves in QuickBasic 4.0. USGS Open-File Report 89-137 A.

SOUTHEASTERN GEOLOGY
V. 43, No. 4, June 2005, p. 193-214

SPECULATIONS REGARDING THE SUBSURFACE GEOMETRY OF THE ELBERTON GRANITE FROM SPARSE WIDE-ANGLE REFLECTION DATA

MOHAMED O. KHALIFA

Department of Geology
South Valley University
Qena, Egypt

ROBERT B. HAWMAN

Department of Geology
University of Georgia
Athens, GA 30605

ABSTRACT

This pilot study used wide-angle seismic reflections to investigate the tectonic relationship between the Elberton granite and surrounding rocks. The principal goal of the study was to image the base of the granite. In contrast with previous COCORP normal-incidence profiles in the region, field experiments for this study were designed to image the uppermost 12 km of the crust. Shot-receiver offsets were chosen to avoid interference with shear waves and to take advantage of the increase in reflection coefficients near the critical angle to image relatively subtle contrasts in acoustic impedance between the Elberton and underlying gneisses. Seismic sources were timed, instantaneous blasts at dimension-stone quarries. These were recorded with a portable array of 19 three-component seismographs. Receiver spacings of 50 m yielded recording apertures of about 1 km for each blast; nine blasts were recorded, with source-receiver distances ranging from 7.8 to 23.4 km. Shot gathers for five of the blasts (7.8-14.9 km) show coherent signals arriving shortly after the direct P wave that are interpreted as postcritical reflections from a layered complex. Although the data coverage is very sparse, the migrated events consistently appear with small apparent dip at depths between two and four km. Corresponding zero-offset travel times are similar to travel times for scattered reflections recovered from reprocessed COCORP data. The wide-angle data extend those observations along strike, 5 km to the southwest and 20 km to the northeast of the COCORP line. It is suggested that the layered complex is laterally continuous and that it marks the base of the granite. The granite itself appears to be 2-3 km thick; this is underlain by 1-2 km of layered rocks. Possible interpretations of this layering include migmatites, mafic cumulates, or a mylonitic shear zone at the base of the granite possibly formed during late Alleghanian thrusting. The migrated sections also show southeast-dipping reflectors that span a depth of 5-10 km and that correlate with previously reported southeast-dipping events in COCORP lines. The transition from horizontal to dipping reflections beneath the Elberton granite supports the hypothesis that the granite is a tabular body that does not extend deeper than 2-3 km. A high-amplitude, well resolved, multicyclic event at depths between 10 and 11 km is interpreted as the master decollement. A similar event in regional COCORP sections loses much of its signal strength southeast of the Brevard Zone. The wide-angle results constrain the depth of this feature beneath the southeast flank of the Inner Piedmont and suggest that it is layered, with a thickness of roughly 500 m.

INTRODUCTION

The southern Appalachians have been crossed by numerous seismic reflection pro-

files. Middle to late Paleozoic thrusting of Valley and Ridge and Blue Ridge rocks over relatively undeformed platform sediments of the North American craton is now well established. However, the style and extent of thrusting beneath the outboard terranes of the crystalline core (the Inner Piedmont and Carolina Terrane) remain controversial. In COCORP (Cook et al., 1979) and ADCOH (Coruh et al., 1987) seismic reflection profiles, strong, continuous reflections associated with the sole thrust and platform sediments beneath the Blue Ridge and the northwest flank of the Inner Piedmont give way to weaker, more scattered reflections beneath the Elberton Granite (Inner Piedmont) and the Carolina Terrane.

It is not clear whether the sole thrust steps down into basement rock and terminates beneath the northwest flank of the Carolina Terrane in a zone of southeast-dipping reflections possibly marking the root zone for the Blue Ridge/Inner Piedmont nappes (Iverson and Smithson, 1982), or whether the sole thrust and associated platform sediments continue southeast beneath the Carolina Terrane and the Coastal Plain, indicating a Blue Ridge / Inner Piedmont root zone somewhere beneath the continental shelf (Cook et al., 1979; Harris and Bayer, 1979). A summary diagram illustrating the two competing models can be found in Cook et al. (1981).

A number of attempts have been made to constrain the age of late Paleozoic thrusting by dating unmetamorphosed plutons. The Elberton Granite (age: 320 m.y.; see below), intruded near the southeast flank of the Inner Piedmont, has figured prominently in these studies because it is the only pluton crossed by COCORP seismic lines. Competing models for the Elberton granite include a rooted body extending to depths greater than 8 km, a tabular intrusion, and the upper portion of a larger pluton decapitated by thrust faulting (see Figure 2 in Jurdy and Phinney, 1983). Unfortunately, attempts to constrain the geometry of the granite have been frustrated by the poor quality of the seismic images.

In Summer 2000, we conducted a pilot study to test the feasibility of using quarry blasts to generate stronger reflections. The experiments were performed using small-aperture arrays of three-component instruments, with instantaneous blasts at dimension-stone quarries in the area as seismic sources. The principal aim of this study was to place constraints on the geometry of the granite body and the nature of its contacts with surrounding rocks. Specifically, the goals of the experiments were: 1) to image the base of the Elberton granite and underlying units and 2) to take advantage of the relative seismic transparency of the Elberton granite to study the nature of the master decollement in the transition zone between the Inner Piedmont and Carolina Terrane.

In this paper, we show examples of data before and after processing and offer a preliminary interpretation based on very sparsely sampled migrated sections.

GEOLOGIC AND TECTONIC SETTING

Rocks of the Inner Piedmont (Figure 1a) consist of upper-amphibolite facies mica schists, amphibole gneiss, granite gneiss, and smaller amounts of quartzite, amphibolite, and metagabbro (Griffin, 1971; Hatcher and Zietz, 1980; Hatcher et al., 1987). Protoliths probably included late Precambrian to early Cambrian sediments and mostly felsic volcanics (Dallmeyer, 1989). Peak metamorphism (pressure: 7-9 kbar; temperature: 725° C) was reached at 350 - 360 m.a. (Devonian), during the Acadian orogeny (Dallmeyer, 1989). Ages within the Inner Piedmont gradually decrease to the southeast. The structure is dominated by recumbant folds overturned to the northwest (Griffin, 1971; Coruh et al., 1987). The adjacent Carolina Terrane (Belair, Kiokee, Charlotte, and Carolina Slate Belts) includes felsic metavolcanics, pyroclastics and intrusives, mafic dikes and sills, and associated argillites and graywackes of late Precambrian to early Cambrian age. It has been interpreted as an island arc sequence (Whitney et al., 1978) developed on basement of uncertain affinity (Secor et al., 1986; Hatcher, 1989). The sequence was metamorphosed and thrust northwestward during the

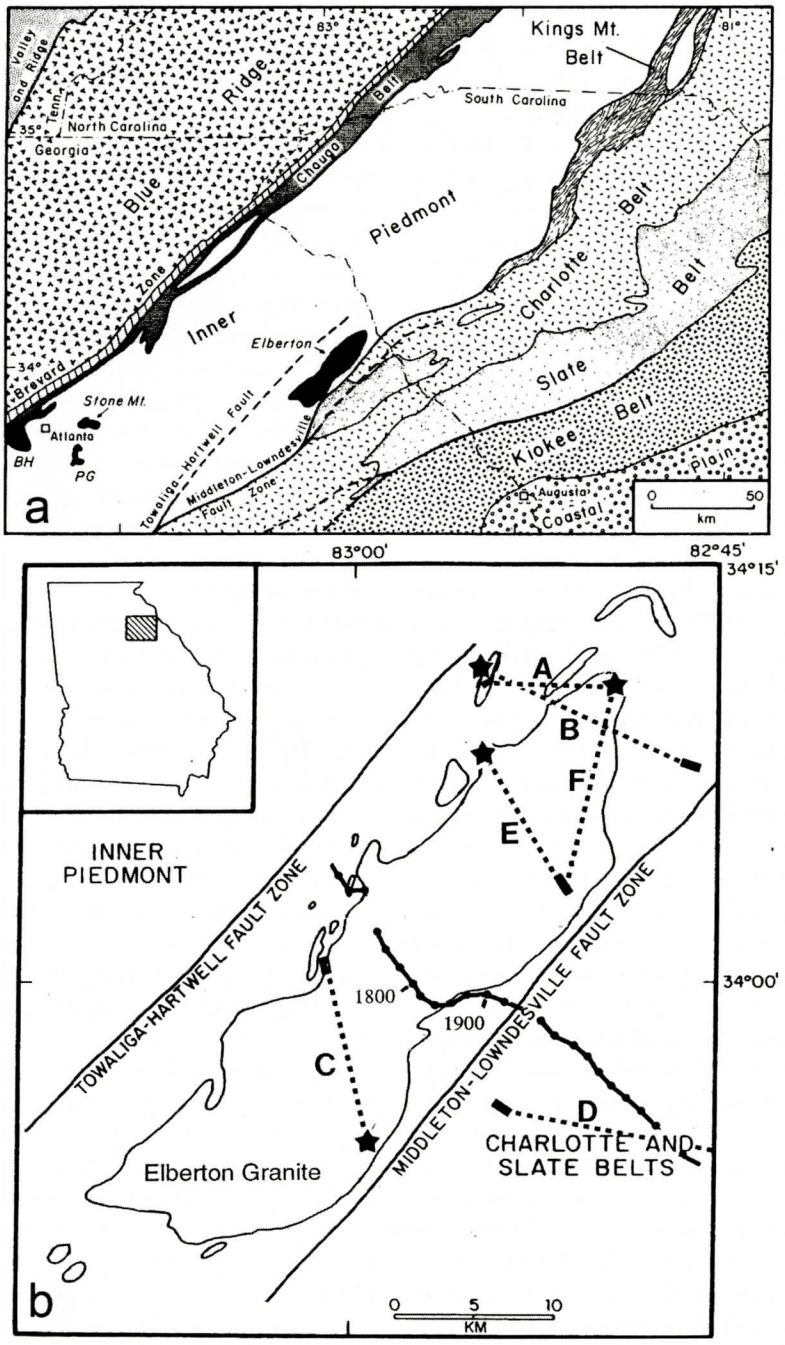

Figure 1 a. Geologic map of northeast Georgia and surrounding states (after Dallmeyer et al., 1981) showing the regional setting of the Elberton Granite. Other granite bodies of similar age are shown in black; BH = Ben Hill granite, PG = Panola granite. b. Larger-scale map of the Elberton Granite (after Ellwood, 1980 and Jurdy and Phinney, 1983), showing the main body of the granite and several outliers. Solid line with dots is COCORP line 1, with vibrator station numbers for reference. Dotted lines are raypaths for shots recorded for the present study; stars are the blast locations and heavy bars are the seismic array locations. The blasts recorded for raypath D (Table 2) are just off the map, at a distance of roughly 23 km from the center of the array.

Taconic and Alleghanian orogenies (Dallmeyer, 1989). Recent evidence suggests that the shear zone marking the boundary between the Inner Piedmont and Carolina Terrane (the Central Piedmont suture, known locally as the Middleton-Lowdnesville zone in Georgia and the Carolinas) extends into southern Virginia, where it is known as the Hyco shear zone (Hibbard et al., 1998).

ELBERTON GRANITE

The Elberton granite is a northeast trending, roughly 60 km by 10 km exposure of fine-grained granite intruded near the southeast flank of the Inner Piedmont in northeast Georgia (Figures 1a, 1b). The remarkably uniform chemical composition of the granite suggests that it was intruded as a single body (Ellwood and Whitney, 1980). Estimated depth of emplacement was 13-16 km (pressure: 4.5 - 5.0 kbar) at temperatures of roughly 675° C (Dallmeyer et al., 1981). Subhorizontal contacts with overlying gneisses of the Inner Piedmont suggest that the present erosional surface is close to the original top of the pluton, with an "undulatory" exposure pattern in the northeast section of the pluton suggesting an irregular upper surface (Ellwood and Whitney, 1980). Whole-rock U-Pb ages of roughly 320 m.y. are interpreted as the age of emplacement (Dallmeyer et al., 1981). Younger ages of 235 - 245 m.y. are probably associated with rapid uplift and cooling to temperatures of 300° - 350° C associated with Alleghanian thrusting (Dallmeyer, 1989).

The granite is roughly bounded by (but not in direct surface contact with) the Hartwell extension of the Towaliga Fault to the northwest and the Middleton-Lowndesville fault zone to the southeast (Figure 1a). In contrast with the cataclasis along the Towaliga fault seen farther to the southwest near Pine Mountain (West et al., 1995), evidence for displacement along the Hartwell extension in the Elberton area is restricted to abrupt changes in lithology. Identification of the fault is based largely on magnetic anomalies. In contrast, rocks within the Middleton-Lowndesville fault zone are intensely sheared, with northwest-vergent folds recording an earlier ductile phase of deformation followed by brittle faulting and cataclasis; this in turn was followed by intrusions of aplite dikes and additional faulting (Ellwood et al., 1980). Recent interpretations suggest that the Middleton-Lowndesville zone may represent a low-angle normal fault associated with gravitational collapse of the orogen (Dennis, 1991). Except for the aplite dikes, these fault-related features are not seen within the Elberton, suggesting that most of the non-extensional deformation along the fault zones preceded its emplacement.

Based on the present dip of magnetic foliation, Ellwood et al. (1980) proposed a southeastward rotation of the Elberton about a northeast-trending axis. They also suggested that the paleomagnetic data are not consistent with large scale thrusting (displacements: 200 - 400 km) of the Elberton (or a sheet containing the Elberton). However, the associated change in paleomagnetic latitude is small compared with the uncertainties associated with the 300 - 350 m.y. pole positions (Jurdy and Phinney, 1983). Based on heat-flow measurements, Costain et al. (1986; 1989) proposed that the Elberton is rooted, with a thickness of roughly 8 km. Geologic evidence summarized by Ellwood (1982), on the other hand, suggests that the Elberton was emplaced as a tabular body.

RESULTS OF EARLIER SEISMIC REFLECTION PROFILING

The Elberton granite is crossed by COCORP line 1 (Figure 1b). Line 4, a short strike line, follows the 5-7 km-wide Middleton-Lowndesville shear zone and just misses the southeast flank of the pluton. Unfortunately, no plotted sections of this shorter line have been published. Early versions of common-midpoint (CMP) stacks (Cook et al., 1979; 1981) show little coherent signal beneath the Elberton between 0 and 3 s TWT (two-way time). Furthermore, reflections associated with the sole thrust and overthrust platform sediments beneath the Blue Ridge (TWT: 2.5 - 3 s) become significantly weaker and less continuous as they pass beneath the southeast half of the Inner Piedmont. Reflections directly beneath (0-3 s TWT) the surface

exposure of the Middleton-Lowndesville zone are virtually absent. Starting at VP 1875 beneath the Elberton, and continuing to the southeast beneath the northwest flank of the Charlotte Belt, is a more coherent band of southeast-dipping reflections (TWT: 2 - 6 s). As noted in the introduction, interpretation of this feature remains controversial. It could represent a buried passive margin consisting of either a sequence of relatively undeformed sediments or an imbricated sedimentary sequence annealed to the edge of the continent during emplacement of the overlying thrust plate (Cook et al., 1979). Alternatively, it could mark the root zone of the Blue Ridge/Inner Piedmont nappes (Iverson and Smithson, 1982).

Coherency filtering and migration of the CMP stacks do little to improve the image beneath the Elberton and Middleton-Lowndesville zone (Phinney and Roy-Chowdhury, 1989). Prestack migration, however, enhances the continuity of the reflection packet at 3-4 s (10-12 km), suggesting that the sole thrust and perhaps the platform sediments inferred beneath the Blue Ridge may continue beneath the Elberton (Jurdy and Phinney, 1983). Besides confirming the transparency of the crust directly beneath the Middleton-Lowdnesville zone (0-3 s TWT; 0-9 km), prestack migration also reveals numerous southeast-dipping reflections at depths of 4-10 km (1.4 - 3.3 s TWT) beneath the pluton which are similar to reflections well beyond the pluton's flanks. As noted by Jurdy and Phinney (1983), this suggests that the base of the Elberton is much shallower than the 8-km depth proposed by earlier workers (Costain et al., 1986).

Unfortunately, the portion of the section for two-way times less than 1 s (depths less than 3 km) is not well defined because of front-end mutes applied to suppress coherent noise with low apparent velocity. The noise may represent refracted P or S waves multiply reflected within the weathered zone (Jurdy and Phinney, 1983). As an alternative to surgical muting of these arrivals, Jurdy and Phinney (1983) experimented with low-cut filtering and apparent-velocity filtering of shot gathers prior to CMP stacking. The resulting stacks show scattered reflections at two-way times of about 1 second (depth: 2 - 3.5 km) which they tentatively identified as the base of the pluton. They also noted that reflections at 3-4 s (9-12 km) continue uninterrupted beneath the pluton from the northwest, suggesting that the sole thrust is younger than the granite.

Table 1. Comparison of field parameters: COCORP and wide-angle experiments.

	COCORP	Wide-Angle
Seismic Source	5 Vibrators	Instantaneous quarry blasts
Receivers	7.5-Hz, single component	4.5-Hz, three component
Recording System	96-channel MDS-10	twenty PRS-4 seismographs
Receiver Spacings	67 m	50-100 m
Source-Receiver Distances	0.47 - 6.83 km	7.77 - 23.40 km (not continuous; range for all blasts)

FIELD EXPERIMENTS

In contrast with earlier seismic profiling conducted by COCORP, the experiments described here targeted the uppermost 12 km of the crust. Recording parameters for the two experiments are compared in Table 1. We used instantaneous blasts at dimension-stone quarries as seismic sources. Two types of blast were recorded: "line shots", which used vertical drillholes, and "lifting shots", which used horizontal drillholes. Both types of blast are designed to detach large blocks intact. The blasts were timed with a seismograph at the quarry; generally this was deployed 100-200 m from the shot (see Hawman, 1996, for a description of the timing strategy).

Recording in the field was done with a small-aperture array of 19 stand-alone seismographs with three-component, 4.5-Hz geophones. Receiver spacings were kept small (50 m) to avoid spatial aliasing of high-frequency signals. Shot-receiver distances (7.8-23.4 km) were chosen to avoid overlap of P-wave reflections with interfering S waves (Hunter et al., 1984), thus elim-

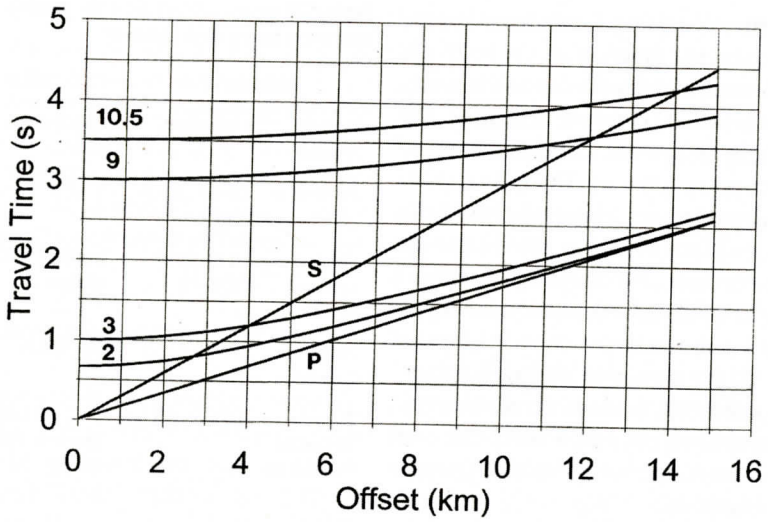

Figure 2. Travel times for direct and reflected P waves and direct S waves. "Offset" is the distance between source and receivers. Velocity for direct P waves: 5.8 km/s; for direct S waves: 3.4 km/s. Average crustal velocity for P-wave reflections: 6 km/s. Reflection travel times were computed for horizontal reflectors at depths of 2, 3, 9, and 10.5 km. The results suggest that interference with direct S and surface waves can be avoided by recording at minimum offsets ranging from 3 km for target depths of 2 km to about 14 km for target depths of 9-10 km.

inating the need for severe muting or apparent-velocity filtering. The goal here was to record at distances great enough to ensure that all P-wave reflections of interest arrived before the direct S wave. Travel times computed for simple models (Figure 2) suggested the use of minimum offsets ranging from 3 km for target depths of 2 km (corresponding to the smallest depth estimate for the base of the Elberton) to about 14 km for target depths of 9-10 km (the estimated depth of the sole thrust) to avoid interference with direct S and surface waves. Recording at large offsets ("wide angles") also took advantage of the increase in reflection coefficients near the critical angle to image relatively subtle constrasts in acoustic impedance between rock units of similar composition. It was hoped that the expected contrast in fabrics (nonfoliated granite in contact with foliated and otherwise layered metamorphic rocks) would also enhance reflectivity.

The arrays were deployed at several widely spaced locations within the granite to provide wide-angle "point soundings" of the principal discontinuities above basement. Raypaths sampled a variety of azimuths to the north and south of the COCORP line; recordings were concentrated in the northern half of the granite, where quarries are most active (Figure 1b). The blasts are referred to in the text and Figure 1b by their source-receiver raypaths. Raypath A refers to two separate blasts at the same quarry, recorded with instruments deployed along partially overlapping stretches of road. Raypath D refers to three separate blasts at the same quarry, recorded on the same day with the same array.

Table 2. Summary of wide-angle experiments with dimension-stone quarry blasts. Raypaths are plotted in Figure 1b.

Date	Raypath	Blast Type	Distance Range, km	Detectable Signal?
6/2/00	A	line	8.00 - 9.04	yes
6/7/00	D	line	22.49 - 23.40	no
6/7/00	D	line	22.28 - 23.19	no
6/7/00	D	line	22.49 - 23.40	no
6/9/00	C	line	11.53 - 12.48	yes
6/13/00	B	lifting	14.01 - 14.91	yes
6/15/00	A	line	7.77 - 9.02	yes
7/13/00	E	line	10.17 - 10.93	no
7/18/00	F	line	13.09 - 14.18	yes

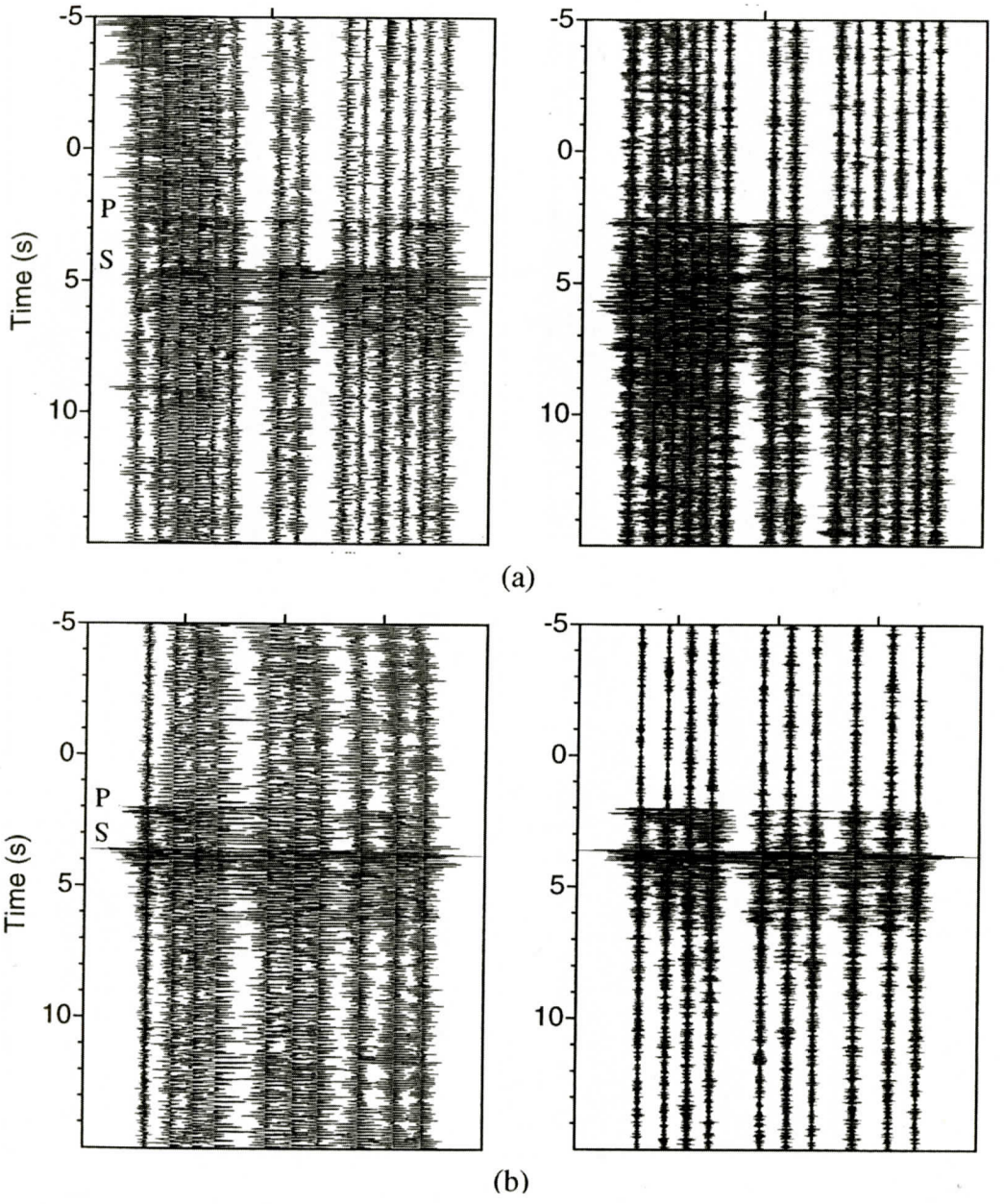

Figure 3. Field records for four dimension-stone quarry blasts recorded over the Elberton granite, northeast Georgia. The left plot in each pair is the raw field record, with only a 60-Hz notch filter applied. P and S mark the direct P wave and S wave, respectively. The right plot shows the gather after the application of an additional trapezoidal bandpass filter to suppress background noise. a. Gather for raypath B (Figure 1b). This blast was a lifting shot. Original offset range of recording: 14.01-14.91 km; offset range shown, after removal of noisy traces: 14.20-14.91 km. Corner frequencies for bandpass filter: 15, 26, 44, 55 Hz. b. Gather for raypath C (line shot). Original offset range: 11.53-12.48 km; offset range shown, after removal of noisy traces: 11.53-12.09 km. Corner frequencies for bandpass filter: 20,25,60,70 Hz.

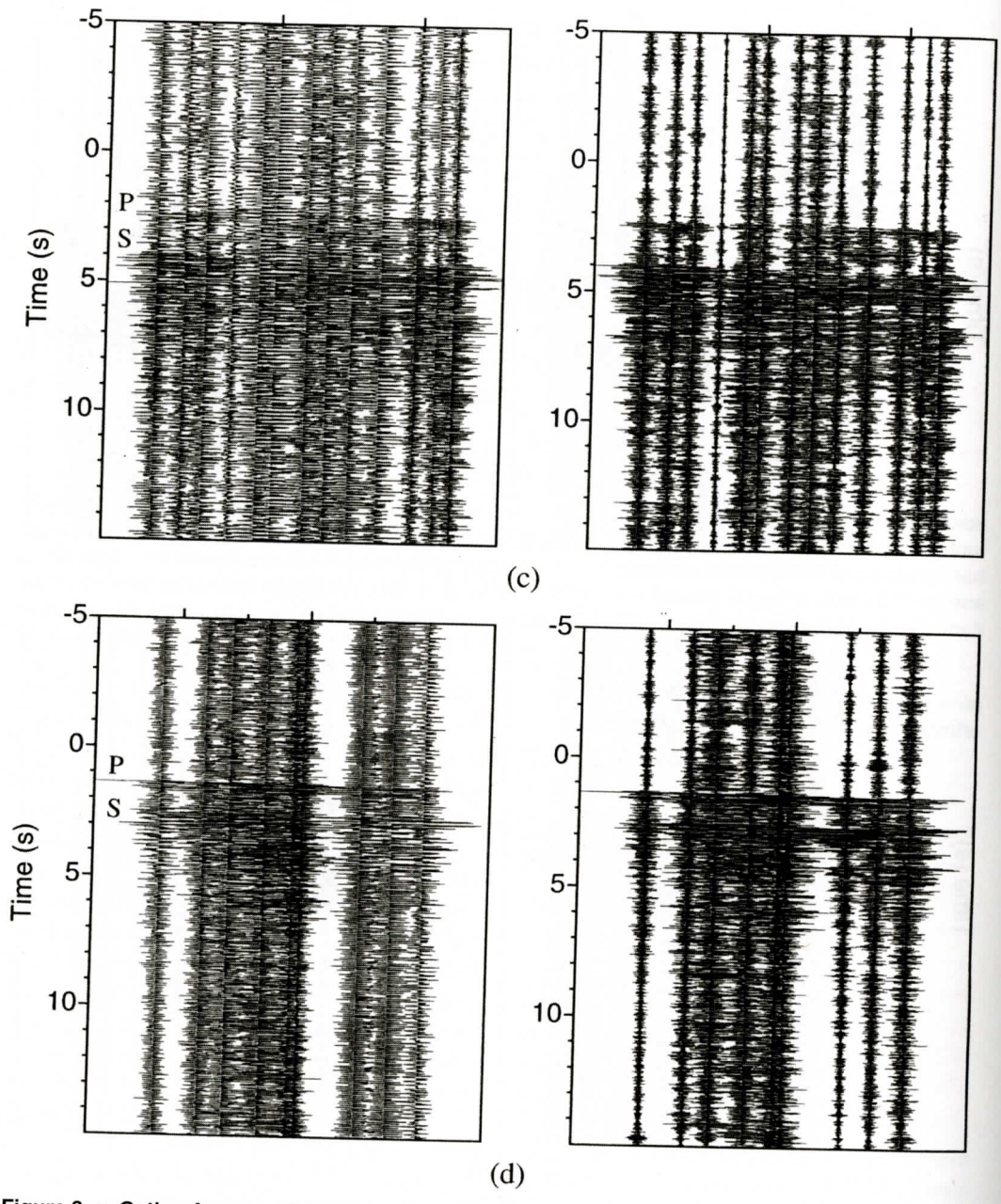

Figure 3. c. Gather for raypath F (line shot). Offset range: 13.09-14.13 km. Corner frequencies for bandpass filter: 13,19,33,45 Hz.d. Gather for raypath A (line shot). Original offset range: 7.77-9.02 km; offset range shown, after removal of noisy traces: 7.77-8.19 km. Corner frequencies for bandpass filter: 15,25,45,60 Hz

DATA PROCESSING

Of the nine blasts recorded (Table 2), five generated detectable signal. Field records show strong direct P and S waves (Figure 3). Amplitude spectra of traces free of traffic noise show signal energy at frequencies as high as 45-50 Hz. Predictive deconvolution (Robinson and Treitel, 1980; Yilmaz, 1987) with a prediction distance of one sample was used to improve res-

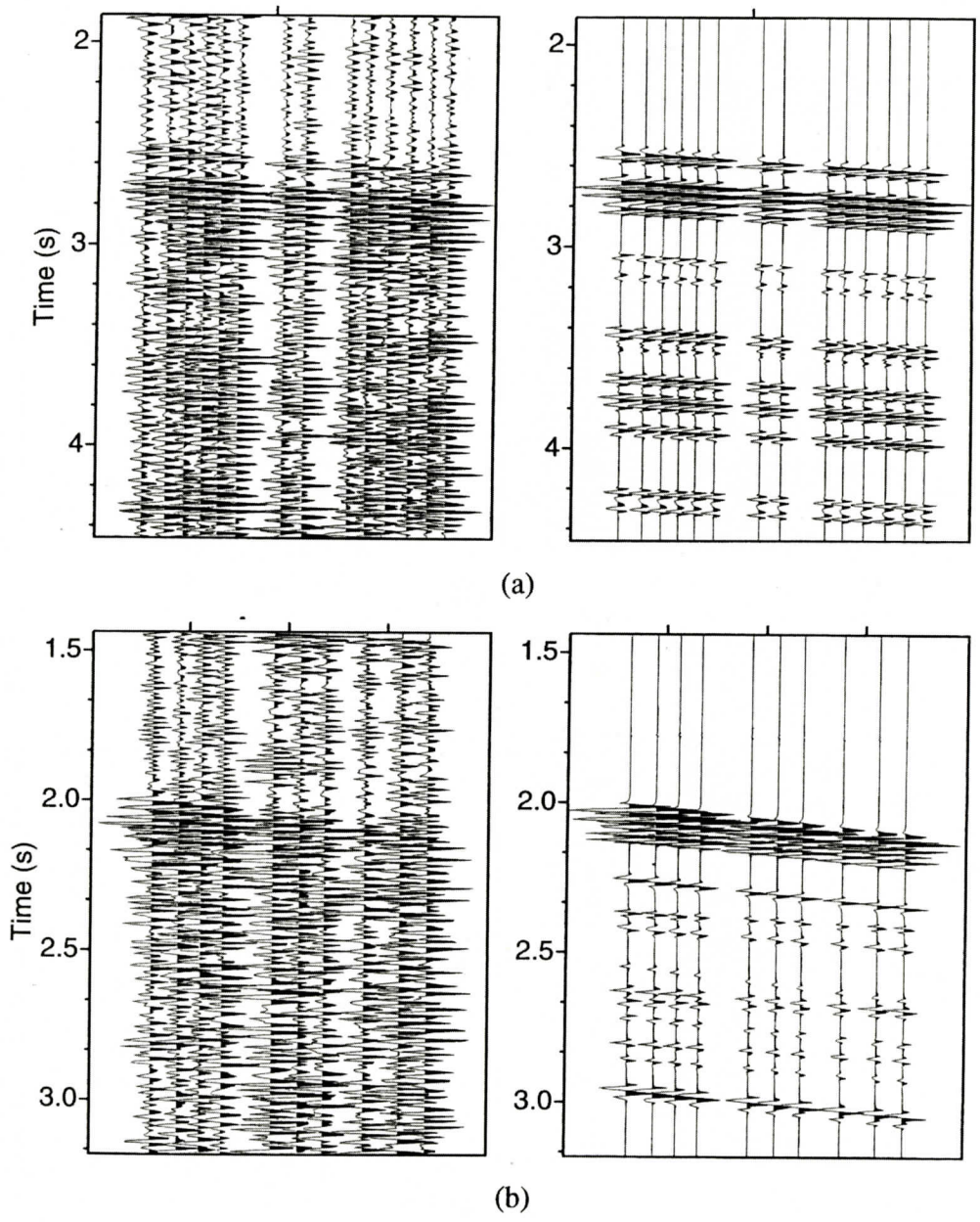

Figure 4. Records after corrections for statics (left) and after the application of a coherency filter to isolate the most reliable events for migration (right). The gathers on the right were generated by inverse stacking of coherency-filtered slant stacks (not shown). The coherency filtering and inverse stacking procedures are outlined in Kong et al. (1985). Compare with the time windows displayed in Figure 3; the windows shown here begin shortly before the arrival of the direct P wave and end before the arrival of the direct S wave.
a. Gather for raypath B (Figure 1b). Portions of the gather with a semblance (coherency) value less than 0.45 have been removed. b. Gather for raypath C. Coherency filter setting: 0.45.

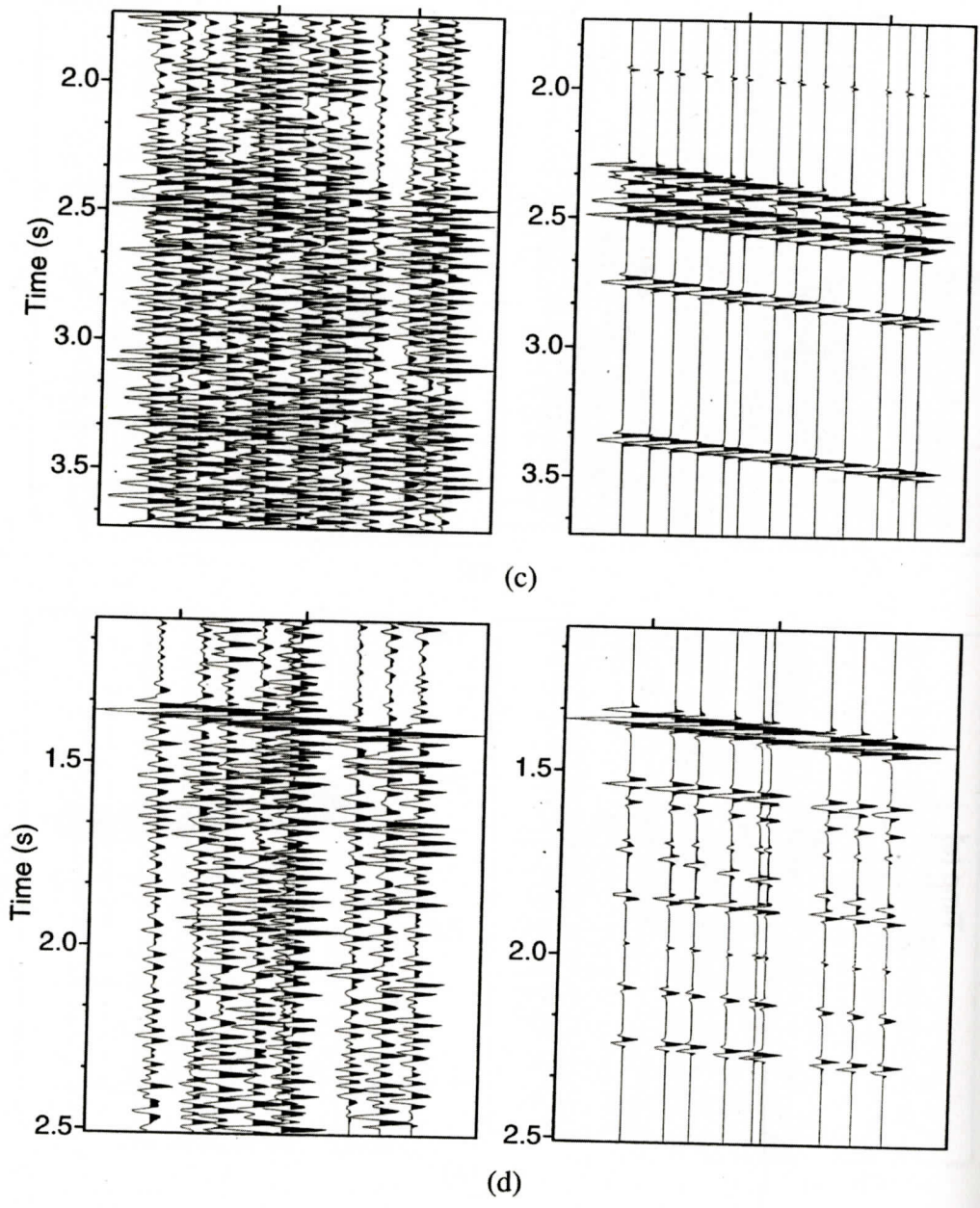

Figure 4 c. Gather for raypath F. Coherency filter setting: 0.6 d. Gather for raypath A. Coherency filter setting: 0.6

olution by whitening the spectrum (i.e., roughly equalizing the contribution of all frequency components) of each trace. Notch filters were applied to eliminate noise at 60 Hz and other narrow-band noise generated by local industry. A trapezoidal bandpass filter was also applied to suppress incoherent noise.

Statics corrections were determined by alignment of first arrivals. The traces in each shot gather first were shifted by applying a reduction velocity corresponding to the apparent velocity of the direct P wave (generally about 5.8 km/s). This reduction velocity was adjusted in cases where slant stacks of the uncorrected gathers

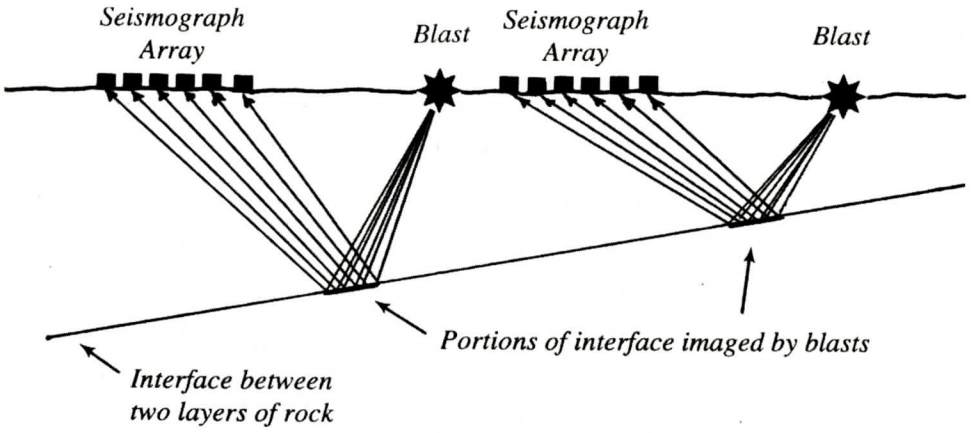

Figure 5. Schematic cross section showing the geometry of the wide-angle seismic experiments over the Elberton granite. For small dips, the portion of an interface sampled by each blast is roughly half the length of the seismograph array.

suggested a different (generally higher) value. Variations in reflection travel time caused by topography and lateral variations in near-surface velocity then were estimated by cross-correlation of first arrivals in the velocity-reduced gathers (Hawman et al., 2000; Hawman, 2004). Although these static corrections were determined from refracted arrivals, the fairly steep near-surface raypaths for the latter resulted in improved coherence for reflections as well (Figure 4).

The static-corrected shot gathers then were slant stacked (Phinney et al., 1981) to provide objective measures of travel time and apparent velocity for coherent arrivals (Hawman and Phinney, 1992; Hawman, 2004). Extremely noisy traces were removed prior to stacking. No attempt was made to extract reflections arriving after the direct S wave. Reflection continuity was evaluated by computing the semblance, a measure of coherence with values ranging from zero to one (Douze and Laster, 1979). The semblance was used to derive a coherency filter (Kong et al., 1985) to isolate the most reliable portions of the slant stack for each shot gather. An example for this data set is shown in Khalifa and Hawman (submitted manuscript). The slant-stack process is reversible (Kong et al., 1985); the equivalent coherency-filtered shot gathers are shown alongside the input static-corrected gathers in Figure 4. As noted by Kong et al. (1985), the filter parameters must be chosen carefully to avoid generating artifacts in the coherency-filtered shot gathers (and ultimately in the migrated sections). All events passed by the coherency filter should be observable (albeit partly obscured by noise) in the input gather. The semblance cutoff value was raised until this criterion was met.

The coherency-filtered slant stacks then were migrated using an algorithm for depth migration described in Hawman (2004). The velocity model used for migration consists of 6 layers and was based on travel times of direct P waves and laboratory velocity measurements for granites at confining pressures up to 4 kbar (Birch, 1960). The velocities in this model range from 5.5 km/s in the uppermost 0.5 km to 6.2 km/s beginning at 6 km depth.

MIGRATION RESULTS

Given the very sparse nature of the data set, a few comments regarding the migration algorithm and the appearance of migrated sections are in order here. Briefly, the algorithm maps each sample in the slant stack into a dipping interface in the subsurface image. The apparent velocity fixes the angle of incidence of the wavefront across the array; this together with the travel time fixes the subsurface location and dip of the reflecting interface. For gentle dips,

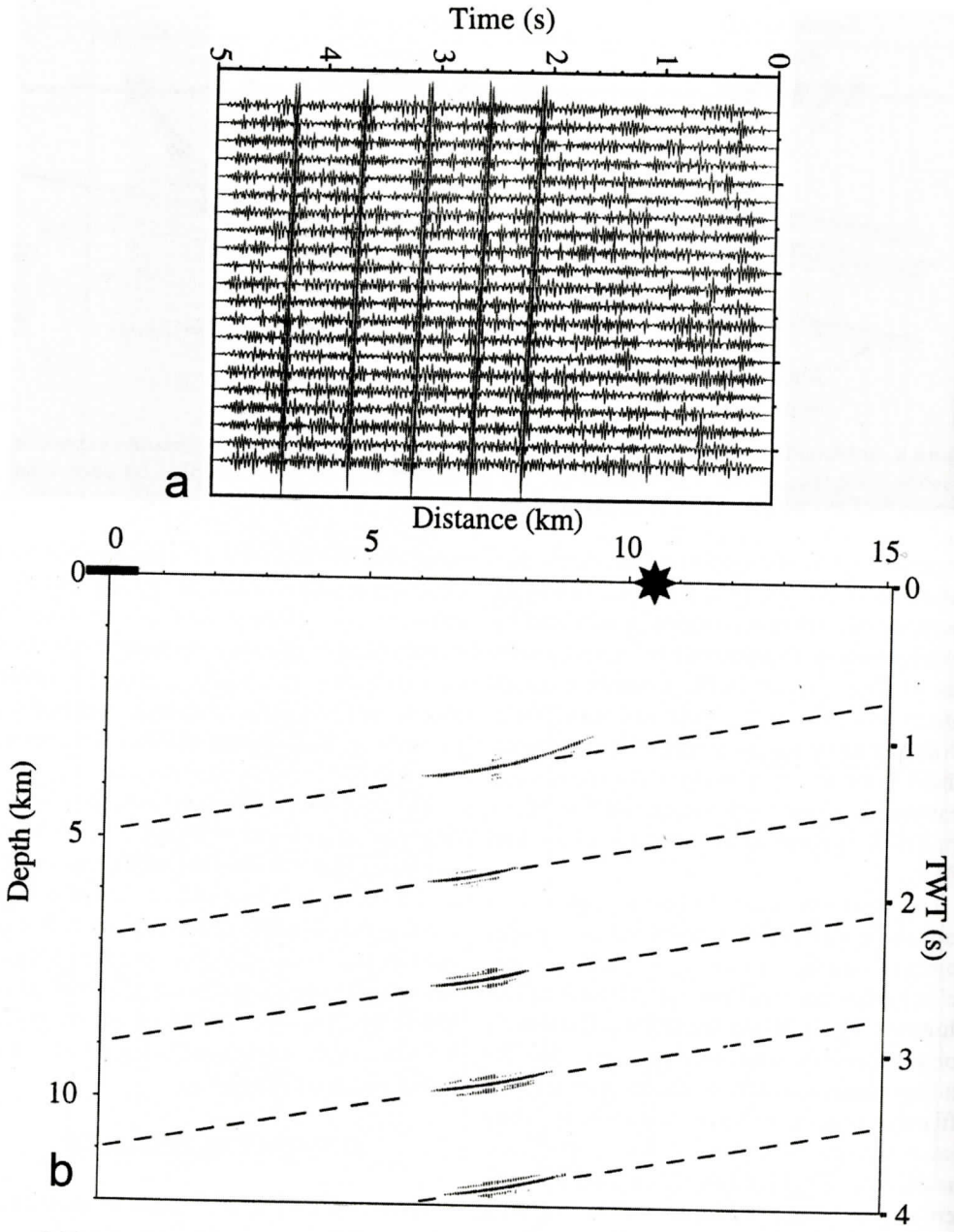

Figure 6. Tests of the migration algorithm using synthetic data as input. a. Synthetic shot gather generated for a series of planar dipping interfaces (dip = 10 degrees). Travel times were computed for a constant velocity of 6 km/s. Signal and random noise bandwidth (15 - 50 Hz), random noise level, station spacing (50 m), and distance range (10-11 km) are representative of the data actually recorded. b. Depth migration of the shot gather in part a. The right axis shows the corresponding two-way, vertical-incidence travel times (TWT). The blast and seismograph array locations are shown by the star and heavy bar, respectively. Dashed lines show the positions of reflecting interfaces for the input model. The migrated image for each interface extends well beyond the zone of reflection points actually sampled by the blast (Figure 5). Weaker reflection bands immediately above and below each migrated interface are artifacts generated by sidelobes of the symmetric input wavelet.

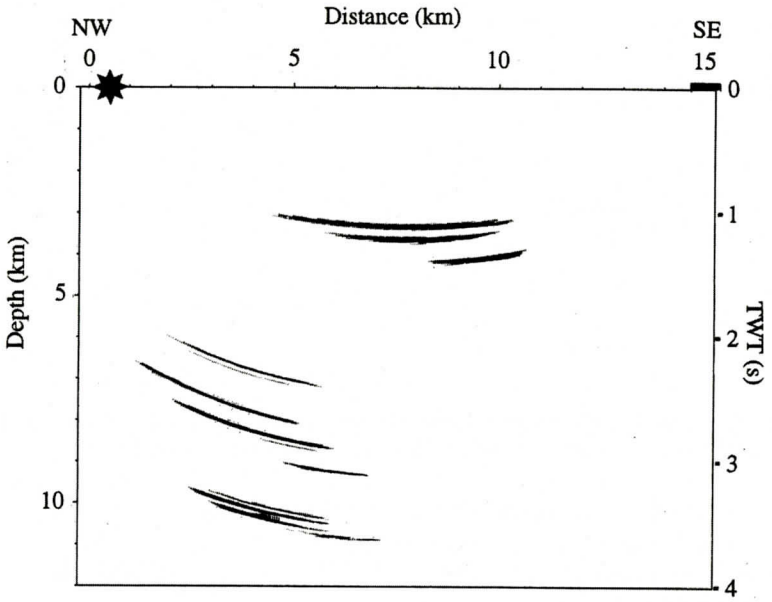

Figure 7. Cross section showing the results of depth migration of the coherency-filtered slant stack of the record for raypath B (Figure 1b). For Figures 7 through 10, the vertical sampling increment is 10 m and the horizontal sampling increment is 50 m. The right axes show the corresponding two-way, vertical-incidence travel times (TWT) computed for the migration velocity model, for comparison with earlier COCORP surveys. These times differ very little from the times computed for a constant velocity of 6 km/s. Locations of the blasts and seismograph arrays are indicated by the stars and horizontal bars, respectively. The considerable smearing of the images is due largely to the small aperture of the recording arrays. For the migration shown in this figure, the semblance cutoff is 0.8 for events in the uppermost 4 km, 0.6 for events between 4 and 9.5 km, and 0.45 for events below 9.5 km.

the portion of an interface actually sampled by a given shot will be roughly half the width of the recording array (Figure 5). In the migrated sections, the interface segments are smeared well beyond this halfwidth. The degree of smearing (or, the width of "migration smiles") is determined by the degree of smearing (uncertainty in ray parameter) in the slant stack, which in turn is controlled by the array aperture and signal bandwidth. Thus the migration smiles represent confidence regions within which the sampled interfaces are constrained to lie.

This smearing effect is illustrated in Figure 6, which shows the response of the migration algorithm to a series of planar, dipping interfaces. Station spacing, total array aperture, noise level, and signal bandwidth for the synthetic input gather (Figure 6a) are similar to corresponding values for the actual field gathers. Weaker reflection bands immediately above and below each migrated interface (Figure 6b) are artifacts generated by sidelobes of the symmetric input wavelet.

For the very small array apertures considered here, replacing the dipping interfaces with single point scatterers at positions coinciding with the midarray reflection points generates a very similar response. The resulting diffractions arrive with virtually the same travel times and apparent velocities as the corresponding reflections, and with a similar degree of smearing in the slant stack, thus yielding a very similar migrated image. Distinguishing between scattered and reflected energy therefore requires considerably more data coverage than the very limited number of sources and receivers used for this study can provide. Even if it is assumed that all coherent signals are reflections, the migrated sections shown in Figures 7-10 represent only partial images of the subsur-

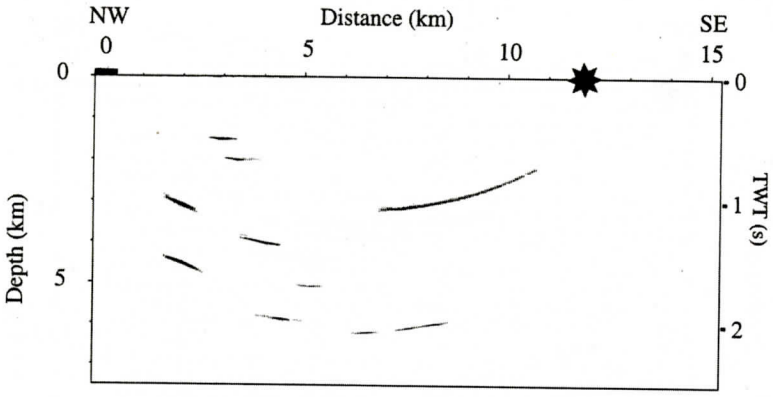

Figure 8. Results of depth migration for the record for raypath C (Figure 1b). The semblance cutoff is 0.8 for events between 1 and 2 km and 0.45 for events between 2 and 7 km.

face. The subset of features illuminated by the experiments is controlled by the distribution of blasts and recording arrays as well as by the geologic structure. With these caveats in mind, we briefly describe the migrated sections and offer a preliminary interpretation.

Section B

Figure 7 shows the migrated section generated for a coherency filter setting with a cutoff semblance value of 0.8 for the uppermost 4 km, 0.6 for depths between 4 and 9.5 km, and 0.45 for depths greater than 9.5 km. This decrease allowed for the loss of coherence due to statics generated by deeper velocity variations not accounted for by the statics determined from first arrivals. Shot-receiver distances for traces included in the slant stack ranged from 14.20-14.91 km. Ray paths for this blast are almost perpendicular to strike (Figure 1b). At depths between 9.5 and 11 km (corresponding to a two-way, zero-offset travel time or TWT of 3.2-3.6 s), a series of reflectors with gentle apparent dip (4-14 degrees to the southeast) occurs with relatively good horizontal resolution of 2-3 km. Above this is a series of southeast-dipping reflectors (7-20 degrees) at depths between 6 and 9.3 km (2.2-3.1 s). The shallowest reflectors appear as a layered structure at depths between 3 and 4.2 km (1-1.4 s). Horizontal resolution within this package is poor but improves with depth. Apparent dips range from 0 to 8 degrees to the northwest.

Section C

The distance range for traces included in the slant stack used to generate Figure 8 was 11.53-12.09 km. Raypaths are roughly parallel to CO-CORP Line 1 (Figure 1b), at an angle to the regional dip. The migrated section is dominated by horizontal to subhorizontal, well-focused reflectors except for two steeply dipping reflectors at the northwest end of the section and a more poorly resolved reflection near the southeast end. The deepest reflectors, at 5.5-6.2 km (1.9-2.1 s TWT), have very small apparent dips. These are overlain by a horizontal reflector at 5 km (1.7 s). The shallowest reflectors are observed at depths of 1.5-2 km (0.5-0.7 s); these are subhorizontal, with an apparent dip of less than 4 degrees to the southeast.

Section F

Migration results for the remaining sections (Figures 9-10) are shown for two coherency filter settings. Increasing the cutoff setting produces more focused images with fewer events. The distance range for traces included in the slant stack for this recording was 13.09-14.13 km. Source-receiver raypaths (Figure 1b) are almost perpendicular to the raypaths for Section B. In the section generated with the lower cutoff setting (Figure 9a), the deepest reflector is ob-

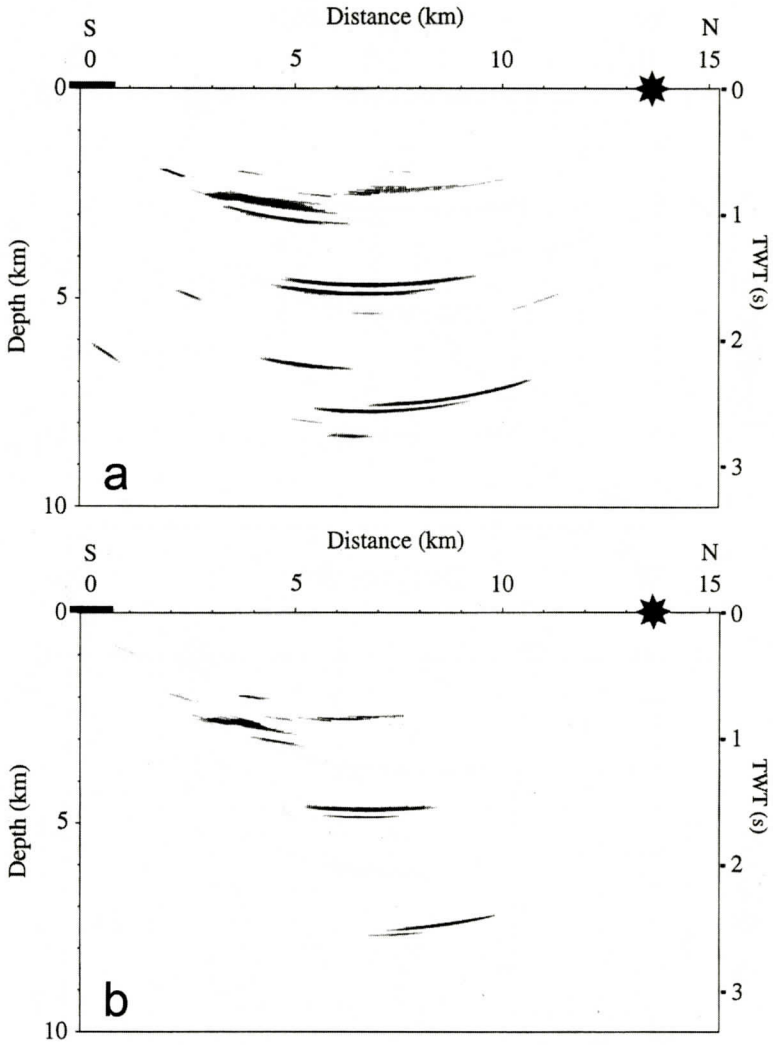

Figure 9. Results of depth migration for raypath F (Figure 1b). a. Semblance cutoff for coherency-filtered slant stack: 0.45. b. Semblance cutoff: 0.6. The higher cutoff generates a more focused image with fewer migrated events.

served at 8.5 km (2.8 s TWT) and is well resolved (resolution width: 1 km). A multicyclic reflector appears at 7.8 km (2.6 s) with poorer horizontal resolution. At a depth of 6.6 km (2.2 s), a well resolved, north-dipping reflector is observed. A horizontal, multicylcic reflector appears at depths between 4.7 and 5 km (1.6-1.7 s) but horizontal resolution is relatively poor (4 km). The shallowest complex consists of two interfaces (depth: 2.5-3 km; 0.9-1 s) that dip gently to the north; above this is an interface at 2 km depth (0.7 s) that is subhorizontal.

Section A

The distance range for this recording was 7.77-9.02 km, but due to traffic noise only the portion recorded between 7.77 and 8.19 km was used to generate the migrated section (Figure 10). In the section generated with the lower coherency-filter setting (Figure 10a), the deepest reflector (5.5 km; 1.9 s) is flat and well resolved. A poorly resolved but mostly horizontal event is observed at 3.8 km (1.3 s). Apparent dips range from zero to 15 degrees to the west.

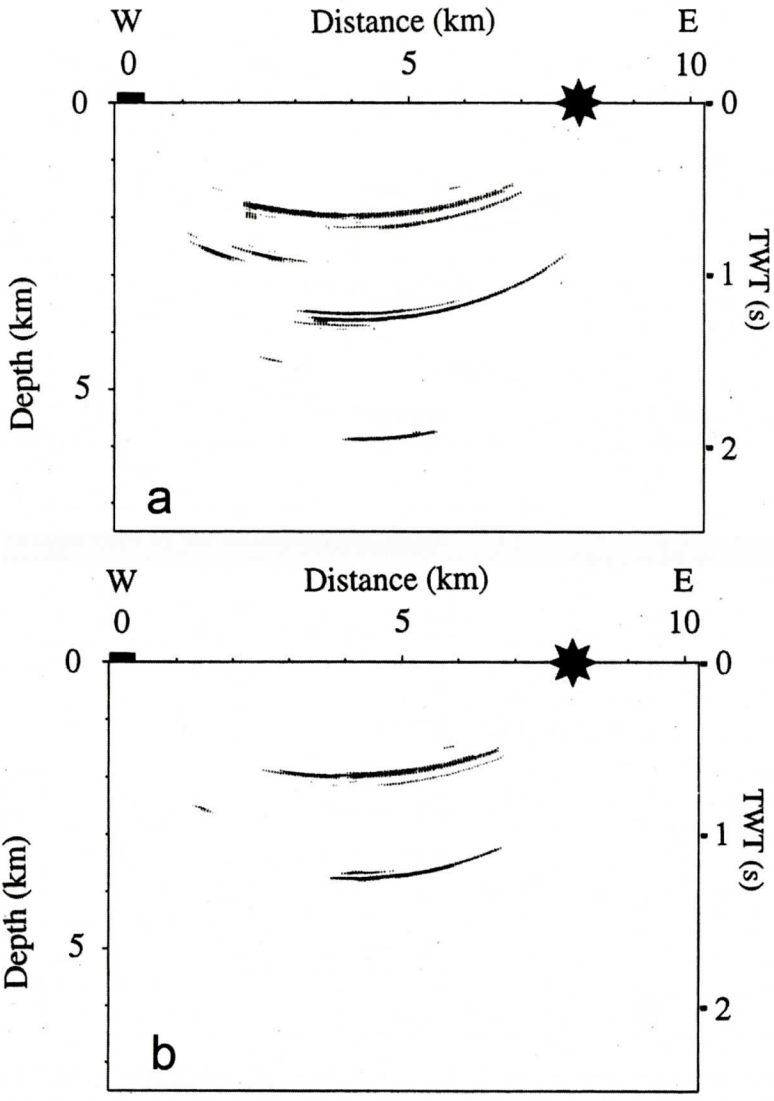

Figure 10. Results of depth migration for raypath A (Figure 1b). a. Semblance cutoff for coherency-filtered slant stack: 0.45. b. Semblance cutoff: 0.6

Two east-dipping events are observed at depths of 2.4-2.7 km (0.8-0.9 s) with an apparent dip of 15 degrees. The shallowest events appear at depths of about 2 and 2.2 km (0.7 s). These are subhorizontal, with large resolution widths.

INTERPRETATION

As noted earlier, the reflector distributions for the migrated sections described above are strongly controlled by the sparse recording geometries. They are of interest, however, because the wide-angle recordings sample parts of the granite not crossed by COCORP lines, and because they sample the crust at larger angles of incidence. The combined results from both surveys are summarized in the fence diagram shown in Figure 11. This was constructed from line drawings of Figures 7, 8, 9b, and 10b, and COCORP sections reprocessed by Iverson and Smithson (1983) and Jurdy and Phinney (1983). Travel times for the COCORP sections were

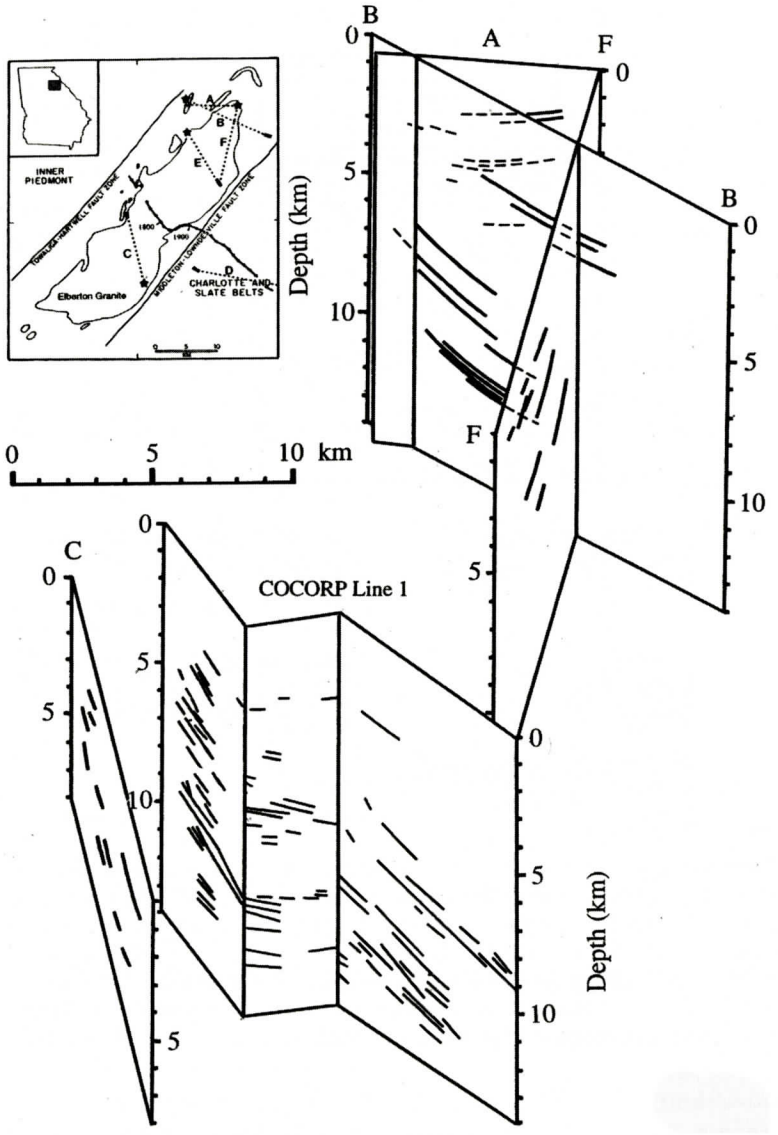

Figure 11. Fence diagram showing line drawings of migrated wide-angle data (Figures 7, 8, 9b, and 10b) and COCORP sections reprocessed by Iverson and Smithson (1983) and Jurdy and Phinney (1983). Depths for the COCORP sections were approximated assuming an average velocity of 6 km/s. The inset map is reproduced from Figure 1b.

converted to approximate depths assuming an average velocity of 6 km/s. The main elements of our geologic interpretation are summarized in the schematic shown in Figure 12.

Structure Within the Top 4 km

In this depth range, the wide-angle migrated sections contain reflectors that, in the COCORP data, are either obscured by coherent noise or not observed at all. Reflectors at about 3 km appear in sections B, C, and F (Figures 7-9). In section B (Figure 7), these appear as a layered complex at depths between 3 and 4.2 km (1-1.4s). In section C, these appear as discrete reflectors with variable apparent dips at depths

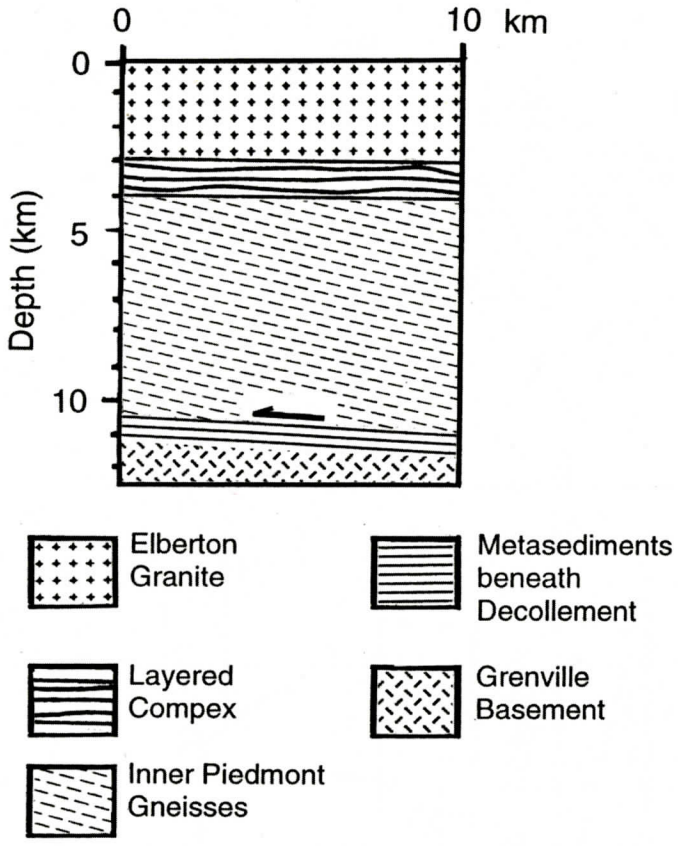

Figure 12. Generalized interpretation of the migrated sections over the Elberton granite, drawn mainly from Line B (Figure 7). The granite extends to a depth of 2-3 km, where it is underlain by a layered complex 1-2 km thick. Possible interpretations of this complex include cumulate layering or migmatites at the base of the pluton as originally emplaced, or a mylonitic shear-zone associated with thrust faulting. Southeast-dipping interfaces at depths of 6-9.5 km become more prominent just southeast of the granite. The sole thrust lies at a depth of 10-11 km and appears to be associated with a package of layered rocks (metasediments?) roughly 0.5 km thick.

between 3 and 4.5 km (1-1.5 s TWT) (Figure 8). In sections F and A, they occur as pairs of multicyclic reflectors, at 2.5 and 4.5 km (0.9 - 1.5 s) in section F (Figure 9a), and at 2 and 3.8 km (0.7 and 1.3 s) in section A (Figure 10a). These depths are consistent with the scattered reflections recovered by Jurdy and Phinney (1983) at about 1 s and observed by Iverson and Smithson (1983) between 1.2 and 1.4 s (3.5-4 km). The wide-angle data extend those observations along strike, 5 km to the southwest and 20 km to the northeast of the COCORP line.

Taken together, the results suggest a layered complex beginning at 2-3 km depth and bottoming out at roughly 4-4.5 km. The combined data suggest that this complex is laterally continuous, supporting the interpretation of Jurdy and Phinney (1983) that it marks the base of the Elberton granite. The near-absence of reflections above 2-3 km is consistent with an intrusive body that is seismically transparent. As noted by Jurdy and Phinney (1983), the hypothesis that the granite is a tabular body that does not extend deeper than 2-3 km is also supported by the transition from horizontal to southeast dipping reflections at slightly greater depths (see below).

The layered complex is similar to reflection packages interpreted by Lynn et al. (1981) as layering near the base of other granitic

batholiths. Some of those packages are 0.5-2.5 km thick. Lynn et al. (1981) propose four alternative mechanisms for generation of the layering: 1) underplating of the plutons by basaltic magma; 2) melting of crustal rocks by mantle basalts, yielding cumulate layers of mafic composition; 3) layering associated with migmatites; and 4) thrust-fault contacts between the base of the batholith and sedimentary rocks or mylonitic shear zones of finite thickness. It is well known that a sequence of thin layers can generate reflections with greatly increased amplitudes through constructive interference. The effect depends on the scale of layering, the layer velocities, the angle of incidence, and the frequency content of the signal (Fountain et al., 1984; Braile and Chiang, 1986). Within shear zones, fine-scale layering coupled with contrasts in the degree of anisotropy between adjacent layers (weak anisotropy within feldspar-rich layers; strong anisotropy with the slow velocity oriented vertically within mica-rich layers) enhances reflectivity (Fountain et al., 1984). Anastomozing structure within a shear zone beneath the Elberton Granite could help to explain the variations in apparent dips and thicknesses of the shallow layered complexes seen in the reprocessed COCORP and wide-angle migrated sections. If the reflections are from a shear zone, they should extend into the Carolina Terrane, well beyond the southeast flank of the granite. Reflections over this depth range in the COCORP portion of Figure 11, however, do not continue southeast of the Middleton-Lowndesville fault zone. This would be consistent with later motion along that fault zone (Dennis, 1991); alternatively, it simply could be related to the difficulty of recovering reflections over this depth range in COCORP sections, as noted earlier.

Structure Between 4 and 10 km

Directly beneath this layered complex, the wide-angle migrated sections show a zone that is relatively reflector-free, underlain by gently dipping reflectors beginning at roughly 6 km (Figures 8, 9a, 10a). In section F (Figure 9a), these events appear at 6.6 km (2.2 s TWT) with apparent dips to the north, followed by a package at 7-7.5 km (2.4-2.5 s) with apparent dips to the south. Section B (Figure 7) is unique in showing southeast-dipping interfaces (dip range: 7-20 degrees) that span a depth range of 6-9.3 km (2-3.1 s). This could have been due to experiment geometry; two of the blasts (F and C) were recorded along raypaths at appreciable angles to the dip direction and the third blast (A) was recorded at smaller offsets where reflections arriving from depths greater than 5 km were more susceptible to shear-wave interference.

These southeast-dipping features are well correlated with southeast-dipping events in COCORP Line 1. The COCORP line shows apparent dips ranging from 15 degrees (Jurdy and Phinney, 1983) to about 20 degrees (Iverson and Smithson, 1983). These events do not appear in the sections reprocessed by Phinney and Roy-Chowdhury (1989) except for a hint of the southeast dipping arrivals after 3 seconds. Interestingly, the dipping reflectors in the wide-angle section are parallel to the southeast projection of the Towaliga-Hartwell fault zone.

Structure at Depths Greater Than 10 km

Section B (Figure 7) is the only wide-angle migrated section that shows reflectors at 10-11 km (3.3-3.6 s); for the other blasts recorded at smaller distances, these reflectors may have been obscured by interfering shear waves. Reprocessed COCORP sections (Iverson and Smithson, 1983; Jurdy and Phinney, 1983) show weaker, sporadic arrivals beneath the Elberton at two-way travel times that are consistent with this deepest event. The reflector in the wide-angle migrated section is multicyclic, subhorizontal, relatively high in amplitude, and well resolved. Reflections with similar characteristics in profiles across other crystalline terranes have been interpreted as mylonitic shear zones (Smithson et al., 1979; Hurich et al., 1985). We interpret this event as a package of reflections from the master decollement. As noted earlier, COCORP sections show a marked decrease in strength for this event southeast of

the Brevard Zone. The wide-angle results constrain the depth of this feature beneath the southeast flank of the Inner Piedmont and suggest that it is layered. However, questions regarding the composition of rocks within the fault zone (whether they are mylonites or relatively undeformed platform sedimentary rocks) remain unresolved.

CONCLUSIONS

Results from Pilot Study

A wide-angle reflection study using instantaneous blasts at dimension-stone quarries has recovered reflections to a depth of 11 km beneath the Elberton granite. Of the nine blasts recorded, five generated recognizable signal. Coherent events arriving shortly after the direct P wave are interpreted as postcritical reflections from a layered complex. Although the data coverage is very sparse, the migrated events consistently appear with small apparent dip at depths between two and four km. It is suggested that the layered complex is laterally continuous and that it marks the base of the granite. This is consistent with an earlier interpretation of scattered events observed in COCORP sections reprocessed by Jurdy and Phinney (1983). The wide-angle data extend those observations 5 km to the southwest and 20 km to the northeast of the COCORP line.

The migrated sections also show southeast-dipping reflectors that span a depth of 5-10 km and that correlate with previously reported southeast-dipping events in COCORP lines (Cook et al., 1979, 1981). As noted by Jurdy and Phinney (1983), the transition from horizontal to dipping reflections beneath the Elberton granite supports the hypothesis that the granite is a tabular body that does not extend deeper than 4 km. A high-amplitude, well resolved, multicyclic event at depths of 10-11 km is interpreted as the master decollement. A similar event in COCORP sections loses much of its signal strength southeast of the Brevard Zone. The wide-angle results constrain the depth of this feature beneath the southeast flank of the Inner Piedmont and suggest that it is layered, with a thickness of roughly 500 m.

Suggestions for Follow-up Work

One of the main limitations of this pilot experiment was the very small recording array; the 50-m station spacing resulted in a recording aperture of only 1 km for each blast. Clearly, a more definitive quarry-blast study would require more instruments. Alternatively, one could deploy a similar number of instruments over a much wider area within the granite to record signals from a single vibrator. Here the receivers would remain fixed and the source would move, a geometry similar to that employed for recent onshore-offshore seismic studies of continental margins (Brocher and Moses, 1990). For a source interval of 50 m, the result would be a set of large-aperture receiver gathers recorded over a range of azimuths that would allow one to construct three-dimensional images of the granite and sole thrust and to study their reflectivity as a function of incidence angle. Overlap of coverage with COCORP Georgia Lines 1 and 5 would allow a direct comparison of near-vertical and wide-angle reflections from the same targets. Recordings of instantaneous quarry blasts could be used as a guide in determining optimum offsets for the vibrator work. The quarry blasts also would provide the clearest first arrivals (no correlation sidelobes) and strongest shear waves (for supplementary studies of physical properties). To better constrain velocities for migration, one could record a reversed refraction profile (total aperture: about 30 km) along the axis of the granite; for this part of the work, one could use much larger blasts at crushed-stone quarries to generate adequate signal at distances greater than 15 km.

Specific objectives of this work would include:

1) Determining the source of reflections observed from depths between 2 and 4 km. Basal reflections extending beyond the Elberton would indicate a thrust fault contact well above the sole thrust. Basal reflections restricted to the region directly below the granite, on the other hand, would suggest that the Elberton was em-

placed as a tabular body, with the original contact with underlying rocks preserved; this would provide important information regarding the geometry of the pluton as originally emplaced.

2) Construction of detailed, three-dimensional images of the sole thrust, to establish its continuity beneath the Elberton granite. Clearly imaged disruptions of reflection continuity beneath the Elberton would argue in favor of post-thrust emplacement of the granite.

ACKNOWLEDGMENTS

We thank Jeffrey E. Clippard and Jennifer A. Kucinskis for their assistance in the field, and Gilles Allard and Jim Whitney for helpful discussions. This study would not have been possible without the help and cooperation of many persons in the Elberton granite industry. In particular, we thank Thomas A. Robinson of the Elberton Granite Association; Vince Fernandez of Blue Ribbon Quarries, Inc.; James Boyd of Boyd Granite Company, Inc.; John Dye and John Oldham of Dye Granite, Inc.; James Adams and Anthony Adams of Gold Eagle Quarries, Inc.; and Rusty Adams and Mark Adams of Star Granite Company, Inc. Comments by reviewers Nicholas Hayman and Tom Taylor improved the manuscript. This work was supported by the National Science Foundation (Grant EAR-0124249) and by grants from the Wheeler-Watts Fund and the Gilles and Bernadette Allard Fund, both administered by the Department of Geology, University of Georgia.

REFERENCES CITED

Birch, F., 1960, The velocity of compressional waves in rocks to 10 kilobars, 1, Journal of Geophysical Research, v. 65, p. 1083-1102.

Braile, L. W., and Chiang, C. S., 1986, The continental Mohorovicic Discontinuity: Results from near-vertical and wide-angle seismic reflection studies, *in* Reflection Seismology: A Global Perspective, edited by Barazangi, M. and Brown, L., p. 257-272, American Geophysical Union.

Brocher, T. M., and Moses, M. J., 1990, Wide-angle seismic recordings obtained during the TACT multichannel reflection profiling in the northern Gulf of Alaska, U. S. Geological Survey Open File Report, v. 90-663, 40 p.

Cook, F. A., Albaugh, D. S., Brown, L. D., Kaufman, S., Oliver, J. E., and Hatcher, R. D., Jr., 1979, Thin-skinned tectonics in the crystalline southern Appalachians: COCORP seismic reflection profiling of the Blue Ridge and Piedmont, Geology, v. **7**, p. 563-567.

Cook, F. A., Brown, L. D., Kaufman, S., Oliver, J. E., and Petersen, T. A., 1981, COCORP seismic profiling of the Appalachian orgen beneath the Coastal Plain of Georgia, Geological Society of AmericaBulletin, v. 92, p. 738-748.

Coruh, C., Costain, J. K., Hatcher, R. D., Jr., Pratt, T. L., Williams, R. T., and Phinney, R. A., 1987, Results from regional vibroseis profiling: Appalachian ultra-deep core hole site study: Geophysical Journal of the Royal Astronomical Society, v. 89, p. 147-156.

Costain, J. K., Hatcher, R. D., Jr., and Coruh, C., 1989, Appalachian ultradeep core hole (ADCOH) project site investigation: Regional seismic lines and geologic interpretation, *in* Hatcher, R. D., Jr., Thomas, W. A., and Viele, G. W., eds., The Appalachian-Ouachita Orogen in the United States: Boulder, Colorado, Geological Society of America, The Geology of North America, v. F-2, Plate 12.

Costain, J. K., Speer, J. A., Glover, L., III, Perry, L., Dashevsky, S., and McKinney, M., 1986, Heat flow in the Piedmont and Atlantic Coastal Plain of the southeastern United States, Journal of Geophysical Research, v. 91, p. 2123-2135.

Dallmeyer, R. D., 1989, Late Paleozoic thermal evolution of crystalline terranes within portions of the U. S. Appalachian orogen *in* Hatcher, R. D., Jr., Thomas, W. A., and Viele, G. W., eds., The Appalachian-Ouachita Ouachita Orogen in the United States: Boulder, Colorado, Geological Society of America, The Geology of North America, v. F-2, p. 417-444.

Dallmeyer, R. D., Hess, J. R., and Whitney, J. A., 1981, Postmagmatic cooling of the Elberton granite: bearing on the late Paleozoic tectonothermal history of the Georgia Inner Piedmont, Journal of Geology, v. 89, p. 585-600.

Dennis, A. J., 1991, Is the central Piedmont suture a low-angle normal fault?, Geology, v. 19, p. 1081-1084.

Douze, E. J., and Laster, S. J., 1979, Statistics of semblance, Geophysics, v. 44, p. 1999-2003.

Ellwood, B. B., 1980, Magnetization of the Elberton Granite, *in* Stormer, J. C., and Whitney, J. A., Geological, Geochemical, and Geophysical Studies of the Elberton Batholith, Eastern Georgia, Georgia Department of Natural Resources, Georgia Geological Survey, Guide Book 19, p. 80-97.

Ellwood, B. B., 1982, Paleomagnetic evidence for the continuity and independent movement of a distinct major crustal block in the southern Appalachians, Journal of Geophysical Research, v. 87, p. 5339-5350.

Ellwood, B. B., and Whitney, J. A., 1980, Magnetic fabric of the Elberton granite, northeast Georgia, Journal of Geophysical Research, v. 85, p. 1481-1486.

Ellwood B. B., Whitney, J. A., Wenner, D. B., Mose, D., and Amerigian, C., 1980, Age, paleomagnetism, and tec-

tonic significance of the Elberton granite, northeast Georgia Piedmont, Journal of Geophysical Research, v. 85, p. 6521-6533.

Fountain, D. M., Hurich, C. A., and Smithson, S. B., 1984, Seismic reflectivity of mylonite zones in the crust, Geology, v. 12, p. 195-198.

Griffin, V. S., 1971, The Inner Piedmont belt of the southern crystalline Appalachians, Geological Society of America Bulletin, v. 82, p. 1885-1898.

Harris, L. D., and Bayer, D. C., 1979, Sequential development of the Appalachian orogen above a master decollement - a hypothesis, Geology, v. 7, p. 568-572.

Hatcher, R. D., Jr., Tectonic synthesis of the U. S. Appalachians, 1989, *in* Hatcher, R. D., Jr., Thomas, W. A., and Viele, G. W., eds., The Appalachian-Ouachita Orogen in the United States: Boulder, Colorado, Geological Society of America, The Geology of North America, v. F-2, p. 511-535.

Hatcher, R. D., and Zietz, I., 1980, Tectonic implications of regional aeromagnetic and gravity data from the southern Appalachians, in The Caledonides in the U.S.A., edited by Wones, D. R., Department of Geological Sciences, Virginia Polytechnic Institute and State University, Memoir 2, p. 235-244.

Hatcher, R. D., Costain, J. K., Coruh, C., Phinney, R. A., and Williams, R. T., 1987, Tectonic implications of new Appalachian Ultradeep Core Hole (ADCOH) seismic reflection data from the crystalline southern Appalachians, Geophysical Journal of the Royal Astronomical Society, v. 89, p. 157-162.

Hawman, R. B., 1996, Wide-angle, three-component seismic reflection profiling of the crust beneath the East Coast Gravity High, southern Appalachians, using quarry blasts, Journal of Geophysical Research, v. 101, p. 13933-13945.

Hawman, R. B., 2004, Using delay-fired quarry blasts to image the crust: A comparison of methods for deconvolving mixed-delay source wavelets, Bulletin of the Seismological Society of America, v. 94, p. 1476-1491.

Hawman, R. B., and Phinney, R. A., 1992, Structure of the crust and upper mantle beneath the Great Valley and Allegheny Plateau of eastern Pennsylvania, Part 2: Gravity modeling and migration of wide-angle reflection data, Journal of Geophysical Research, v. 97, p. 393-415.

Hawman, R. B., Prosser, C. L., and Clippard, J. E., 2000, Shallow seismic reflection profiling over the Brevard zone, South Carolina, Geophysics, v. 65, p. 1388-1401.

Hibbard, J. P., Shell, G. S., Bradley, P. J., Samson, S. D., and Wortman, G. L., 1998, The Hyco shear zone in North Carolina and southern Virginia: Implications for the Piedmont Zone-Carolina Zone boundary in the southern Appalachians, American Journal of Science, v. 298, p. 85-107.

Hunter, J. A., Pullan, S. E., Burns, R. A., Gagne, R. M., and Good, R. L., 1984, Shallow seismic reflection mapping of the overburden-bedrock interface with the engineering seismograph - some simple techniques, Geophysics, v. 49, p. 1381-1385.

Hurich, C. A., Smithson, S. B., Fountain, D. M., and Humphreys, M. C., 1985, Seismic evidence of mylonite reflectivity and deep structure in the Kettle dome metamorphic core complex, Washington, Geology, v. 13, p. 577-580.

Iverson, W. P., and Smithson, S. B., 1982, Master decollement root zone beneath the southern Appalachians and crustal balance, Geology, v. 10, p. 241-245.

Iverson, W. P., and Smithson, S. B., 1983, Reprocessing and reinterpretation of COCORP southern Appalachian profiles, Earth and Planetary Science Letters, v. 62, p. 75-90.

Jurdy, D. M., and Phinney, R. A., 1983, Seismic imaging of the Elberton granite, Inner Piedmont, Georgia, using COCORP southern Appalachian data, Journal of Geophysical Research, v. 88, p. 5865-5873.

Khalifa, M. O., and Hawman, R. B., Short Note: Wide-angle seismic imaging of the Elberton granite, Georgia: A pilot study using instantaneous blasts at dimension-stone quarries, submitted to Geophysics.

Kong, S. M., Phinney, R. A., and Roy-Chowdhury, K., 1985, A nonlinear signal detector for enhancement of noisy seismic record sections, Geophysics, v. 50, p. 539-550.

Lynn, H. B., Hale, L. D., and Thompson, G. A.,1981, Seismic reflections from the basal contacts of batholiths, Journal of Geophysical Research, v. 86, p. 10633-10638.

Phinney, R. A., and Roy-Chowdhury, K., 1989, Reflection seismic studies of crustal structure in the eastern United States, *in* Pakiser, L. C., and Mooney, W. D., eds., Geophysical Framework of the Continental United States: Boulder, Colorado, Geological Society of America Memoir 172, p. 613-653.

Phinney, R. A., Roy-Chowdhury, K., and Frazer, L. N., 1981, Transformation and analysis of record sections, Journal of Geophysical Research, v. 86, p. 359-377.

Robinson, E. A., and Treitel, S., 1980, Geophysical Signal Analysis, Prentice-Hall, Inc., 466 pp.

Secor, D. T., Snoke, A. W., and Dallmeyer, R. D., 1986, Character of the Alleghanian orogeny in the southern Appalachians, III, Regional tectonic relations, Geological Society of America Bulletin, v. 97, p. 1345-1353.

Smithson, S. B., Brewer, J., Kaufman, S., Oliver, J., and Hurich, C. A., 1979, Structure of the Laramide Wind River Uplift, Wyoming, from COCORP deep reflection data and from gravity data, Journal of Geophysical Research, v. 84, p. 5955-5972.

West, T. E., Secor, D. T., Pray, J. R., Boland, I. B., and Maher, H. D., 1995, New field evidence for an exposure of the Appalachian decollement at the east end of the Pine Mountain terrane, Georgia, Geology, v. 23, p. 621-624.

Whitney, J. A., Paris, T. A., Carpenter, R. H., and Hartley, M. E., 1978, Volcanic evolution of the southern Slate Belt of Georgia and South Carolina: A primitive oceanic island arc, Journal of Geology, v. 86, p. 173-192.

Yilmaz. O., 1987, Seismic Data Processing, Society of Exploration Geophysicists, Tulsa, Oklahoma, 526 p.

SOUTHEASTERN GEOLOGY
V. 43, No. 4, June 2005, p. 215-227

EOCENE DISPERSAL OF THE ECHINOID GENUS *ECHINOCYAMUS* IN THE SOUTHEASTERN UNITED STATES

LOUIS G. ZACHOS

Nonvertebrate Paleontology Laboratory
Texas Memorial Museum
J. J. Pickle Research Campus, Building 122
10100 Burnet Road
Austin, Texas 78758-4445
lg_zachos@alumni.utexas.net

ABSTRACT

Seven species of *Echinocyamus* have been described from the Eocene deposits of the western hemisphere: *E. avilensis*, *E. caribbeanensis*, *E. parvus*, *E. macneili*, *E. huxleyanus*, *E. meridionalis*, and *E. bisexus*. *Echinocyamus bisexus*, *E. huxleyanus* and *E. macneili* are shown to be junior synonyms of *E. parvus*, and the remaining species are assigned to other genera. *Echinocyamus parvus* occurs in a narrow chronostratigraphic range, which correlates closely with the deposition of the Gosport Sand in southern Alabama and the Bartonian/Priabonian transition. The rapid dispersal of the species from North Carolina through Georgia and into Alabama is evidence for a short-term reversal of the current flowing through the Suwannee Channel. Stressful environmental conditions may have caused deviant reproductive adaptation in the species, and eventually led to the extinction of the genus from North America until the late Oligocene.

INTRODUCTION

The echinoid genus *Echinocyamus* (Order Clypeasteroida, Family Fibulariidae) is represented by numerous species ranging from the Eocene into the Recent. Mortensen (1948) noted that the genus is characteristically found in the Tertiary (particularly the Eocene) of the circum-Mediterranean area. The Recent species are found in the Caribbean, the coast of western Europe, the Mediterranean, eastern Africa, the Indo-Pacific, and Hawaii (Ghiold and Hoffman, 1986).

Seven species of *Echinocyamus* have been described from the Eocene deposits of the western hemisphere. *E. avilensis* Lambert from Cuba, *E. caribbeanensis* Kier from Barbados, *E. parvus* Emmons from North Carolina, *E. macneili* Cooke, *E. huxleyanus* Meyer, and *E. meridionalis* Meyer from Alabama, and *E. bisexus* Kier from Georgia.

Details are given in Systematic Paleontology to show that three of the species (*E. bisexus*, *E. huxleyanus* and *E. macneili*) are junior synonyms of *E. parvus*, and none of the remaining species should be included in the genus *Echinocyamus*. The genus is represented in the Eocene of North America by a single species, *E. parvus*.

MATERIAL AND METHODS

Ghiold and Hoffman (1984) noted that paleogeographic conclusions are inherently narrative. Circumstantial evidence, both positive and constraining (i.e., negative), is required to reveal significant aspects of the paleobiology and distribution of *Echinocyamus* in the Eocene of North America.

The author has collected over a period of several decades from the Tertiary deposits of the southeastern United States (from Texas to North Carolina), and these data are an important source of information. Collecting methodology included regular bulk sampling of outcrops when searching for these small echinoids. Nearly all specimens came from washed and screened samples. Collections deposited with the Texas Memorial Museum, Austin, Texas

(TMM), Louisiana State University Museum of Geoscience, Baton Rouge, Louisiana (LSUMG), Florida Museum of Natural History, Gainesville, Florida (FLMNH), and the U.S. National Museum of Natural History, Washington, DC (USNM) and some material from private collections were also reviewed.

AGE AND OCCURRENCE

Echinocyamus parvus (or its synonyms) has been reported from Alabama, Georgia and North Carolina. Detailed location information is given in the Appendix. The reported strata include the Lake City Limestone (lower Claiborne or Lutetian), the Gosport Sand (upper Claiborne or Bartonian), the Moodys Branch Formation (lower Jackson or Priabonian), and the Castle Hayne Limestone (lower to upper Claiborne). However, *E. parvus* is associated with the protoscutellid echinoid *Periarchus lyelli* in all occurrences except one, where it is associated with *Protoscutella plana*. Protoscutellids first appeared in the southeastern United States region (Stefanini, 1924) and the family occurs throughout the region from North Carolina to Texas. Zullo and Harris (1987) and Harris and Laws (1997) described biostratigraphic zonation of the Castle Hayne Limestone using protoscutellids. They showed that the transition from *P. plana* to the closely related *P. lyelli* corresponds to a discrete period of time at the boundary between the middle and late Eocene (Bartonian-Priabonian). *Echinocyamus parvus* first appears in North Carolina at this time, coexisted with *P. lyelli* for a short period, and then disappeared from the western hemisphere, not known from North America again until the late Oligocene, probably 12 to 14 million years later.

Little Stave Creek, Alabama

Specimens of *E. parvus* have been collected from washed samples of the Gosport Sand at this locality, along with juveniles of *Periarchus lyelli*.

Claiborne Bluff, Alabama

This is the type locality for *E. huxleyanus* (= *E. parvus*). Clark and Twitchell (1915) noted that it is found "...in some abundance..." in the Gosport Sand, and there are several specimens other than the type at the USNM. The fibulariid echinoid *Fibularia texana* is also known from the Gosport Sand at this location (Zachos and Molineux, 2003).

Conecuh River, Alabama

Recent study of several closely-spaced exposures along the Conecuh River has resulted in the collection of a number of specimens of small echinoids. Although the exact collecting location for the type of *E. macneili* (= *E. parvus*) is not known, abundant *E. parvus* were collected from a small creek on the east side of the Conecuh River that agrees with the locality description given by Cooke (1959). Faunal evidence from the *Echinocyamus*-containing beds and adjacent strata on the Conecuh indicates that the *Echinocyamus* beds are age equivalent to the Gosport Sand at Claiborne Bluff and on Little Stave Creek. The underlying section contains *Periarchus lyelli* and *Fibularia texana*, as well as the Lisbon index fossil *Cubitostrea sellaeformis* – the distinctive "saddle" oyster. The *Echinocyamus* beds contain some Gosport molluscan species, including *Bathytormus protextus* and *Turritella carinata*, as well as *F. texana* and abundant fragments of *P. lyelli*. The uppermost beds are more calcareous and lack *Echinocyamus*, but contain abundant whole *P. lyelli*. All of the section above the *Cubitostrea* ledge is lithostratigraphically Moodys Branch, although the matrix contains up to 30% quartz grains and 30% glauconite grains in a carbonate matrix, and the entire section represents the equivalent of the upper Lisbon-Gosport-Moodys Branch sequence seen at the classic section at Claiborne Bluff. The quartz grains are indistinguishable from the quartz found in the Gosport at Claiborne (unfrosted, clear, angular to subangular monocrystalline grains). No definitive age for these beds between unquestioned Lisbon and Moodys Branch has been clearly reported in the

literature. Cooke (1939) suggested that the Gosport and Moodys Branch were equivalent to some extent. MacNeil (1946) described the section along the Conecuh River and noted the ambivalent age treatment. Toulmin (1977) and the Alabama Geological Survey geologic map of Covington County (SM66, 1968) both included this section in the Moodys Branch Formation and showed it directly overlying the Lisbon Formation.

Choctawatchee River, Alabama

Cooke (1959) reported *E. parvus* from exposures doubtfully attributed to the Moodys Branch Formation from this locality near Geneva, Alabama. Material in the USNM confirms this identification. These beds are similar in nature to those on the Conecuh River, and the same age considerations apply.

United States Geological Survey (USGS) Test Well 5 (34H337), Glynn County, Georgia

The types and additional specimens of *E. bisexus* (= *E. parvus*) were collected from depth interval between 342 and 354 m in this well. Kier (1980) reported the interval was in the Lake City Formation (lower Lisbon equivalent). This was according to a determination by S.M. Herrick of the USGS based on first occurrences of what were at the time considered to be diagnostic benthic foraminifera (S.M. Herrick letter to P.M. Kier, January 9, 1967). There are several slides in the USNM with foraminifera, mollusks, brachiopods and crinoids picked from samples in this depth range. Notable is the occurrence of the foram *Discorbis inornatus*, which Applin and Jordan (1945) considered characteristic of the Lake City Formation. Miller (1986) stated that the paleontologic criteria for differentiation of the Avon Park and Lake City Formations were lacking. He specifically reported *D. inornatus* near the top of the upper Claiborne in Georgia. Kier did not give an exact location of USGS Test Well #5, but records from the USGS in Atlanta, Georgia place it about 3.2 km from USGS Test Well #26, which was described by Jones and others (2002). The depth-correlated zone in Test Well #26 to the echinoid-bearing horizon in Test Well #5 is interpreted to be near the top of the upper Claiborne section, significantly higher than the Lake City, and temporally equivalent to the Gosport Sand in Alabama. The associated echinoid fauna includes *Fibularia texana*, *Periarchus lyelli*, and *Durhamella floridana*, which also indicate upper Claiborne equivalence, although Carter and Hammack (1989) reported that the echinoids suggested a Jacksonian age for the zone.

East Coast Limestone, Inc. quarry, Maple Hill, North Carolina

Specimens of *E. parvus* were found in spoil, but in sandy matrix associated with *Protoscutella plana*. *Periarchus lyelli* also occurs in the highest section in this quarry, although it was not found in direct association with *E. parvus*.

Lanier quarry, Maple Hill, North Carolina

Kier (1980) reported both *E. parvus* and *E. bisexus* from this quarry, and this has been confirmed by material in the USNM and by later collections. *Echinocyamus parvus* is associated with *P. lyelli*.

Ideal Cement Corp. quarry, Castle Hayne, North Carolina

Reported by Kier (1980) and confirmed by material in the USNM.

Martin-Marietta quarry, Catherine Lake, North Carolina

This quarry was opened after Kier's 1980 study. Abundant *E. parvus* are found with *P. lyelli*. The variant described by Kier (1968) as *E. bisexus* is also found at this locality.

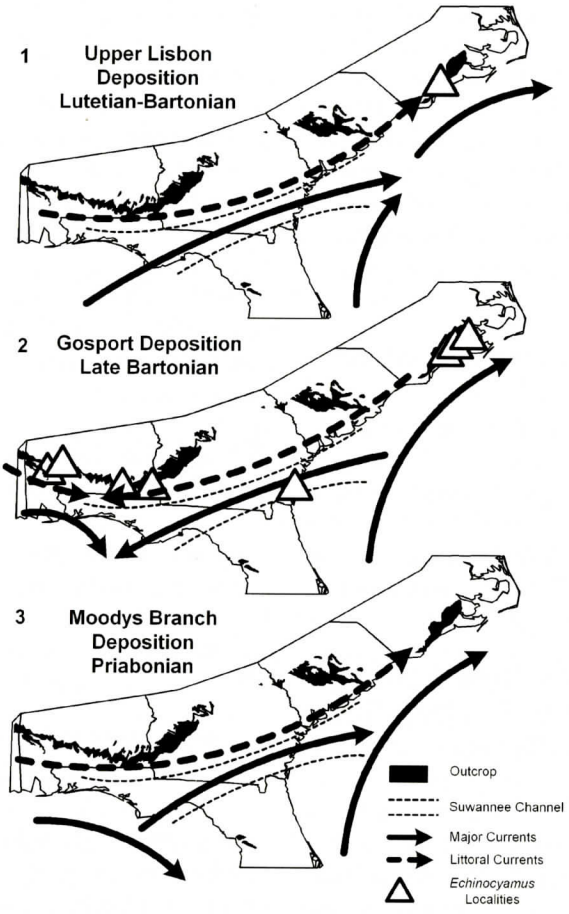

Figure 1. Eocene dispersal of *Echinocyamus parvus* in southeastern United States. Outcrop of upper Lisbon and Gosport (upper Claiborne) sediments is shown for reference. 1, Major ocean and littoral currents and location of Suwannee Channel during deposition of Upper Lisbon and equivalents, Lutetian-Bartonian. Single occurrence of *E. parvus* associated with *Protoscutella plana* in Pender County, North Carolina. 2, Reversal of currents through Suwannee Channel, with dispersal of *E. parvus* into Georgia and Alabama during deposition of Gosport and equivalents, Late Bartonian. 3, Reestablishment of currents through the Suwannee Channel during deposition of Moodys Branch and equivalents, Priabonian, with disappearance of *Echinocyamus*.

Thomas Farm, Onslow County, North Carolina

The exact location is not known, but was about "10 miles northwest of Jacksonville" (Kellum, 1926), and judging from Kellum's map it was within 2 or 3 km of Catherine Lake. The Kellum material is at the USNM.

Craven County, North Carolina

Emmons (1858) gave the type locality for *E. parvus* as Craven County, but no other information is available. The type itself has been missing for nearly a century. Emmons also reported *Periarchus lyelli* from Craven County.

The stratigraphic and geographic distribution of *E. parvus* is constrained by non-occurrences (absences). Negative evidence is suspect in the paleontological record, but in this case there are several things that reduce the uncertainty. Kidwell and Holland (2002) note that biomineralized taxa are reasonably well represented in the geologic record, especially at the genus or high-

er taxonomic level. The occurrences of other echinoid genera, particularly *Fibularia*, where *Echinocyamus* is absent serve as proxies, or what Kidwell and Holland (2002) term "taphonomic control taxa". Finally, when *E. parvus* is found it is usually found in abundance, which negates the Signor-Lipps effect (see Newman and Palmer, 1999). Decreased spatial or temporal resolution due to mixing by postmortem transport or poor collecting methodology is a problem in accurate determination of appearance or extinction of a taxon, but makes absence data more robust by increasing the likelihood that specimens from outside the targeted stratum will occur in a sample, if the samples are large enough to capture such occurrences.

Lower Claiborne, Texas to Alabama

The genus has not been reported from Lisbon (or equivalents) or older beds of Florida, Alabama, Mississippi, Louisiana, or Texas. Hundreds of specimens of *Fibularia texana* and juvenile sand dollars have been collected from the lower Claiborne beds of Texas without a single *Echinocyamus*.

Lower Castle Hayne Limestone, North and South Carolina

The genus does not occur in the oldest sections of the Castle Hayne Formation and is not known in association with *Protoscutella conradi*, *P. tuomeyi*, nor susbspecies of *P. mississippiensis*.

Moodys Branch Formation, Mississippi and Alabama

The only reported Moodys Branch occurrences are from the Gosport-equivalent sections discussed previously. No *Echinocyamus* are known from the Moodys Branch exposures at Jackson, Mississippi or Claiborne Bluff or Little Stave Creek in Alabama.

Lower Ocala (Inglis beds), Florida

The genus has never been reported from the Ocala Limestone of Florida. A large washed sample at the FLMNH taken from the Inglis beds of the Ocala Limestone (Moodys Branch equivalent) along the Cross Florida Barge Canal in Citrus County, Florida contained 15,324 echinoids, including 7,071 *Fibularia vaughani* and more than 4,000 juvenile sand dollars, but not a single *Echinocyamus*.

Creola member, Yegua Formation, Texas and Louisiana

A fossiliferous zone in the upper portion of the Yegua Formation was described by Stenzel (1940) and named by him the Creola member. Stratigraphically below the Moodys Branch at the Creola Bluff (Montgomery Landing) locality on the Red River in Louisiana, the section was correlated by Stenzel with the Gosport Sand of Alabama. The type section is now below water level, but no echinoids of any type have been found in Stenzel's collections at the TMM and LSUMG. In addition, no *Echinocyamus* have been reported from the Moodys Branch Formation at Montgomery Landing.

PALEOGEOGRAPHIC SIGNIFICANCE

The Suwannee Channel, extending from the Florida panhandle through southern Georgia, was a negative structure during the middle and late Eocene, and experienced strong current flow from the Gulf of Mexico into the Atlantic Ocean north of the Blake Nose (Popenoe and others, 1987). This structural feature has been called variously the Gulf trough, Suwannee Strait or Suwannee Channel (see McKinney, 1984). During the Lutetian and Bartonian (Lisbon deposition) deep-water conditions across the Florida/Bahamas platform and southern Georgia permitted spillover of currents from the Gulf of Mexico into the Atlantic Ocean via the Suwannee Channel (Figure 1-1). Popenoe and others (1987) have shown that the current magnitude through the Suwannee Channel was di-

rectly related to water depth. A eustatic fall in sea level during the late Bartonian (Gosport deposition) is evidenced by an unconformity at the top of the Avon Park Formation that implies very shallow, possibly subaerial, conditions across the Florida-Bahamas platform and seaward migration of the coastline along the Gulf of Mexico from at least Texas to Alabama. This coincides with the dispersal of *Echinocyamus* into Alabama from North Carolina, and indicates a reversal of surface current flow bringing planktonic *Echinocyamus* larvae into the Gulf of Mexico (Figure 1-2). The deposition of the Gosport Sand itself is likely the result of a convergence of littoral currents and longshore drift across this 65 km stretch of northern Gulf of Mexico shoreline. There are two modern analogues: the shell beaches formed by the convergence of littoral currents along the Texas Coastal Bend (Watson, 1971) and the extensive shell deposits centered at Sanibel Island, Florida – an analogue first described by Gardner (1957). A reversal of current through the Suwannee Channel would also have created a convergence off the coast of North Carolina, which may have resulted in the thick bryozoan-echinoderm grainstone/packstone facies described by Coffey and Read (2004) in the upper Castle Hayne Limestone. These high-energy current regimes are the favored habitat for the extant species *Echinocyamus pusillus* (Telford, and others, 1983). The subsequent rise in eustatic sea level during deposition of Jackson Stage (Priabonian) sediments reestablished the earlier current regime (Figure 1-3). Environmental conditions, most importantly changes in current patterns and larval dispersal paths but possibly including sea temperature and nutrition sources, became inhospitable for *Echinocyamus* and led to its subsequent disappearance from North America.

The Suwannee Channel has been envisioned as a barrier to faunal mixing (Cheetham, 1963) and a boundary between facies (Chen, 1965), or a coincidental topographic feature with only minor relationship to faunal distribution (Carter and McKinney, 1992). It can also be recognized as an avenue for faunal mixing and propagation. The panmictic populations and lack of vicariance of the endemic protoscutellids from the upper Texas coast to North Carolina during the middle Eocene indicates that the Gulf trough was not a barrier to larval dispersal. Rather, the suspected reversal that explains dispersal of *Echinocyamus* into the Gulf of Mexico could have been episodic, ensuring panmixis of the protoscutellid population. Lambert and Thiéry (1925) and Kier and Lawson (1978) collectively list 29 species of *Echinocyamus* from the Lower to Upper Eocene of Africa and Europe. The sudden appearance of a single species relatively late in the Eocene and its rapid dispersal from North Carolina to Alabama is evidence that the genus was exotic to North America. The ultimate source of the species may have been via the equatorial current from Africa (see discussions of paleocurrents by Poddubiuk and Rose, 1984; Chirat, 2000).

SYSTEMATIC PALEONTOLOGY

Family Fibulariidae Gray, 1855
Genus *Echinocyamus* van Phelsum, 1774
***Echinocyamus parvus* Emmons, 1858**
Figures 2-3, 2-4, 2-5, 2-6, 2-7
***Echinocyamus parvus* Emmons, 1858: 307, fig. 244; Clark and Twitchell, 1915: 119; Kellum, 1926: 14; Cooke, 1942: 28, pl. 1, figs. 6-8; 1959: 31, pl. 9, figs. 9-11; Kier, 1966: figs. 10, 11, 13b; Toulmin, 1977:360; Kier, 1980:34, pl. 10, figs. 5-10.**
***Echinocyamus huxleyanus* Meyer, 1886: 85, pl. 3, fig. 23; Gregorio, 1890: 251, pl. 43, fig. 15 (after Meyer); Clark and Twitchell, 1915: 119, pl. 57, figs. 1a-d; Cooke, 1942: 29, pl. 1, figs. 1-5; 1959: 32, pl. 9, figs. 12-14; Kier, 1966: figs. 10, 11, 12e; Toulmin, 1977: 360.**
***Echinocyamus macneili* Cooke, 1959: 32-33, pl. 9, figs. 6-8; Kier 1966: figs. 10, 11, 13a; Toulmin, 1977: 360.**
***Echinocyamus bisexus* Kier, 1968: 12-21, figs. 11-23, pl. 3, figs 1-6, pl. 4, figs. 1, 2; 1980: 34-35, pl. 10, fig. 11.**

Diagnosis: Small, rarely more than 6 mm length. Petals relatively short, pore series parallel to slightly divergent, pore pairs oblique and

non-conjugate. One hydropore; four (sometimes only three) genital pores, diameters larger in females (Figure 2-7), distance between pores variable. Peristome round, two more or less conspicuous buccal pores in each ambulacrum, no buccal tubes or peristomial points, no ambulacral grooves. Tubercles irregularly arranged, but distinct ring of tubercles surrounds peristome. Accessory pores distinct, restricted to adoral ambulacra. Periproct located about midway between peristome and posterior of test, submarginal in some immature specimens (Figure 2-4). Ten internal radiating walls or buttresses, two associated with each ambulacrum.

Discussion: Clark and Twitchell (1915) reported the type missing from Williams College. Handwritten notes in the type collection at the USNM indicate that at the time Twitchell transferred several other types from Williams College to the USNM. Cooke (1959) reported that the type was not located with Emmons' other types at Williams College. Markes Johnson of Williams College (personal communication) reports that the Emmons collection was transferred to the Smithsonian many years ago, but searching of the collections at the USNM revealed only vertebrate material derived from the Emmons Collection and the echinoid types transferred by Twitchell. Emmons listed the type locality as Craven County, North Carolina. Clark and Twitchell (1915) indicated that the specimen was "Very probably from the Trent marl" (which was thought to be Claiborne in age and underlying the Castle Hayne), but Kellum (1926) stated that he had "... found it ... associated with typical Castle Hayne forms and therefore considers it as belonging to that horizon." Emmons' figure certainly appears to represent the species we refer to *E. parvus,* and is much narrower than *E. wilsoni* Kier (1997) from the Oligocene Belgrade Formation in Onslow County, N.C. Emmons noted that the crinoid *Microcrinus conoideus* was also from the Eocene of Craven County "...and associated with *Echinocyamus parvus*". The author has found *Microcrinus* with *Echinocyamus* at the Lanier quarry at Maple Hill, North Carolina, and it also occurs in the samples from USGS Test Well 5 from Glynn Co., Georgia. Emmons also listed *Periarchus lyelli* from the Eocene of Craven County.

Echinocyamus huxleyanus Meyer was described from the Gosport Sand at Claiborne Bluff in Alabama. *Echinocyamus macneili* was described from a single specimen collected from beds along the Conecuh River in southeastern Alabama, reportedly from the Moodys Branch Formation (but see earlier discussion). Comparison with recent collections of abundant *Echinocyamus* from the type area along the Conecuh River reveals no significant differences. None of these specimens can be confidently differentiated from specimens of *E. parvus* from North Carolina.

Mortensen (1948) noted that the size of the genital pores differs between males and females of species of *Echinocyamus* due to differences in the genital papillae. Kier (1968) suggested that the large, widely-spaced genital pores in *E. bisexus* indicated production of large, yolky eggs, implying a lecithotropic (non-feeding) larval stage. The genital pores are developed in the paired interambulacra (rather than in the genital plates). The occurrence of genital pores in the interradii has been reported for other clypeasteroid echinoids (Mortensen, 1948, describes this for *Clypeaster rosaceus, Peronella peronii*, and *Laganum putnami,* although he does not suggest a cause) and so is not surprising in *E. parvus*. Kier further stated that it is impossible to distinguish males of *E. bisexus* from males of *E. parvus*. He subsequently found *E. bisexus* in samples from the Lanier quarry in North Carolina, but could only distinguish very small, sexually precocious forms with developed genital pores (in the interradii). This is also the case for specimens from the Martin-Marietta quarry at Catherine Lake (Figure 2-3) – with the implication that either the adult females of *E. bisexus* are indistinguishable from *E. parvus*, or juveniles of *E. bisexus* fail to survive to adulthood as a result of this accelerated sexual maturity. Given the overall rarity of preserved juveniles of any echinoid, the fossil record may under-record such aberrancy.

Although sexual dimorphsm expressed in the size and arrangement of genital pores is characteristic of *E. parvus* throughout its range, ex-

Figure 2. All images at same scale, 1-6 and 9-11 coated with NH_4Cl. 1,2, *Periarchus lyelli*, USNM 526246, Locality Ala-1, aboral and oral views. 3, *Echinocyamus parvus*, "bisexus" variant, USNM 526253, Locality NC-1, aboral view. 4, *E. parvus*, USNM 526252, Locality Ala-3, oral view. 5,6, *E. parvus*, USNM 526251, Locality Ala-1, aboral and oral views, male. 7, *E. parvus*, USNM 559481, Locality Ala-2, aboral view, female. Figured by Clark and Twitchell (1915, Pl. LVII, Figs. 1a-d) as *E. huxleyanus*. 8, *P. lyelli*, USNM 526250, Locality Ala-4, acid-etched, section showing internal buttressing, viewed from aboral side. 9, 10, *P. lyelli*, USNM 526249, Locality Ala-3, aboral and oral views, 11, *P. lyelli*, USNM 526247, Locality Ala-3, aboral view. 12, *P. lyelli*, USNM 526248, Locality Ala-3, photographed wet, section showing internal buttressing, viewed from aboral side.

treme deviant stages (*E. bisexus*) are known only from Georgia and North Carolina (and only from juvenile forms in the latter case). The question is whether this has led to the development of two sympatric species, or if the *E. bisexus* form is an individual deviancy. The early sexual maturity shown by the *E. bisexus* form could be considered a form of heterochrony (specifically progenesis), but the formation of genital pores outside the genital plates is not part of the normal ontogeny of any echinoid. It is unlikely that the two distinct forms indicate phenotypic plasticity within *E. parvus*, expressing itself as multiple development modes or poecilogony, which has not been reported in echinoids.

Lawrence and Herrera (2000) list several characteristics of stress-induced deviant reproduction in echinoderms. *E. bisexus* shows the characteristics of (1) accelerated sexual maturity, (2) increased egg size – with implication of change from typical planktotrophic (feeding) to lecithotropic (non-feeding) larvae. If, as concluded here, *E. bisexus* is a deviant form of *E. parvus*, there is the suggestion of an adaptive response to environmental stress. Pearse (1969) studied the causes of reproductive periodicities in tropical echinoids and concluded that nutrient availability and sea temperature were likely the most important parameters determining the timing of gametogenesis. The small size of some of the *E. bisexus* forms is evidence that they were at most only weeks past metamorphosis, when settlement of the larvae must have been on hospitable substrate at acceptable temperature and salinity. Environmental conditions changed rapidly enough to force the accelerated sexual maturity and increased egg and yolk size but not immediately kill the animal. Because of limited internal volume of the echinoid, gonad growth occurs at the expense of digestive organs. Starvation could have been the impetus for the changes seen, possibly coupled with an abrupt change in sea temperature. The modern species *E. pusillus* feeds primarily on diatoms and other organic debris adhering to substrate particles (Telford and others, 1983). Any conditions affecting the abundance of diatoms in the bottom sediment could have indirectly stressed the *E. parvus* population.

Genus *Fibularia* Lamarck, 1816

Fibularia avilensis (Lambert, 1931), new combination

Echinocyamus avilensis Lambert, 1931: 298-299, fig. 2.

Diagnosis: Small, globose. Petals relatively short, pore series parallel to slightly divergent, pore pairs oblique and non-conjugate. Four genital pores. Peristome round, periproct circular, located about midway between peristome and posterior of test. No internal buttresses.

Discussion: *Echinocyamus avilensis* Lambert, as noted by Kier (1968), was never adequately figured, and the location of the type is not known. The reported dimensions of the species, as well as Lambert's interchanged usage of the genera *Echinocyamus* and *Fibularia* (see Mortensen, 1948; confirmed by Lambert's (1931, p. 299) explicit reassignment of *Fibularia jacksoni* Hawkins 1927 to *Echinocyamus*), indicates that this species should be referred to the latter genus.

Genus *Fibulaster* Lambert and Thiéry, 1925

Fibulaster? caribbeanensis (Kier, 1966), new combination

Echinocyamus caribbeanensis Kier, 1966: 7-8, figs. 10-12, pl. 1, figs. 4, 5.

Diagnosis: Small, thick test. Petals relatively short, pore series parallel to slightly divergent, pore pairs oblique and non-conjugate, anterior petal (III) longer than others. Four genital pores. Peristome round, sunken, two more or less conspicuous buccal pores in each ambulacrum, no buccal tubes or peristomial points, no ambulacral grooves. Accessory pores along suture between ambulacral and interambulacral plates past petals. Periproct marginal to submarginal, protruding slightly. Internal structure unknown.

Discussion: Two paratypes of this species are retained in the collections of the USNM (USNM 328794 and USNM 328795). Both specimens show a degree of inflation more typical of *Fibularia* than *Echinocyamus*. *Echinocyamus caribbeanensis*, with its slightly protruding and marginal or nearly marginal periproct is tentatively referred to *Fibulaster*.

Fibulaster? caribbeanensis was described from the Scotland Formation on Barbados, from the Upper, Middle, and Lower Chalky Mount members and the older Murphys Member, suggesting a middle through upper Eocene range (Vaughan, 1945). However, more recent studies of the stratigraphy of Barbados (Speed, 1983) indicate a lack of stratigraphic coherence in the Chalky Mount area of Barbados, casting uncertainty on the accurate age of occurrence. The faunal associations tend to indicate a Bartonian or Priabonian age.

Family Protoscutellidae Durham, 1955
Genus *Periarchus* Conrad, 1866
***Periarchus lyelli* (Conrad, 1834)**
Figures 2-1, 2-2, 2-8, 2-9, 2-10, 2-11, 2-12
***Periarchus lyelli* (Conrad). See Zachos and Molineux, 2003 for full synonymy.**
***Echinocyamus meridionalis* Meyer, 1887: 12, pl. 2, figs. 21, 21a; Gregorio, 1890: 251, pl. 43, figs 13, 14 (after Meyer); Cooke, 1942: 29; 1959: 32, pl. 9, figs. 4, 5; Kier, 1966: fig. 10; Toulmin, 1977: 360.**
***Fibularia meridionalis* (Meyer). Clark and Twitchell, 1915: 121, pl. 57, figs. 3a-d.**

Diagnosis: Petals poorly defined in juveniles less than 6 mm length. Apical system eccentric anteriorly, often sunken (Figure 2-9), this region of test weak; genital pores undeveloped in juveniles. Periproct circular to elongate, nearer posterior margin in small juveniles, closer to midpoint between peristome and margin in larger juveniles. Ambulacral grooves present in larger juveniles, buccal tubes or peristomial points protrude into peristome (Figures 2-2, 2-10) and complex internal buttressing (Figures 2-8, 2-12) present at all sizes.

Discussion: The holotype of *E. meridionalis*, USNM 559486, is broken in the apical region of the test. This affords a look at the internal structure of the test and reveals complex radial internal buttresses. Four additional specimens, USNM 559485, one figured by Cooke (1959), are missing from the USNM collection. The fragment noted by Cooke (1942, p. 29), USNM 166502, and specimens from the Conecuh River localities also show complex internal buttresses. Immature individuals of *Periarchus lyelli* show identical internal structure. Clark and Twitchell (1915) reported only rudimentary petals or genital pores, an indication of immaturity common in the Protoscutellidae. In addition, the primitive stage of petal development of specimens referred to *E. meridionalis* is the same as that seen in the early stages of an ontogenetic series of *P. lyelli*. The location of the periproct is more marginal than expected for *P. lyelli*, but the location of the periproct appears to migrate towards the peristome during early growth of the individual. Clark and Twitchell (1915, p. 122) noted "faint radiating creases" (ambulacral grooves) on some specimens. The breakage of the peripetalous region on the holotype is characteristic of damage seen in immature protoscutellids, and uncharacteristic of fibulariids, which usually break along the ambitus or transversely.

Clark and Twitchell (1915, p. 122) noted that *E. meridionalis* "...occurs in comparative abundance..." in the Gosport Sand at Claiborne, Alabama. Meyer (1887) also reported it from Jackson, Mississippi, probably from the Moodys Branch Formation. These occurrences would be expected for juveniles of *Periarchus lyelli*.

ACKNOWLEDGMENTS

Appreciation is extended to J. Thompson, M. Florence, D. Levin, and T. Peters, Smithsonian Institution, Washington, D.C. for their assistance with the USNM collections; and also to R. Barnum and L. Gunning, Alexandria, VA for their hospitality during my stays in the Washington area. Specimens from Little Stave Creek were provided by C.L. Garvie, Leander, TX, and from the Conecuh River by M. Dye, Birmingham, AL. Information on well 34H337 was provided by R. Allen, USGS, Atlanta, GA. The manuscript benefited from critical reviews by C. Ciampaglio, Wright State University, Celina, OH; A. Molineux, Texas Memorial Museum, Austin, TX; and R. Portell, Florida Museum of Natural History, Gainesville, FL.

REFERENCES CITED

Applin, E. R. and Jordan, L., 1945, Diagnostic foraminifera from subsurface formations in Florida, Journal of Paleontology, v. 19, no. 2, p. 129-148.

Carter, B. D. and Hammack, R. E., 1989, Stratigraphic distribution of Jacksonian (Priabonian) echinoids in Georgia: Comparison and suggested correlations with Florida and the Carolinas, Palaios, v. 4, p. 86-91.

Carter, B. D. and McKinney, M. L., 1992, Eocene echinoids, the Suwannee Strait, and biogeographic taphonomy, Paleobiology, v. 18, no. 3, p. 299-325.

Cheetham, A. H., 1963, Late Eocene zoogeography of the eastern Gulf coast, Geological Society of America Memoir 91, 113 p.

Chen, C. S., 1965, The regional lithostratigraphic analysis of Paleocene and Eocene rocks of Florida, Florida Geo-

logical Survey Bulletin 45, 105 p.

Chirat, R., 2000, The so-called 'cosmopolitan palaeobiogeographic distribution' of Tertiary Nautilida of the genus *Aturia* Bronn 1838: the result of post-mortem transport by oceanic palaeocurrents, Palaeogeography, Palaeoclimatology, Palaeoecology, v. 157, p. 59-77.

Clark, W. B. and Twitchell, M. W., 1915, The Mesozoic and Cenozoic Echinodermata of the United States, United States Geological Survey Monograph 54, 341 p.

Coffey, B. P. and Read, J. F., 2004, Mixed carbonate-siliclastic sequence stratigraphy of a Paleogene transition zone continental shelf, southeastern USA, Sedimentary Geology, v. 166, p. 21-57.

Conrad, T. A., 1834, Observations on the Tertiary and more recent formations of a portion of the southern states, Journal of the Academy of Natural Sciences of Philadelphia, v. 7, no. 1, p. 116-154.

Conrad, T. A., 1866, Check list of the invertebrate fossils of North America: Eocene and Oligocene, Smithsonian Miscellaneous Collections, v. 7, no. 200, p. 1-41.

Cooke, C. W., 1939, Equivalence of the Gosport sand to the Moodys marl, Journal of Paleontology, v. 13, no. 3, p. 337-340.

Cooke, C. W., 1942, Cenozoic irregular echinoids of eastern United States, Journal of Paleontology, v. 16, no. 1, p. 1-62.

Cooke, C. W., 1959, Cenozoic echinoids of eastern United States, United States Geological Survey Professional Paper 321, 106 p.

Durham, J. W., 1955, Classification of clypeasteroid echinoids, California University Publications in Geological Sciences, v. 31, no. 4, p. 73-198.

Emmons, E., 1858, Report of the North Carolina Geological Survey: Agriculture of the Eastern Counties; Together with Descriptions of the Fossils of the Marl Beds. Raleigh, Henry D. Turner, 314 p.

Gardner, J. A., 1957, Little Stave Creek, Alabama – Paleoecologic study, Chapter 20, p. 573-587. *In* H. S. Ladd, Treatise on Marine Ecology and Paleoecology, vol. 2, Paleoecology, Geological Society of America Memoirs 67.

Ghiold, J. and Hoffman, A., 1984, Clypeasteroid echinoids and historical biogeography, Neue Jahrbuch Geologie Paläontologie, Mh., v. 9, p. 529-538.

Ghiold, J. and Hoffman, A., 1986, Biogeography and biogeographic history of clypeasteroid echinoids, Journal of Biogeography, v. 13, p. 183-206.

Gray, J. E., 1855, An arrangement of the families of Echinida, with descriptions of some new genera and species, Proceedings of the Zoological Society, London, v. 23, p. 35-39.

Gregorio, A. de, 1890, Monographie de la faune éocènique de l'Alabama, Annales de Géologie et de Paleontologie, Palermo, v. 7-8, 316 p.

Harris, W. B. and Laws, R. A., 1997, Paleogene stratigraphy and sea-level history of the North Carolina Coastal Plain: global coastal onlap and tectonics, Sedimentary Geology, v. 108, p. 91-120.

Hawkins, H. L., 1927, Descriptions of new species of Cainozoic echinoidea from Jamaica, p. 76-84, *In* B. W. Arnold and H. L. Clark, 1927, Jamaican fossil echini, Memoirs of the Museum of Comparative Zoology at Harvard College, v. 50, no., 1, 76-84 p.

Jones, L. E., Prowell, D. C., and Maslia, M. L., 2002, Hydrogeology and water quality (1978) of the Floridan Aquifer System at U.S. Geological Survey Test Well 26, on Colonels Island, near Brunswick, Georgia, United States Geological Survey Water-Resources Investigations Report 02-4020, 44 p.

Kellum, L. B., 1926, Paleontology and stratigraphy of the Castle Hayne and Trent marls in North Carolina, United States Geological Survey Professional Paper 143, 56 p.

Kidwell, S. M. and Holland, S. M., 2002, The quality of the fossil record: implications for evolutionary analyses, Annual Review of Ecology and Systematics, v. 33, p. 561-588.

Kier, P. M., 1966, Four new Eocene echinoids from Barbados, Smithsonian Miscellaneous Collections, v. 151, no. 9, 28 p.

Kier, P. M., 1968, Echinoids from the Middle Eocene Lake City Formation of Georgia, Smithsonian Miscellaneous Collections, v. 153, no. 2, 45 p.

Kier, P. M., 1980, The echinoids of the Middle Eocene Warley Hill Formation, Santee Limestone, and Castle Hayne Limestone of North and South Carolina, Smithsonian Contributions to Paleobiology, no. 39, 102 p.

Kier, P. M., 1997, Oligocene Echinoids of North Carolina, Smithsonian Contributions to Paleobiology, no. 83, 37 p.

Kier, P. M. and Lawson, M. H., 1978, Index of Living and Fossil Echinoids 1924-1970, Smithsonian Contributions to Paleobiology, no. 34, 182 p.

Lamarck, J. B. P. A. de, 1816, Histoire naturelle des animaux sans vertèbres, 3, Paris, 586 p.

Lambert, J., 1931, Note sur le groupe des *Oligopygus* la nouvelle famille des *Haimeidae* et sur quelques Échinides fossiles de Cuba. Bulletin de la Société Géologique de France, Série 5, Tome 1, p. 289-304.

Lambert, J., and Thiéry, P., 1925, Essai de nomenclature raisonnée des Échinides, Libraire L. Ferrière (Chaumont), 607 p.

Lawrence, J. M. and Herrera, J., 2000, Stress and deviant reproduction in echinoderms, Zoological Studies, v. 39, no. 3, p. 151-171.

McKinney, M. L., 1984, Suwannee Channel of the Paleogene Coastal Plain: support for the "carbonate suppression" model of basin formation, Geology, v. 12, p. 343-345.

MacNeil, F. S., 1946, The Tertiary formations of Alabama, Southeastern Geological Society, 4th Field Trip Guidebook, 91 p.

Meyer, O., 1886, Contributions to the Eocene paleontology of Alabama and Mississippi, Alabama Geological Survey Bulletin 1, p. 63-85.

Meyer, O., 1887, Beiträg zur Kenntniss der Fauna der Alttertiärs von Mississippi und Alabama, Bericht der

Senckenbergische Naturforschende Gesellchaft, Abhandlungen, p. 1-22.

Miller, J. A., 1986, Hydrogeologic framework of the Floridan Aquifer System in Florida and in parts of Georgia, Alabama, and South Carolina:Regional Aquifer-System Analysis, United States Geological Survey Professional Paper 1403-B, p. B1-B91.

Mortensen, Th., 1948, A Monograph of the Echinoidea, IV(2), Clypeastroida, C. A. Reitzel, Copenhagen, 471 p.

Newman, M. E. J. and Palmer, R. G., 1999, Models of Extinction: A Review, Sante Fe Institute Working Paper 99-08-061, 49 p.

Pearse, J. S., 1969, Reproductive periodicities of Indo-Pacific invertebrates in the Gulf of Suez. II. The echinoid *Echinometra mathaei* (de Blainville), Bulletin of Marine Science, v. 19, no. 3, p. 580-613.

Poddubiuk, R. H. and Rose, E. P. F., 1984, Relationships between mid-Tertiary echinoid faunas from the central Mediterranean and eastern Caribbean and their palaeobiogeographic significance, Annales Geologiques des Pays Helleniques, v. 32, p. 115-128.

Popenoe, P., Henry, V. J., and Idris, F. M., 1987, Gulf trough – the Atlantic connection, Geology, v. 15, p. 327-332.

Speed, R. C., 1983, Structure of the accretionary complex of Barbados, I: Chalky Mount, Geological Society of America Bulletin, v. 94, p. 92-116.

Stefanini, G., 1924, Relations between American and European Tertiary echinoid faunas, Geological Society of America Bulletin, v. 35, p. 827-846.

Stenzel, H. B., 1940, The Yegua problem, University of Texas Publication 3945, Austin, p. 847-910.

Telford, M., Harold, A. S., and Mooi, R., 1983, Feeding structures, behavior, and microhabitat of *Echinocyamus pusillus* (Echinoidea: Clypeasteroida), Biological Bulletin, v. 165, p. 745-757.

Toulmin, L. D., 1977, Stratigraphic distribution of Paleocene and Eocene fossils in the eastern Gulf Coast region (2 volumes), Geological Survey of Alabama, Monograph 13, 602 p.

Vaughan, T. W., 1945, American old and middle Tertiary larger foraminifera and corals, Part I – American Paleocene and Eocene larger foraminifera, Geological Society of America Memoir 9, 175 p.

Van Phelsum, M., 1774, Brief aan Cornelius Nozeman over de Gewelv-Siekken of Zee-Engeln, Rotterdam, 145 p.

Watson, R. L., 1971, Origin of shell beaches, Padre Island, Texas, Journal of Sedimentary Petrology, v. 41, no. 4, p. 1105-1111.

Zachos, L. G. and Molineux, A., 2003, Eocene echinoids of Texas, Journal of Paleontology, v. 77, no. 3, p. 491-508.

Zullo, V. A. and Harris, W. B., 1987, Sequence stratigraphy, biostratigraphy, and correlation of Eocene through lower Miocene strata in North Carolina, Cushman Foundation for Foraminiferal Research, Special Publication 24, p. 197-214.

APPENDIX

Localities

Ala-1, Little Stave Creek, upper section, approximately 1 km north of Jackson, SE/4 Sec. 20, T7N, R2E, Clarke County, Alabama. Geographic coordinates: 31° 33' 21" N 87° 53' 19" W; UTM Zone 16 (NAD27) coordinates: Easting 415,650m Northing 3,491,370m

Ala-2, Claiborne Bluff, left bank of Alabama River at US Highway 84 bridge, NW/4, Sec. 25, T7N, R5E, Monroe County, Alabama. Geographic coordinates: 31° 32' 48" N 87° 30' 57" W; UTM Zone 16 (NAD27) coordinates: Easting 451,050m Northing 3,490,120m

Ala-3, Right bank of Conecuh River at mouth of Fall Creek, 200 m upstream of County Road 42 bridge, west of Andalusia, SW/4 SE/4 Sec. 29, T4N, R15E, Covington County, Alabama. Geographic coordinates: 31° 16' 45" N 86° 34' 12" W; UTM Zone 16 (NAD27) coordinates: Easting 540,933m Northing 3,460,429m

Ala-4, Creek on left side of Conecuh River, 80 meters south of County Road 42 bridge, west of Andalusia, NW/4 NE/4 NE/4 Sec. 32, T4N, R15E, Covington County, Alabama. Geographic coordinates: 31° 16' 36" N 86° 34' 7" W; UTM Zone 16 (NAD27) coordinates: Easting 541,056m Northing 3,460,147m

Ala-5, Railroad bridge over Choctawatchee River at Geneva, NW/4 SW/4 Sec. 28, T1N, R16W, Geneva County, Alabama. Geographic coordinates: 31° 1' 39" N 85° 51' 21" W; UTM Zone 16 (NAD27) coordinates: Easting 609,200m Northing 3,433,040m

Ga-1. U.S.G.S. Test Well #5 (34H337) located on the west side of the railroad tracks, between London and Albermarle Streets, in Brunswick, Glynn County, Georgia. Geographic coordinates: 31° 8' 24" N 81° 29' 43" W UTM Zone 17 coordinates (NAD27): Easting 452,785m Northing 3,445,038m

NC-1, Martin-Marietta quarry, south of County Road 1223, about 2.25 km NNE of Catherine Lake, Onslow County, North Carolina. Geographic coordinates: 34° 50' 10" N 77° 33' 3" W; UTM Zone 18 (NAD27) coordinates:

Easting 266,725m Northing 3,857,645m

NC-2, East Coast Limestone, Inc. quarry, 1.3 km SW of intersection of State Roads 50 and 53, 2.5 km WNW of Maple Hill, Pender County, North Carolina. Geographic coordinates: 34° 39' 53" N 77° 43' 22" W; UTM Zone 18 (NAD27) coordinates: Easting 250,500m Northing 3,839,040m

NC-3, Lanier quarry, about 4.25 km SSE of Maple Hill, 0.6 km south cemetery off County Road 1532, Pender County, North Carolina. Geographic coordinates: 34° 37' 36" N 77° 40' 35" W; UTM Zone 18 (NAD27) coordinates: Easting 254,645m Northing 3,834,715m

NC-4, Ideal Cement Co. quarry, south of junction of Island Creek with Northeast Cape Fear River, at end of County Road 2023, 7.2 km NE of Castle Hayne, New Hanover County, North Carolina. Geographic coordinates: 34° 22' 35" N 77° 49' 36" W; UTM Zone 18 (NAD27) coordinates: Easting 240,080m Northing 3,807,325m

NC-5, J. M. Thomas Farm, "10 miles northwest of Jacksonville", Onslow County, North Carolina (Kellum, 1926, Locality 10636).

NC-6, Craven County, North Carolina (Emmons, 1858).

SOUTHEASTERN GEOLOGY
V. 43, No. 4, June 2005, p. 229-247

SAND TEXTURE AND COMPOSITION IN SMALL, SOUTHERN APPALACHIAN STREAMS: INDICATIONS OF SEDIMENT ORIGIN AND TRANSPORT PROCESSES

DAVID C. SHELLEY[1] AND C. BRANNON ANDERSEN[2]

[1] *Department of Geological Sciences*
University of South Carolina
Columbia, South Carolina, 29208
[2] *Department of Earth and Environmental Sciences*
Furman University
Greenville, South Carolina 29613

ABSTRACT

Sand grains associated with intense chemical weathering during residence in pedogenic and alluvial storage environments have been described in clastic fluvial sediment loads. These phases are labile, but their behavior in stream sediments has not been systematically studied. The purpose of this study was to determine the abundance of weathered particles in stream sediments from two streams in Mountain Lake watershed, Paris Mountain, South Carolina. The distribution of weathered particles was then compared with stream profile, sand composition, and texture data in order to assess controls on weathered particle distribution in light of bulk downstream trends. An undifferentiated assemblage of schists and gneisses underlies the watershed. Sixty-five sample localities were established along Kaufman and Hartness Creeks, which are second order systems. All samples were analyzed for grain size distribution. Grain mounts of the medium sand fraction of 20 selected samples were prepared for petrographic analysis. The results indicate that sediments in Mountain Lake watershed are texturally and compositionally immature. Both streams show a slight downstream trend with respect to improved sorting. Kaufman Creek shows a slight downstream trend with respect to increasing grain sizes. There are no systematic downstream changes in weathered particle abundance or bulk composition, but sediment compositions in the two creeks are very distinct. The lack of alluvial storage, related to the steep slope, and rapid export of material minimize *in situ* alteration within the streams, even of the labile weathered particles. Individual site slope and mineralogic composition are not correlated, indicating that the influence of slope on sediment maturation is scale dependent. Disaggregation of weathering rims on coarser clasts and continued soil particle input along the streams may partially mask early attrition of weathered particles. When integrated with other studies, the results suggest that significant loss of weathering rims is detectable between 2.3 to 4.8 km of net downstream transport in the Southern Appalachians. Because the lack of alluvial storage limits *in situ* weathering of sediment, variations in sediment composition reflect variations in source rock distribution as modified by soil processes.

INTRODUCTION

Interpreting the mechanisms related to alteration of clastic fluvial sediments is of key importance in distinguishing source rock and environmental signals preserved in the sedimentary record. Accordingly, many studies have focused on petrographic examination of modern stream sands to assess different sediment populations reflecting different sources, environmental conditions, transport histories, and weathering mechanisms (Cameron and Blatt, 1971; Mann and Caravoc, 1973; Basu, 1976; Mack, 1981; Franzinelli and Potter, 1983; McBride and Picard, 1987; Girty and others, 1988; Grantham and Velbel, 1988; Johnsson and others, 1988; Johnsson, 1990b, a; Johnsson

and Meade, 1990; Girty, 1991; Johnsson and others, 1991; Savage and Potter, 1991; Heins, 1993; Johnsson, 1993; Robinson and Johnsson, 1997). A relatively separate body of literature has focused on the controls on downstream textural changes in modern rivers, particularly sediments in the gravel size range (Jones and Humphrey, 1997; Hoey and Bluck, 1999; Rice, 1999; Jones, 2000; Heller and others, 2001; Rice and Church, 2001; Surian, 2002; Brummer and Montgomery, 2003; Constantine and others, 2003).

The net effects of alteration are related to both the intensity and duration of exposure to physio-chemical environments that are not in equilibrium with a given sedimentary particle (Johnsson, 1993). Distinguishing the effects of intensity versus duration of exposure can be difficult in an absolute, quantitative sense, especially in the rock record. However, qualitative data concerning the relative influences of these rates along given transport distances under specific environmental conditions are more easily estimated and are of value when interpreting the sedimentary record (Savage and Potter, 1991). Along a link, defined as a channel segment between tributaries, if bank failure, hill slope failure, and runoff are minimized, then changes in bulk sediment composition will be due primarily to *in situ* alteration. If the net rate of alteration is greater than the average rate of grain transport through the link (i.e. the time spent in the bedload plus the time spent in temporary storage in alluvial deposits), then strong differences should be noted over very small distances. If the average rate of grain transport through the link is greater than the rate of alteration, however, no significant compositional trends should be detected.

A number of studies of clastic fluvial sediments have also noted that bedload sediments often contain intensely weathered particles associated with residence time in colluvial (saprolite, regolith, and soil) and/or alluvial (stream bar and floodplain) depositional environments (Grantham and Velbel, 1988; Johnsson, 1990a; Johnsson and Meade, 1990; Pope, 1995). Johnsson (1990b) suggests that weathered particles, including soil grain types and grains with weathering rims, are likely susceptible to mechanical abrasion and rapid mass loss during transport. This may be a primary control on coupling of chemical/mechanical processes influencing grain size and grain size normalized compositional changes in fluvial sediments. A simple, theoretical box model helps conceptualize how these changes and processes are related (Figure 1). Although downstream loss of weathering rims on larger size fractions, including cobbles, has been shown to be an important control on the expression of downstream fining trends in mountainous streams (Heller and others, 2001), there have been few systematic attempts to assess the controls on the production, transport, and fate of weathered particles in the sand fraction. In one of the few examples of weathered particle studies, Grantham and Velbel (1988) note that the relative abundance of garnet grains with weathering rims begins to decline after about 4.8 km of transport in the southern Appalachians, but these numbers are only loosely constrained. Further study of such weathered particles, however, may provide very sensitive proxies for interpretation of weathering and transport processes influencing bedload materials in modern systems (Grantham and Velbel, 1988; Johnsson, 1993; Heller et al., 2001).

The purpose of this paper is to assess the controls on the distribution and behavior of weathered particles in stream sediments from a small, steep, weathering-limited watershed in a low-

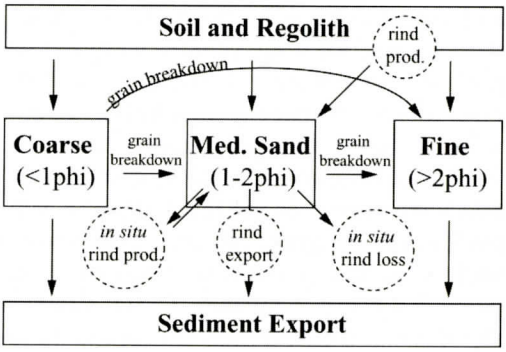

Figure 1. Theoretical box model for potential sources, fates, and processes related to the abundance of medium grains with weathering rims.

order, subtropical basin. Mountain Lake watershed, located on Paris Mountain, in Greenville, South Carolina, provides two small streams that have been sampled at a high resolution to examine the bulk texture and composition in addition to the weathered particle abundance. The dataset provides a thoroughly documented reference point for comparison with similar studies of headwater stream sediments and serves as a springboard for further research in the local area.

REGIONAL SETTING

The 295 ha Mountain Lake watershed (Figure 2) is located on the northeast flank of Paris Mountain (34° 56'N, 82° 22'W) in Greenville, South Carolina, USA. Paris Mountain is a monadnock that lies in the Inner Piedmont Terrain about 20 km southeast of the Blue Ridge escarpment. Tectonically, the area is part of the Paris Mountain thrust sheet, which is one of four regional thrust sheets that form a composite stack known as the Inner Piedmont province (Horton and McConnell, 1991). The lithologies underlying the watershed include a complex assemblage of biotite schist, muscovite schist, quartz muscovite schist, and biotite gneiss with varying amounts of sillimanite and kyanite (Niewendorp, 1997). Structurally, the watershed is characterized by a complex array of imbricate thrusts resulting in a complex metamorphic stratigraphy of different types of schists and gniesses, with deeper metamorphic units exposed to the east and south.

The study area is in the east central portion of the Paris Mountain USGS 7.5-minute quadrangle. The highest elevation in the watershed is the peak of Paris Mountain, at approximately 690 m above sea level. The lowest point at Mountain Lake lies at an elevation of 342 m. The total relief is 348 m.

Hartness and Kaufman Creeks dominate the surface hydrologic system of the study area. Analysis of channels marked on the Paris Mountain USGS 7.5-minute quadrangle indicate that both creeks are second-order systems (Strahler, 1952). In the northern portion of the watershed, the 2.3 km-long Kaufman Creek

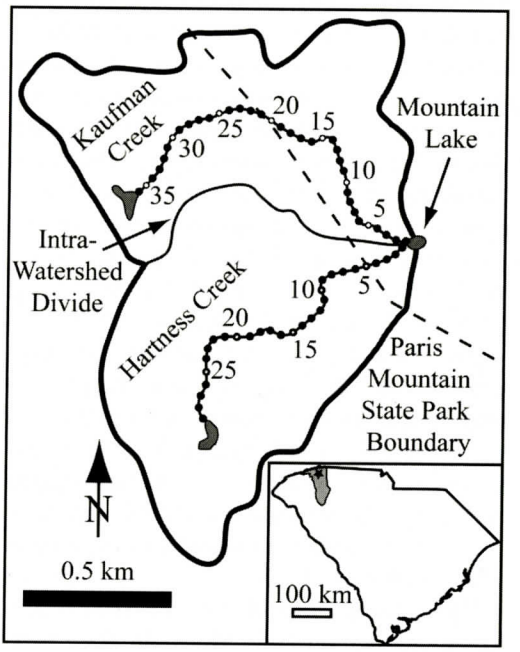

Figure 2. Map of Mountain Lake watershed, located on Paris Mountain in northern Greenville Co., South Carolina. Dots represent sampling localities at 50 m intervals along Kaufman Creek (north, n= 36) and Hartness Creek (south, n=29); numbering begins at the confluence and counts upstream.

drains 1.40 km^2 and descends 154 m along its course for an average slope of 0.067. Kaufman Creek cuts across regional structural trends for most of its lower course. In the southern portion of the watershed, the 1.9 km-long Hartness Creek drains 1.55 km^2 and descends 118 m for an average slope of 0.062.

Outcrops occur in the channels as either metamorphic lithologies with steeply dipping foliation that directs water along strike or as gently convex-up exposures of biotite gneiss. Both stream channels are characterized by a series of step pools connected by waterfalls and segments of straight channel. Niewendorp (1997) traced several faults that coincide with or extend directly under relatively straight reaches of Hartness Creek between sites 1-10, 14-22, and 22-29, suggesting some structural control of the drainage.

Lateral spread of high water is clearly confined by the steep topography and abundant

rock outcrops along the banks. The banks are thin accumulations of soil held in place by riparian vegetation, which includes rhododendron, dog hobble, and other herbaceous species. The adjacent slopes and ridges are characterized by thin, mature Ultisols (Camp, 1975) colonized by an oak-hickory forest mixed with mountain laurel. Small, discontinuous outcrops are common. Many slopes in the upper watershed show evidence of significant soil creep, but large alluvial fans are not observed.

The watershed is characterized by a subtropical climate. The average annual daily maximum temperature for Greenville County is 22° C, but monthly averages range from 11° to 31° C. The annual average daily minimum temperature is 11° C, but monthly averages range from 2° to 21° C. Average annual precipitation is 122.9 cm (Camp, 1975).

The lower portion of the watershed is protected land within Paris Mountain State Park. The upper portions are private property. A few high-value housing developments exist around the margin of the watershed, but the area is still largely undeveloped. The creeks are each currently sourced from small impoundments. Observation of the watershed indicates no significant differences between the drainages for Kaufman and Hartness Creeks, no significant, localized anthropogenic disturbances, and no significant point sources of sandy sediment.

METHODS

Sampling

A total of 65 sampling sites were established at approximately 50 m intervals along the creeks (Figure 2, Hartness, n = 29; Kaufman, n = 36). Elevations of sites were taken from the Paris Mountain USGS 7.5-minute quadrangle map. To test for scale dependency of slope-texture and slope-composition relations, an enlarged copy of the Paris Mountain USGS 7.5-minute quadrangle was used to determine the instantaneous slope for each locality by dividing by the distance between the closest 6 m contour intervals. Representative samples of bedload sediment were collected at each locality with a 1-quart scoop and dried in an oven at 80°C. Although grain size analysis focused on the sand and granule size fractions, observations suggest that the population may be bimodal, with one mode in the sand range and another in the cobble to pebble range. Samples were not collected downstream from Mountain Lake to avoid complications related to sediment storage in the lake.

Grain Size Analysis

Samples were sieved through screens at half-ϕ intervals between -2.0 ϕ and 4.0 ϕ in a Ro-Tap machine for 12 minutes. Particles larger than -2.0 ϕ were omitted due to sampling biases. The grains smaller than 4.0 ϕ comprise only a very small percentage of the total sediment load and were not further separated. Mean and sorting were calculated according to the method of moments (Krumbein and Pettijohn, 1938):

Mean (1st moment): $X_f = (S(f*m))/n$ (eq.1)

Sorting (2nd moment, standard deviation): $s_f = ((S(f*(m-X_f)^2))/100)^{0.5}$ (eq. 2)

In these calculations, f equals the weight percent of each grain size, m equals the midpoint of each grain size range in ϕ, and n equals the total number of samples. The <63 μm fraction was qualitatively observed to be dominated by silt, and, for moment calculations, the midpoint of the range was placed at 6.5 ϕ.

Petrographic Analysis

A riffle split of the medium sand fraction (1.0 to 2.0 ϕ) was selected from twenty localities, embedded in epoxy, and thin sectioned for petrographic analysis. This fraction was chosen both for ease of optical analysis and to facilitate comparison with other studies. All thin sections were stained for potassium feldspar and plagioclase. The classification scheme (Table 1) was modeled after Robinson and Johnsson (1997) but was modified to focus on the limited range of source rocks, to incorporate observed subpopulations, to characterize the lithic composition, and to distinguish between degrees and

Table 1 – Classification scheme for petrographic analysis of the medium sand fraction in Mountain Lake Watershed

Qt = total quartz = Qm+Qs+Qp

Qtm = total moncrystalline quartz = Qm+Qs

Qm = quartz, monocrystalline

Qms = straight extinction

Qmu = undulatory extinction

Qp = quartz, polycrystalline

Qp2-3 = 2-3 grains per crystal

Qp>3 = >3 grains per crystal

Qs = quartz, subgrained

Ft = total feldspar = Fp+Fk

Fp = plagioclase

Fk = potassium feldspar

Mt = total mica = Mb+Mm+Ml

Mm = muscovite

Mb = biotite

At = total accessories = Ao+Ai+Ak+As+Ab+Ap+Au1+Au2

Ao = opaque

Ai = inosilicates (hornblende)

As = sillimanite

Ak = kyanite

Ab = brown garnets

Ap = pink garnets

Au1 = unknown: gray to brown, B(-), textured, ~-relief, possibly zeolite from fault/fracture

Au2 = unknown: clear, 1^0 gray, hi (-) relief, possibly zeolite from fault/fracture

Ot = total other grains = Ya+Pf+Ou+Bi

Ya = alterites

Pf = pedogenic/ferruginous

Ou = other

Bi = biogenic debris

Rt = total rock fragments = Qp+As+Lq+Lf+Lm+La+Ly+Lp

Rtp = total poly-phase rock fragments = Lq+Lf+Lm+La+Ly+Lp

Rq = rock fragments with quartz under the cross hairs

Rf = rock fragments with feldspar under the cross hairs

Rm = rock fragments with micas under the cross hairs = Lmm+Lmb

Ra = rock fragments with accessories under the cross hairs

Ry = rock fragments with alterites under the cross hairs

Rp = rock fragments with pedogenic ferrunginous materials under the cross hairs

Zx = grains with FeO rims

Z1 = minimal rinds (0-25%)

Z2 = partial rinds (25-50%)

Z3 = complete rinds (>75%)

Table 2 - Summary of slope and texture data for Mountain Lake Watershed.

	Kaufman Creek, distance downstream																			
	1.75	**1.70**	**1.65**	**1.60**	**1.55**	**1.50**	**1.45**	**1.40**	**1.35**	**1.30**	**1.25**	**1.20**	**1.15**	**1.10**	**1.05**	**1.00**	**0.95**	**0.90**	**0.85**	**0.80**
Mean (ϕ)	0.64	0.15	0.25	-0.13	-0.09	-0.13	-0.04	0.04	0.08	-0.30	0.17	0.08	-0.28	-0.30	0.46	0.07	0.33	0.67	0.11	0.49
Sorting	1.58	1.19	1.36	1.06	1.06	1.20	1.16	1.08	1.16	1.10	1.13	1.29	1.06	1.16	1.24	1.05	1.22	1.37	1.26	1.35
Fine (>2.0 ϕ)	1.21	0.57	0.75	0.21	0.22	0.49	0.41	0.32	0.37	0.34	0.48	0.65	0.32	0.43	0.69	0.33	0.58	0.77	0.59	0.77
Medium (1.0 to 2.0 ϕ)	0.17	0.22	0.29	0.29	0.28	0.29	0.28	0.23	0.30	0.27	0.20	0.29	0.21	0.32	0.20	0.20	0.23	0.20	0.29	0.22
Coarse (> 1.0 ϕ)	1.12	0.64	0.81	0.63	0.63	0.66	0.66	0.61	0.68	0.60	0.59	0.73	0.59	0.61	0.66	0.57	0.68	0.91	0.71	0.82
Fines/Medium	7.02	2.54	2.62	0.73	0.77	1.68	1.50	1.37	1.23	1.27	2.36	2.25	1.52	1.36	3.48	1.59	2.58	3.89	1.99	3.46
Medium/Coarse	0.15	0.35	0.35	0.46	0.45	0.44	0.42	0.38	0.44	0.44	0.34	0.40	0.36	0.52	0.30	0.36	0.33	0.22	0.41	0.27
Elevation	504	498	498	498	498	498	498	492	486	486	480	480	480	480	480	468	462	450	438	426
Site Slope	0.250	0.011	0.011	0.011	0.011	0.011	0.031	0.036	0.036	0.015	0.015	0.015	0.015	0.015	0.050	0.083	0.071	0.125	0.083	0.083

	Kaufman Creek, distance downstream															
	0.75	**0.70**	**0.65**	**0.60**	**0.55**	**0.50**	**0.45**	**0.40**	**0.35**	**0.30**	**0.25**	**0.20**	**0.15**	**0.10**	**0.05**	**0.00**
Mean (ϕ)	0.43	0.77	0.25	0.07	0.31	0.45	0.58	0.17	0.30	0.31	0.86	1.06	0.89	1.12	0.94	0.80
Sorting	1.37	1.41	1.20	1.32	1.50	1.30	1.23	1.31	1.24	1.34	1.10	1.47	1.09	1.22	1.37	1.64
Fine (>2.0 ϕ)	0.78	0.97	0.44	0.73	1.04	0.64	0.55	0.71	0.53	0.68	0.47	1.05	0.56	0.69	0.84	1.48
Medium (1.0 to 2.0 ϕ)	0.25	0.13	0.29	0.28	0.28	0.25	0.22	0.27	0.27	0.29	0.14	0.07	0.11	0.07	0.11	0.12
Coarse (> 1.0 ϕ)	0.86	0.88	0.71	0.73	0.93	0.80	0.74	0.74	0.73	0.82	0.60	1.05	0.51	0.73	0.93	1.08
Fines/Medium	3.19	7.60	1.50	2.62	3.67	2.53	2.52	2.61	1.97	2.32	3.46	14.72	4.91	10.08	7.47	12.09
Medium/Coarse	0.29	0.14	0.41	0.38	0.30	0.32	0.29	0.37	0.37	0.36	0.22	0.07	0.22	0.09	0.12	0.11
Elevation	414	408	396	390	384	378	378	372	372	372	366	366	366	366	360	354
Site Slope	0.125	0.036	0.036	0.050	0.018	0.018	0.018	0.018	0.018	0.018	0.018	0.018	0.018	0.029	0.029	0.031

Table 2 (continued) - Summary of slope and texture data for Mountain Lake Watershed.

	Downstream distance (Hartness)																			
	1.40	**1.35**	**1.30**	**1.25**	**1.20**	**1.15**	**1.10**	**1.05**	**1.00**	**0.95**	**0.90**	**0.85**	**0.80**	**0.75**	**0.70**	**0.65**	**0.60**	**0.55**	**0.50**	**0.45**
Mean (ϕ)	0.61	0.85	-0.16	0.42	0.21	0.13	-0.20	0.35	0.04	0.01	0.30	0.24	0.67	0.36	0.13	0.50	0.16	0.49	0.51	0.26
Sorting	1.52	1.61	1.29	1.30	1.33	0.95	1.14	1.42	1.25	1.16	1.47	1.35	1.34	1.46	1.41	1.34	1.23	1.31	1.49	1.31
Fine (>2.0 ϕ)	1.15	1.31	0.82	0.68	0.82	0.18	0.51	0.89	0.55	0.39	1.03	0.84	0.78	1.03	0.93	0.89	0.50	0.75	1.08	0.72
Medium (1.0 to 2.0 ϕ)	0.17	0.11	0.21	0.25	0.23	0.19	0.21	0.26	0.30	0.30	0.25	0.23	0.19	0.23	0.28	0.17	0.30	0.20	0.21	0.25
Coarse (> 1.0 ϕ)	0.99	1.17	0.63	0.75	0.71	0.54	0.58	0.87	0.70	0.66	0.87	0.76	0.84	0.88	0.79	0.73	0.70	0.76	0.94	0.74
Fines/Medium	6.57	11.89	3.91	2.76	3.61	0.92	2.48	3.43	1.81	1.29	4.13	3.65	4.06	4.54	3.31	5.33	1.69	3.76	5.15	2.81
Medium/Coarse	0.18	0.09	0.33	0.33	0.32	0.36	0.35	0.30	0.43	0.45	0.28	0.30	0.23	0.26	0.35	0.23	0.42	0.26	0.22	0.34
Elevation	474	468	462	456	450	438	432	426	426	420	414	414	408	402	396	396	390	390	384	384
Site Slope	0.250	0.031	0.042	0.042	0.071	0.083	0.125	0.036	0.016	0.016	0.016	0.028	0.050	0.036	0.042	0.025	0.025	0.017	0.017	0.017

	Downstream distance (Hartness, continued)									Averages					
										Kaufman		Hartness		Watershed	
	0.40	**0.35**	**0.30**	**0.25**	**0.20**	**0.15**	**0.10**	**0.05**	**0.00**	**Avg**	**SD**	**Avg**	**SD**	**Avg**	**SD**
Mean (ϕ)	0.22	0.44	0.05	0.06	0.19	0.26	0.48	0.37	0.08	0.31	0.29	0.28	0.27	0.20	0.29
Sorting	1.53	1.49	1.24	1.33	1.47	1.36	1.59	1.65	1.59	1.25	0.14	1.38	0.15	1.27	0.16
Fine (>2.0 ϕ)	1.16	1.07	0.61	0.74	0.98	0.77	1.41	1.59	1.43	0.61	0.24	0.88	0.27	0.66	0.29
Medium (1.0 to 2.0 ϕ)	0.26	0.22	0.25	0.29	0.30	0.27	0.16	0.19	0.26	0.23	0.04	0.23	0.05	0.24	0.05
Coarse (> 1.0 ϕ)	0.91	0.93	0.68	0.73	0.88	0.80	0.97	0.94	0.84	0.73	0.13	0.80	0.15	0.74	0.14
Fines/Medium	4.44	4.86	2.41	2.56	3.28	2.82	8.85	8.58	5.59	3.32	1.43	4.16	2.35	3.06	2.08
Medium/Coarse	0.29	0.24	0.37	0.40	0.34	0.34	0.16	0.20	0.30	0.33	0.09	0.30	0.09	0.34	0.09
Elevation	384	378	378	372	366	366	360	360	354	480	21.50	422	28.80	451	38.82
Site Slope	0.028	0.028	0.036	0.036	0.042	0.018	0.018	0.018	0.028	0.049	0.058	0.049	0.055	0.049	0.056

types of alteration. Most of the grain populations are standard minerals commonly identified under the microscope. Two types of "weathered particle" grain types were recognized. Alterite (Ya) grains are defined as those grains that have been altered to the point where the original mineralogy can no longer be confidently identified but have not been leached of all mobile elements (Johnsson, 1990b). In Mountain Lake watershed, alterites commonly consist of chlorite and sericite, and many have picked up a light pink stain. This could be due to the presence of remnant K-feldspars, clays that react with the stain, and/or leaching and filling of micropores by the stain solution. Pedogenic ferruginous (Pf) particles are secondary concretions of precipitated iron oxide or residual weathering products of alterites that have been further leached of all mobile phases (Johnsson, 1990b). In Mountain Lake watershed, pedogenic ferruginous particles, characterized by chaotic, thick, reddish-to-opaque oxide minerals, lack good crystal faces and often appear irregular in shape. Many types of otherwise recognizable grains from proximal pedogenic sources have weathering rims produced during residence in colluvial (regolith, sapprolite, soil) and alluvial (bar and floodplain) deposits.

Thin sections were point counted (n = >300; grid spacing of 0.66 mm) using the traditional method in which the entire sedimentary grain is used in the classification rather than the Gazzi-Dickinson method (Ingersoll and others, 1984). In the traditional method, if a single mineral species makes up more than 95% of the visible surface area of a grain, then the grain is classified as monomineralic. If no single mineral species makes up more than 95% of the visible surface area of a grain, then the grain is classified as a polymineralic rock fragment. Quartz is the only phase to be further subdivided into monocrystaline and polycrystaline aggregates. Rock fragments were sub-classified based on the composition of the grain under the crosshairs. Statistical maximum and minimum limits for each grain type counted were calculated using the method of Howarth (1998).

Weathering Rims

The abundance of weathering rims, recognized as reddish-brown material similar to Pf grains, but concentrated in thin convexo-concavo zones along the boundaries of grains that are otherwise identifiable, was also recorded. Grains are considered to have a class one (Z1) rim if reddish alteration covers 1-25% of the total visible circumference and fracture length combined. Class two (Z2) rims cover 25-75% of the total visible circumference and fracture length combined. Class three (Z3) rims cover 75-100% of the total visible circumference and fracture length combined.

RESULTS

The sediments in Mountain Lake watershed are texturally and compositionally immature, but stream profiles, bulk composition, and textural trends reveal significant differences between the two creeks. Data tables have been abbreviated and summarized due to the sheer quantity of data, but a complete dataset of all textural and compositional parameters for each site is available from the authors.

Stream Profiles

The two creeks are characterized by distinctly different profiles (Table 2 and Figure 3). A single, large slope break dominates the Kaufman Creek profile, whereas Hartness Creek is characterized by a much more even slope along its entire length. These same differences are reflected in a plot of the instantaneous slopes, calculated using the nearest 6 m contour intervals, for each site (Figure 4).

Grain Size Data

Sediment samples from Mountain Lake watershed show considerable variability with respect to grain size distributions along a downstream profile (Table 2, Figures 5 and 6). Mean grain sizes from sediment samples in Mountain Lake watershed fall within a range of -0.28 to 1.12 ϕ. The mean grain size in Kaufman

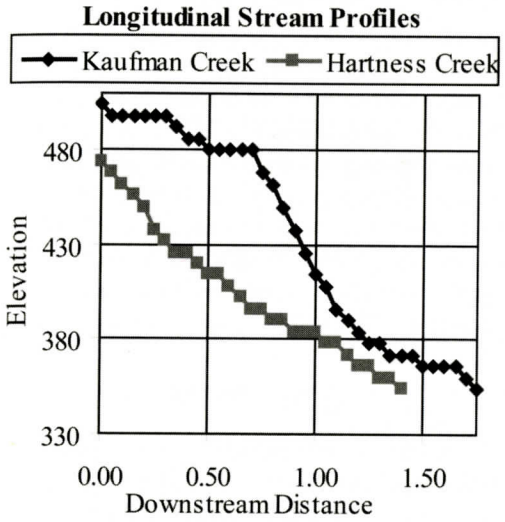

Figure 3. Longitudinal profiles for A) Kaufman Creek and B) Hartness Creek. Profiles are based on the elevations of the sampling sites.

Creek is 0.32 ϕ, while the mean grain size in Hartness Creek is 0.28 ϕ. Sorting coefficients fall within a range of 0.94 to 1.65. On average, the sediments are poorly sorted in both creeks, with only one sample falling into the extreme low end of the moderately sorted category (Folk, 1974). In Kaufman Creek, the mean grain size increases downstream, and sorting improves slightly downstream. In Hartness Creek, mean grain size does not change downstream, but there is a slight trend toward improved sorting.

Textural trends illustrated in Figures 5 and 6 indicate that the most downstream sites seem to behave anomalously. The relative percentages of the coarse and medium sand fractions in both creeks change sharply, as do the sorting in both creeks and the mean grain size in Kaufman Creek. These sites are located near the junction of the streams with Mountain Lake, where the systems essentially form a small delta/estuary system. Anthropogenically induced complications from reduced flow velocity are assumed to be influencing these sites and, accordingly, textural data from the three closest sites to the lake have been discarded for statistical purposes in each creek.

Compositional Data

Compositional analyses indicate significant amounts of alterites, feldspars, micas, and lithic fragments in addition to quartz (Table 3, Figure

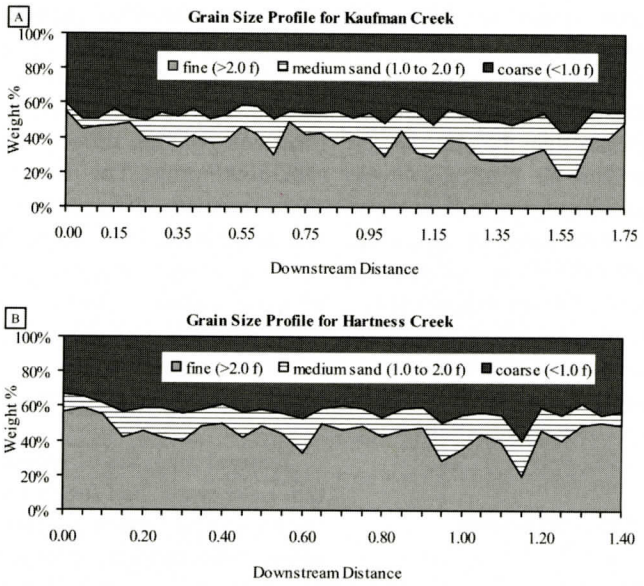

Figure 5. Textural profiles for A) Kaufman Creek and B) Hartness Creek. The choice of "coarse" (< 1.0 ϕ), medium sand (1.0 to 2.0 ϕ), and "fine" (>2.0 ϕ) fractions is based on the box model presented in Figure 1.

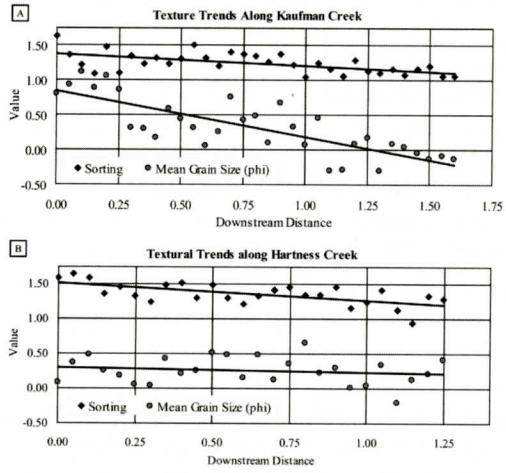

Figure 6. Grain size and sorting trends for A) Kaufman Creek and B) Hartness Creek. The three lowest sites (i.e. lower 0.15 km) are not considered for statistical purposes due to the interference of Mountain Lake. Kaufman Creek shows a trend toward coarser grain sizes (R^2 = 0.6347, y = -0.6595x + 0.8472), but only a very weak trend toward improved sorting (R^2 = 0.3274). Hartness Creek shows a very weak trend toward improved sorting (R^2 = 0.3800), but no trend with respect to grain size (R^2 = 0.0172).

7). Although there are no significant, systematic changes in the sediment composition along the stream profile, Hartness Creek sands are characterized by total feldspar, microcline, and hornblende abundances that are more than one standard deviation greater than the abundances in Kaufman Creek (Figure 8). Kaufman Creek contains a greater amount of quartz than Hartness Creek, as well as local peaks in muscovite abundance. Although difficult to statistically determine, abundances of many individual accessory minerals also suggest different distributions. Sillimanite distribution, for example, is much more consistent along Hartness Creek (11.7 +/- 7.5%, RSD 0.65%), than along Kaufman Creek (2.7 +/- 3.5%, RSD 1.32%).

Weathered Particles

Alterites and pedogenic ferruginous particles are present in low abundances throughout the watershed (Figure 9). Rind abundances are similar in both creeks, and there are no distinct trends with respect to the loss of these phases. Approximately one-fourth of the grains have weathering rims of some degree (Figure 10). Z1 rims are almost twice as common as Z2 and Z3 rims combined. Along the stream profile, there is some variability of the relative proportions of both constituent minerals and rims. However, as sediment moves through the watershed, no single population is observed to systematically change volumetrically at the expense of another.

DISCUSSION

The results show that the overall lack of alluvial storage and rapid export of material minimize the detectable effects of downstream alteration of sedimentary particles at this scale, even those associated with pedogenic sources. The dominant weathering mechanism influencing the stream sediment is the extended residence time in the soil horizons on the adjacent slopes; in situ chemical alteration is minimized by the rapid export. No net influence of mechanical weathering is detected in the sand fraction, although this could be masked partially by the breakdown of larger cobbles, which move more slowly through the system and may break down into sand-sized particles. More work is needed to determine the impact of this effect. Because the lack of alluvial storage limits in situ weathering of sediment, variations in sediment composition reflect variations in source rock distribution. The results of this study are contrasted with studies of larger systems to provide some boundaries on the detectability of alteration in such systems and insight into the potential limits of many methodological assumptions that implicitly underlie similar studies.

Sediment Texture

Textural analyses of sediments from Mountain Lake watershed suggest that sediments are not subject to significant mechanical weathering or hydrodynamic sorting during transport. Similar to the coarsening trends here documented in Kaufman Creek, Brummer and Montgomery (2003) noted downstream coarsening, rather

Table 3 – Summary of medium sand composition (wt%) for Mountain Lake Watershed. A complete dataset is available from the authors.

	Kaufman Creek, downstream distance												Hartness	
	1.75	1.60	1.45	1.30	1.15	1.00	0.85	0.75	0.55	0.25	0.10	0.00	1.35	1.20
Qt	59.74	76.14	61.11	68.98	69.71	72.55	63.82	71.19	67.21	71.43	62.58	57.19	46.89	40.85
Qtm	58.75	74.18	59.15	67.99	67.43	70.59	62.50	70.53	64.61	71.10	61.92	56.21	45.25	38.89
Ft	5.94	3.27	4.25	4.29	5.21	4.90	2.30	4.30	3.90	2.33	2.32	0.65	21.97	22.22
Rt	7.59	7.84	14.38	8.91	9.12	10.78	14.14	7.28	12.99	6.98	10.26	17.65	14.75	15.03
Rtp	6.60	5.88	12.42	7.92	6.84	8.82	12.83	6.62	10.39	6.64	9.60	16.67	13.11	13.07
Mt	7.92	4.25	6.86	6.60	8.79	4.25	7.89	6.29	3.90	7.97	7.62	7.84	3.28	3.92
At	6.60	2.29	8.50	2.64	3.26	3.27	7.57	3.64	4.87	5.98	7.62	5.88	8.52	12.09
Ot	12.21	6.21	4.90	8.58	3.91	4.25	4.28	7.28	7.14	5.32	9.60	10.78	4.59	5.88
Ya	6.27	5.23	3.59	6.60	3.91	2.94	1.32	5.30	3.57	3.99	4.97	4.25	2.62	2.29
Pf	5.61	0.98	0.65	1.98	0.00	1.31	2.96	1.99	3.25	0.66	4.64	4.90	1.64	0.65
Pf+Ya	11.88	6.21	4.25	8.58	3.91	4.25	4.28	7.28	6.82	4.65	9.60	9.15	4.26	2.94
Zt	41.91	43.79	51.31	44.22	40.39	42.48	49.34	50.33	51.30	46.18	39.07	56.54	52.79	33.01
Z1	29.37	34.97	30.39	35.64	30.62	30.72	31.25	38.74	37.34	33.55	24.17	28.76	29.51	26.80
Z2	8.58	5.88	15.03	6.93	6.84	7.19	11.18	6.95	9.74	7.97	11.26	20.59	16.72	4.90
Z3	3.96	2.94	5.88	1.65	2.93	4.58	6.91	4.64	4.22	4.65	3.64	7.19	6.56	1.31

	Hartness Creek, downstream distance								Averages					
									Kaufman		Hartness		Average	
	1.05	0.90	0.75	0.60	0.45	0.30	0.15	0.00	Avg	SD	Avg	SD	Avg	SD
Qt	45.60	46.05	45.54	47.85	47.21	43.89	35.50	41.50	66.80	5.84	44.09	3.81	55.45	4.83
Qtm	43.32	44.74	44.55	46.86	45.57	42.90	33.22	39.54	65.41	5.74	42.49	4.14	53.95	4.94
Ft	24.43	20.72	23.43	24.75	19.34	21.12	23.78	19.93	3.64	1.51	22.17	1.89	12.90	1.70
Rt	11.40	17.43	11.22	14.85	11.80	15.84	24.10	17.65	10.66	3.41	15.41	3.84	13.04	3.62
Rtp	9.12	16.12	10.23	13.86	10.16	14.85	21.82	15.69	9.27	3.29	13.80	3.70	11.54	3.50
Mt	3.58	1.64	5.61	2.97	5.25	7.26	5.21	5.23	6.68	1.68	4.40	1.62	5.54	1.65
At	8.14	11.51	7.92	5.61	7.21	6.93	6.51	12.42	5.18	2.14	8.69	2.45	6.93	2.29
Ot	6.84	2.63	6.27	3.96	9.18	4.95	4.89	3.27	7.04	2.75	5.25	1.90	6.14	2.33
Ya	4.56	1.64	3.96	2.31	4.26	3.30	3.26	0.65	4.33	1.46	2.89	1.22	3.61	1.34
Pf	1.63	0.33	1.65	0.99	3.93	0.66	1.30	2.61	2.41	1.86	1.54	1.07	1.98	1.46
Pf+Ya	6.19	1.97	5.61	3.30	8.20	3.96	4.56	3.27	6.74	2.62	4.43	1.82	5.58	2.22
Zt	49.51	48.68	51.49	46.20	64.26	48.84	49.84	62.09	46.41	5.32	50.67	8.57	48.54	6.95
Z1	31.92	28.95	33.66	31.02	43.28	30.03	27.36	36.93	32.13	4.09	31.95	4.98	32.04	4.53
Z2	12.38	12.83	9.90	9.24	11.80	13.86	16.94	16.99	9.85	4.26	12.56	3.88	11.20	4.07
Z3	5.21	6.91	7.92	5.94	9.18	4.95	5.54	8.17	4.43	1.63	6.17	2.19	5.30	1.91

than conventional downstream fining of sediments in another low order, mountainous, headwater system. Detailed geomorphic analysis in the latter case suggested that the primary control on the coarsening trends is differential transport rates of coarse and fine material, with addition of coarse sediment as a secondary control. The downstream coarsening trend in Kauf-

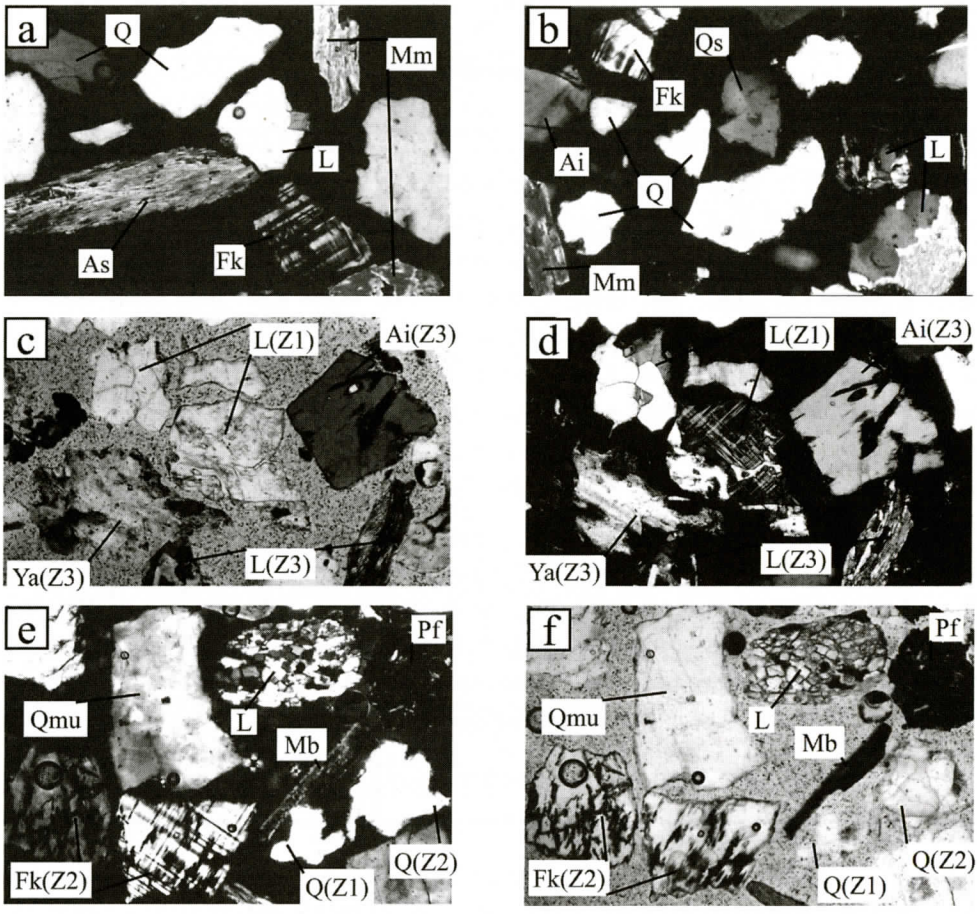

Figure 7. Selected photomicrographs of major phase classifications (Table 1; rim data in parentheses). All fields of view of approximately 4mm. a) and b) are different views under crossed polars. The lithic (L) in a) is composed of quartz (Q) and biotite (Mb). The top right lithic in b) is composed of quartz (Q), biotite (Mb), and pedogenic ferruginous material (Pf); the lower lithic is composed of quartz (Q), muscovite (Mm), and pedogenic ferruginous material (Pf). c) and) are the same view with polars uncrossed and crossed respectively. The upper left lithic is composed of quartz (Q) and biotite (Mb); the middle lithic is composed of potassium feldspar (Fk), alterite (Ya), and biotite (Mb). The bottom lithic is composed of quartz (Q), biotite (Mb), and pedogenic ferruginous material (Pf). e) and f) are the same view with polars crossed and uncrossed respectively. The lithic is composed of quartz (Q), biotite (Mb), and opaque oxides (Ao).

man Creek (Figure 6), with its large, steep slope break, and observed lack of large colluvial deposits in the stream channel, are here interpreted to reflect a similar process at work in Kaufman Creek drainage basin. The more variable slopes in Hartness Creek are associated with a weaker textural signal, suggesting that there are other factors complicating the grain size distribution (Figure 3, Figure 6). The discrepancies between grain size trends in the two creeks are likely related to the fact that Kaufman Creek drainage basin has significantly greater relief (348 m) than Hartness Creek drainage basin (202 m) (Figure 3). These data, combined with the evidence for abundant outcrops and thin soils on the adjacent slopes, support the interpretation of Mountain Lake watershed as a weathering-limited system. Consistent sorting coefficients along both creeks (Figure 6) suggest that the sampling of the me-

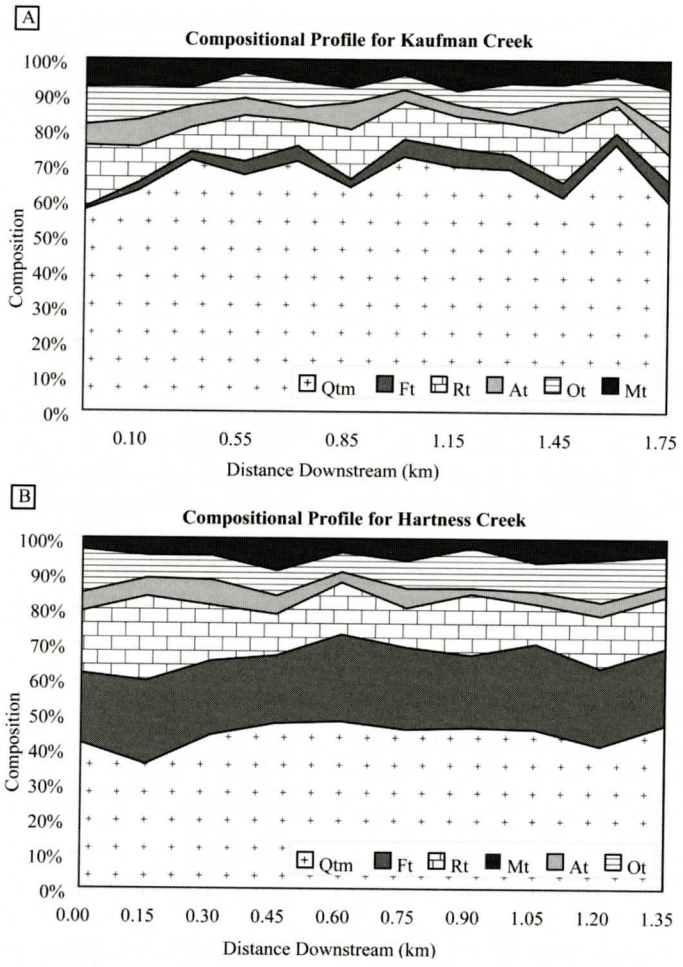

Figure 8. Bulk compositional variation for A) Kaufman Creek and B) Harntess Creek. Neither stream shows significant systematic changes in the relative percentage of any species relative to another.

dium sand fraction for compositional analysis has not been obviously biased by hydrodynamic sorting processes.

Downstream Compositional Trends

The compositional profiles indicate that there are no significant changes in the bulk composition or weathered particle abundance in the medium sand fraction as sediments are transported down the creeks. Several recent studies of modern environments have hypothesized that alluvial storage, related to slope, acts as a dominant control on compositional maturation trends by extending the duration of exposure of sediments to chemical weathering (Schumm, 1968; Franzinelli and Potter, 1983; Grantham and Velbel, 1988; Johnsson and others, 1988; Johnsson and others, 1991; Savage and Potter, 1991; Johnsson, 1993; Jones and Humphrey, 1997; Robinson and Johnsson, 1997). In these systems, sediment is temporarily stored in deposits such as levees, bars, and floodplains. While in storage, sediments are leached of mobile phases due to an extended fluid-sediment contact time. During channel migration, this stored sediment is reincorporated into the system and the overall compositional maturity of the sediment is increased. This relationship between alluvial storage and sedi-

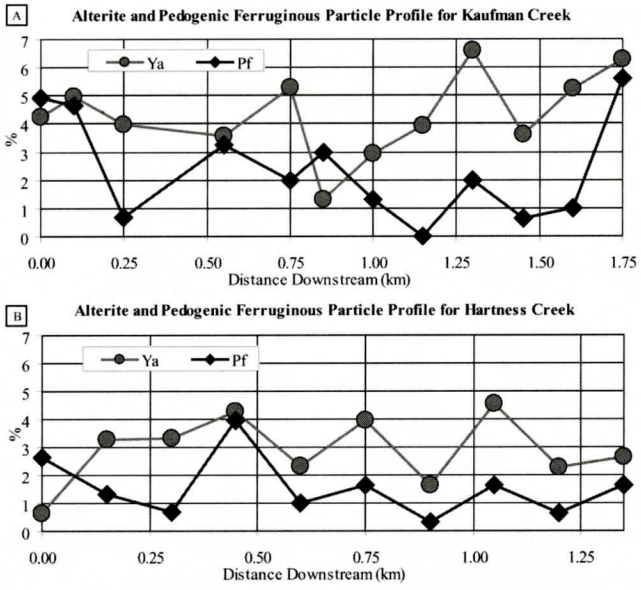

Figure 9. Alterite and pedogenic ferruginous particle profiles for A) Kaufman Creek and B) Harntess Creek. Data show no systematic downstream trends.

ment maturation has been documented in arctic and tropical environments (Franzinelli and Potter, 1983; Grantham and Velbel, 1988; Johnsson et al., 1988; Johnsson et al., 1991; Savage and Potter, 1991; Johnsson, 1993; Jones and Humphrey, 1997; Robinson and Johnsson, 1997).

Together, compositional and weathering rim data from this study support the slope/storage

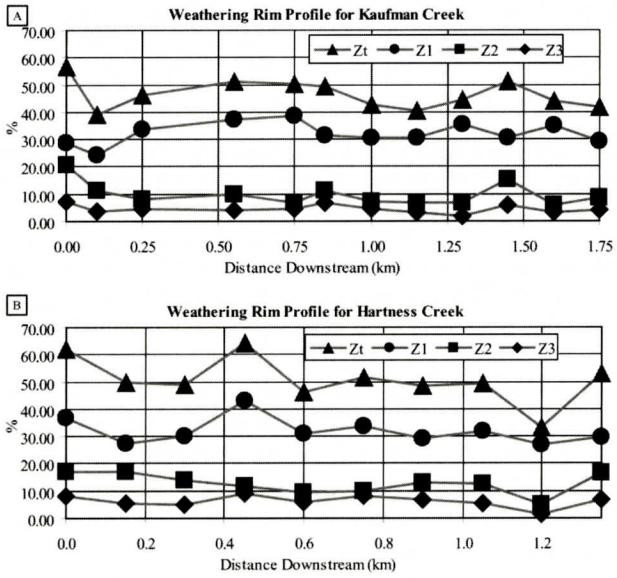

Figure 10. Distribution of weathering rims in A) Kaufman Creek and B) Hartness Creek. Z1 rims cover 1-25% of the combined rim and fracture length of the grain, Z2 rims 25-75%, and Z3 rims 75-100%. There are no systematic downstream changes associated with the bulk profiles, suggesting that the bulk rim population is not affected by mechanical weathering at this scale of observation

hypothesis discussed above by documenting an opposite end-member, where high slopes, rapid transport, and limited alluvial storage are associated with a lack of petrographic changes. However, there is no correlation between local site slope (Figure 4) and either textural (Figures 5, 6) or compositional parameters (Figures 8, 9, and 10) along either creek. This indicates that the effects of slope on sediment texture and composition are scale dependent. At very small scales there are higher order controls that affect sediment texture and composition, such as sediments locally derived from very small drainages on adjacent slopes, log jams along the stream that artificially increase slope, or local channel morphologies that result in hydrodynamic sorting.

In Mountain Lake watershed, the presence of weathering rims and alterites shows that during early evolution these sediments are chemically weathered and not simply formed by the mechanical disagregation of source rocks. Based on the lack of observed alluvial storage, this weathering is inferred to occur in the soil horizon. The consistent abundance of these particles and rims, which are considered very labile phases, suggests that they are not subjected to further significant alteration as they move through the creeks (Johnsson, 1990b). Thus the composition at this early stage of sediment development reflects the mineral composition of the source rocks as modified by soil processes. Although the importance of soil processes has been demonstrated before in tropical environments (e.g., Franzinelli and Potter, 1983; Johnsson, 1990b), these data clearly show that this is true in more temperate environments as well.

The lack of storage in Mountain Lake watershed precludes significant *in situ* chemical weathering in longitudinal bars, but the detection of any particle attrition is potentially complicated by two additional factors (Figure 1). First, the relative increase in coarse clast abundance suggests, but does not prove, that mechanical breakdown of coarse grains is not a significant source for sand-sized particles with weathering rims. Abrasion of highly weathered rims associated with these relatively slow-moving, increasingly abundant clasts may, however, effectively produce weathered sand-sized particles within the stream. Second, the steep banks that lie adjacent to the streams also provide a constant source of fresh, pedogenically derived material along their entire length.

In light of these complications, the lack of a net downstream increase in weathered particle abundance suggests two possibilities. The first possibility is that there is no change at all in any of the weathered particles as they move downstream. If this is true, then the material added by coarse clast breakdown and pedogenic sediment input must be homogeneous. The second possibility is that there is indeed some loss of weathered particles, but it is effectively in equilibrium with the rate of addition by coarse clast breakdown and pedogenic sediment input, and thereby masked. Further research is required to understand the relative importance of these effects on the detectability of alteration trends.

Although no significant compositional alteration has been detected in the present study, results can be integrated with other data to constrain some minimum limits on the distances over which alteration is detectable in the bulk load stream sediments of the southern Appalachians. In a similar study of the Coweeta watershed in North Carolina, Grantham and Velbel (1988) determined that weathering rims on garnets are lost through abrasion in mountain streams somewhere between 0.8 and 4.8 km. Somewhere within this interval, the rate of rim loss due to abrasion in the streambed becomes greater than the rate of rim addition because the rate of attrition of rims surpasses the rate of creation/addition of fresh rims. This distance is likely related to stream network patterns and the tendency for steep headwater streams merge into higher order systems with flatter alluvial valleys over just a few kilometers. In the higher order systems, the rate of input of fresh material from the adjacent slopes is limited by increased distance to the channel and a decrease in slope; simultaneously, the channel slope decreases, thereby increasing the duration of exposure to chemical weathering per unit downstream distance.

These results support previous conclusions that weathered particles are useful tracers of

weathering and transport processes (Grantham and Velbel, 1988; Johnsson, 1993; Heller et al., 2001). Although not necessarily preserved in ancient deposits, careful monitoring of these particles in modern systems should provide a method for relating processes to subtle changes in the bedload that are not evident through analysis of changes in bulk composition alone. As tracers, weathered particles provide a useful tool that should be relatively insensitive to compositional differences between source areas. Thus, results from different basins may provide comparable, parallel proxies that can be used to more confidently assess the impacts of various processes on fluvial sediments.

Compositional Differences Between the Creeks

The lack of downstream changes in bulk sediment mineralogy along Hartness and Kaufman Creeks is consistent with rapid transport of material through the system and suggests that the compositional differences between the streams are not merely sampling artifacts. There are three hypotheses related to this difference. The first scenario involves differences in the bedrock beneath each watershed. Although the geology of Mountain Lake watershed has not been mapped in sufficient detail to distinguish such differences, studies of other small basins have also encountered similar complexities when working with such high-resolution datasets (Mann and Caravoc, 1973; Mack, 1981; Grantham and Velbel, 1988; Heins, 1993; Yuretich and others, 1996). The second potential influence on bulk compositional differences between the streams involves differences in degree or depth of excavation of the weathering horizons on the adjacent slopes. The homogeneous climate and evidence for extremely rapid denudation of the slopes, however, suggests that these differences are minimal. A third possible influence would be the anthropogenic input of sand into the system. Field observations of the watershed and contacts with local residents, however, suggest that the watersheds are virtually identical with respect to degree of development and lack any significant, potential point source(s) for such consistent sand input.

After considering these three hypotheses, the first hypothesis is preferred. Although the complex geology of Mountain Lake watershed has not yet been mapped in detail, the current data suggests that the deeper metamorphic units exposed to the south and the east under the source area for Hartness Creek, produce more feldspar, more hornblende, and less quartz in the medium sand fraction than the shallower units underlying the source area for Kaufman Creek. Grantham and Velbel (1988) note that the Coweeta watershed, which is also in the southern Appalachians, is too complex to map at a high-resolution scale but use petrographic parameters of stream sediments to actually try and distinguish source rock differences. This is likely a function of bulk differences in source rock mineralogy and composition but could also reflect textural differences that selectively include or exclude medium sand-sized crystals of certain phases. Although the structure is likely a significant influence on the physiography of Mountain Lake watershed, lithologic differences between the sub-drainage basins may also be related to the different stream profiles. Kaufman Creek produces high abundances of quartz, which is highly resistant to chemical weathering, and is characterized by 348 m of total relief; Hartness Creek, on the other hand, produces higher abundances of more labile minerals and has only 202 m of total relief.

These results suggest that immature sediments containing abundant unstable phases may prove to be hypersensitive indicators of provenance by preserving a distinct local source rock signature that is of limited value in drawing regional conclusions regarding geology (Butler, 1979; Mack, 1984; Girty and others, 1988; Heins, 1993). Ternary diagrams of quartz/feldspar/rock fragments, for example, can be used to infer two very distinct proximal populations derived from the same source (Figure 11). The error polygons, formed by the 95% confidence intervals calculated according to Howarth (1998), for the Kaufman Creek, Hartness Creek, and watershed averages are mutually exclusive. Because this difference is primarily in the feldspars, the same magnitude

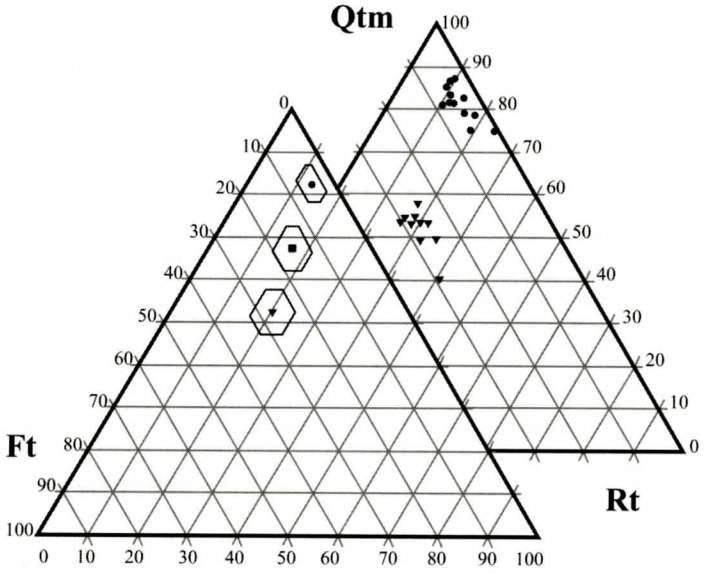

Figure 11. Quartz-Feldspar-Rock Fragment (QFR) ternary diagrams: A) Total samples from Kaufman Creek (closed circles) and Hartness Creek (open triangles). B) Suite averages for Kaufman Creek (closed circles), Hartness Creek (open triangles), and the entire watershed (closed squares). Error polygons for each group represent the 95% confidence levels of the suite means with respect to each species (e.g. Robinson and Johnsson, 1997) were calculated using methods of Howarth (1998). The mutual exclusion of all fields suggests caution when making regional provenance interpretations from immature sediments.

of differences should show up even if these point counts were done according to the Gazzi-Dickinson method, which would reclassify the "rock fragments" recognized in the current study based only on the crystal (or microcrystalline aggregate) directly beneath the crosshairs (Ingersoll et al., 1984). These data support the conclusions of other studies that ternary diagrams by themselves should be interpreted cautiously (Butler, 1979; Mack, 1984; Girty et al., 1988; Heins and Ingersoll, 2000).

Future Work

These results propose several hypotheses for future studies. Further work on the character of medium sand grains in the soil horizons should document the range of phases present and how alteration of grains proceeds. Further work on the age and depth of soil profiles, the transport rate of material from the slopes to the streambed, the rim distribution in deposits of Mountain Lake, and rim distributions associated with longer stream reaches should offer quantitative constraints on the rates and distances associated with these processes. Further work on the distribution of these rims with respect to the parent phase may yield quantitative predictions of compositional changes associated with textural maturation.

CONCLUSIONS

1. Mountain Lake watershed, located on Paris Mountain in Greenville, South Carolina, is a subtropical system drained by Kaufman and Hartness Creeks, which are both second-order, headwater streams. A complex, undifferentiated assemblage of high-grade metamorphic and granitic source rocks underlies the watershed. Bulk samples of bedload sediments, including gravel-, sand-, and clay-sized detritus, were collected from 65 sites along the creeks for textural and petrographic analysis.
2. Textural analysis of Kaufman Creek sediments indicates a downstream trend toward

increased grain sizes. Textural analysis of Hartness Creek sediments indicates no significant grain size trends. Poorly sorted sediments characterize both creeks, and neither creek shows a significant downstream trend with respect to sorting.

3. Quartz, lithic fragments, micas, and feldspars characterize the sediments in Mountain Lake watershed. The relative proportions of these constituents are fairly constant through the watershed. This lack of compositional change is interpreted to be the result of steep slopes, which move sediments out of the system more rapidly than they can be altered *in situ*.

4. There are significant differences between the sediment compositions from the two streams. Hartness Creek contains greater amounts of potassium feldspar than Kaufman Creek, and Kaufman Creek contains significantly more quartz than Hartness Creek. These differences are interpreted to reflect the source rock distribution undetectable by normal surface mapping. Results suggest that immature sediment containing abundant labile phases preserves a very strong, distinct source rock signature but is of limited value in drawing regional generalizations concerning provenance.

5. Roughly 25% of all grains show evidence of iron oxide weathering rims. These rims, along with the presence of alterites and pedogenic ferruginous grains, indicate that sand-sized grains are chemically weathered in Mountain Lake watershed. A complete lack of trends with respect to weathering rims or weathered particle abundance indicates that this weathering is restricted to the soil horizons prior to introduction into the stream. Integration of the current data with the findings of Grantham and Velbel (1988) suggests that these rims may be lost due to mechanical abrasion between 2.0 and 4.8 kilometers of transport.

6. Careful monitoring of labile grain types, including accessory minerals and weathered particles, in different size fractions may help quantitatively constrain subtle parameters related to physical and chemical processes in a given system.

ACKNOWLEDGEMENTS

This study was funded by EPA Grant #NE984049-96-0 to CBA. The Furman University Department of Earth and Environmental Sciences provided additional funds. We thank Clark Niewendorp, Jack Garihan, Bill Heins, Paul Heller, Greg Mack, Timothy Lawton, and Chris Brummer for review, consultation, and help with the project. We also thank the rangers at Paris Mountain State Park for logistical help and Leah Blatzer for help with fieldwork.

REFERENCES

Basu, A., 1976, Petrology of Holocene fluvial sand derived from plutonic source rocks: Implications to paleoclimactic interpretation: Journal of Sedimentary Petrology, v. 46, p. 694-709.

Brummer, C.J., and Montgomery, D.R., 2003, Downstream coarsening in headwater channels: Water Resources Research, v. 39.

Butler, J.C., 1979, Trends in ternary petrologic variation diagrams - fact or fantasy: American Mineralogist, v. 64, p. 1115-1121.

Cameron, K.L., and Blatt, H., 1971, Durabilities of sand size schist and "volcanic" rock fragments during fluvial transport, Elk Creek, Black Hills, South Dakota: Journal of Sedimentary Petrology, v. 41, p. 565-576.

Camp, W.J., 1975, Soil Survey of Greenville County, South Carolina: Washington, D.C., United States Department of Agriculture Soil and Conservation Service, p. 71.

Constantine, C.R., Mount, M.F., and Florsheim, J.L., 2003, The effects of longitudinal differences in gravel mobility on the downstream fining pattern in the Cosumnes River, California: Journal of Geology, v. 111, p. 233-241.

Franzinelli, E., and Potter, P.E., 1983, Petrology, Chemistry, and Texture of Modern River Sands, Amazon River System: Journal of Geology, v. 91, p. 23-39.

Girty, G.H., 1991, A Note on the Composition of Plutoniclastic Sand Produced in Different Climatic Belts: Journal of Sedimentary Petrology, v. 61, p. 428-433.

Girty, G.H., Mossman, B.J., and Pincus, S.D., 1988, Petrology of Holocene Sand, Peninsular Ranges, California and Baja Norte, Mexico - Implications for Provenance-Discrimination Models: Journal of Sedimentary Petrology, v. 58, p. 881-887.

Grantham, J.H., and Velbel, M.A., 1988, The Influence of Climate and Topography on Rock-Fragment Abundance in Modern Fluvial Sands of the Southern Blue Ridge Mountains, North Carolina: Journal of Sedimentary Petrology, v. 58, p. 219-227.

Heins, W.A., 1993, Source rock texture versus climate and

topography as controls on the composition of modern, plutonoclastic sand, in Johnsson, M.J., and Basu, A., eds., Processes Controlling the Composition of Clastic Sediments: Boulder Colorado, Geological Society of America Special Paper 284.

Heller, P.L., Beland, P.E., Humphrey, N.F., Konrad, S.K., Lynds, R.M., McMillan, M.E., Valentine, K.E., Widman, Y.A., and Furbish, D.J., 2001, Paradox of downstream fining and weathering-rind formation in the lower Hoh River, Olympic Peninsula, Washington: Geology, v. 29, p. 971-974.

Hoey, T.B., and Bluck, B.J., 1999, Identifying the controls over downstream fining of river gravels: Journal of Sedimentary Research, v. 69, p. 40-50.

Horton, J.W.J., and McConnell, K.I., 1991, Chapter three: the Western Piedmont, in Horton, J.W.J., and Zullo, V.A., eds., The geology of the Carolinas: Knoxville, University of Tennessee Press, p. 405.

Howarth, R.J., 1998, Improved estimators of uncertainty in proportions, point-counting, and pass-fail test results: American Journal of Science, v. 298, p. 594-607.

Ingersoll, R.V., Bullard, T.F., Ford, R.L., Grimm, J.B., Pickle, J.D., and Sares, S.W., 1984, The effect of grain size on detrital modes: a test of the Gazzi-Dickinson point-counting method: Journal of Sedimentary Petrology, v. 54, p. 103-116.

Johnsson, M.J., 1990a, Overlooked Sedimentary Particles from Tropical Weathering Environments: Geology, v. 18, p. 107-110.

Johnsson, M.J., 1990b, Tectonic Versus Chemical-Weathering Controls on the Composition of Fluvial Sands in Tropical Environments: Sedimentology, v. 37, p. 713-726.

Johnsson, M.J., 1993, The system controlling the composition of clastic sediments, in Johnsson, M.J., and Basu, A., eds., Processes controlling the Composition of Clastic Sediments: Geological Society of America Special Paper, no. 284.

Johnsson, M.J., and Meade, R.H., 1990, Chemical-Weathering of Fluvial Sediments During Alluvial Storage - the Macuapanim Island Point-Bar, Solimoes River, Brazil: Journal of Sedimentary Petrology, v. 60, p. 827-842.

Johnsson, M.J., Stallard, R.F., and Lundberg, N., 1991, Controls on the Composition of Fluvial Sands from a Tropical Weathering Environment - Sands of the Orinoco River Drainage-Basin, Venezuela and Colombia: Geological Society of America Bulletin, v. 103, p. 1622-1647.

Johnsson, M.J., Stallard, R.F., and Meade, R.H., 1988, 1st-Cycle Quartz Arenites in the Orinoco River Basin, Venezuela and Colombia: Journal of Geology, v. 96, p. 263-2771.

Jones, A.P., 2000, Late quaternary sediment sources, storage and transfers within mountain basins using clast lithological analysis: Pineta Basin, central Pyrenees, Spain: Geomorphology, v. 34, p. 145-161.

Jones, L.S., and Humphrey, N.F., 1997, Weathering-controlled abrasion in a coarse-grained, meandering reach of the Rio Grande: Implications for the rock record: Geological Society of America Bulletin, v. 109, p. 1080-1088.

Krumbein, W.C., and Pettijohn, F.J., 1938, Manual of Sedimentary Petrography: New York, Appleton-Century Crofts, 475 p.

Mack, G.H., 1981, Composition of modern stream sand in a humid climate derived from low-grade metamorphic and sedimentary foreland fold-thrust belt of North Georgia: Journal of Sedimentary Petrology, v. 51.

Mack, G.H., 1984, Exceptions to the Relationship between Plate-Tectonics and Sandstone Composition: Journal of Sedimentary Petrology, v. 54, p. 212-220.

Mann, W.R., and Caravoc, V.V., 1973, Composition of sand released from three source areas under humid, low relief weathering in the North Carolina Piedmont: Journal of Sedimentary Petrology, v. 43, p. 870-881.

McBride, E.F., and Picard, M.D., 1987, Downstream Changes in Sand Composition, Roundness, and Gravel Size in a Short-Headed, High-Gradient Stream, Northwestern Italy: Journal of Sedimentary Petrology, v. 57, p. 1018-1026.

Niewendorp, C., 1997, Geologic map of Paris Mountain, 7.5 minute quadrangle, Greenville County, South Carolina, South Carolina Department of Natural Resources, Geological Survey Open-File Report 99.

Pope, G.A., 1995, Internal Weathering in Quartz Grains: Physical Geography, v. 16, p. 315-338.

Rice, S., 1999, The nature and controls on downstream fining within sedimentary links: Journal of Sedimentary Research, v. 69, p. 32-39.

Rice, S.P., and Church, M., 2001, Longitudinal profiles in simple alluvial systems: Water Resources Research, v. 37, p. 417-426.

Robinson, R.S., and Johnsson, M.J., 1997, Chemical and physical weathering of fluvial sands in an arctic environment: Sands of the Sagavanirktok River, North Slope, Alaska: Journal of Sedimentary Research, v. 67, p. 560-570.

Savage, K.M., and Potter, P.E., 1991, Petrology of Modern Sands of the Rios Guaviare and Inirida, Southern Colombia - Tropical Climate and Sand Composition: Journal of Geology, v. 99, p. 289-298.

Schumm, S.A., 1968, Speculations concerning paleohydrologic controls of terrestrial sedimentation: Geological Society of America Bulletin, v. 79, p. 1573-1588.

Strahler, A.N., 1952, Hypsometric (area-altitude) analysis of erosional topography: Geological Society of America Bulletin, v. 63, p. 1117-1142.

Surian, N., 2002, Downstream variation in grain size along an Alpine river: analysis of controls and processes: Geomorphology, v. 43, p. 137-149.

Yuretich, R., Knapp, E., Irvine, V., Batchelder, G., McManamon, A., and Schantz, S.P., 1996, Influences upon the rates and mechanisms of chemical weathering and denudation as determined from watershed studies in Massachusetts: Geological Society of America Bulletin, v. 108, p. 1314-1327.

SOUTHEASTERN GEOLOGY
Duke University
Box 90233
Durham, NC 27708-0233

Returned Service Requested

Non-Profit Org.
U. S. POSTAGE
PAID
Durham, NC
Permit No. 60

BELK LIBRARY
SERIALS DEPT
APPALACHIAN STATE UNIVERSITY
PO BOX 32026
BOONE **NC** **28608**